"DIAGNOSTIC POTENTIAL OF DIFFUSION WEIGHTED MRI IN DIFFERENTIATING BENIGN FROM MALIGNANT OVARIAN MASSES AND CORRELATING WITH HISTOPATHOLOGY"

By

Dr. AMRUTHA RANGANATH

DISSERTATION SUBMITTED TO SRI DEVARAJ URS ACADEMY OF HIGHER EDUCATION AND RESEARCH, KOLAR, KARNATAKA

In partial fulfilment of the requirements for the degree of

DOCTOR OF MEDICINE
IN
RADIODIAGNOSIS

Under the Guidance of

Dr. ANIL KUMAR SAKALECHA, M.D.,
PROFESSOR OF RADIODIAGNOSIS

&

Under the Co-Guidance of

Dr. KALYANI.R, M.D., FICP,
PROFESSOR & HOD OF PATHOLOGY

DEPARTMENT OF RADIODIAGNOSIS,
SRI DEVARAJ URS MEDICAL COLLEGE,
TAMAKA, KOLAR – 563 101.

MAY 2021

SRI DEVARAJ URS ACADEMY OF HIGHER EDUCATION AND RESEARCH, TAMAKA, KOLAR, KARNATAKA

DECLARATION BY THE CANDIDATE

I hereby declare that this dissertation entitled **"DIAGNOSTIC POTENTIAL OF DIFFUSION WEIGHTED MRI IN DIFFERENTIATING BENIGN FROM MALIGNANT OVARIAN MASSES AND CORRELATING WITH HISTOPATHOLOGY"** is a bonafide and genuine research work carried out by me under the guidance of **Dr. ANIL KUMAR SAKALECHA**, Professor, Department of Radiodiagnosis, Sri Devaraj Urs Medical College, Kolar, and co-guidance of **Dr. KALYANI. R,** Professor & HOD, Department of Pathology, Sri Devaraj Urs Medical College, Kolar, in partial fulfilment of University regulation for the award "**M.D. DEGREE IN RADIODIAGNOSIS**", the examination to be held in May 2021 by SDUAHER. This has not been submitted by me previously for the award of any degree or diploma from the university or any other university.

Dr. AMRUTHA RANGANATH,
Postgraduate in Radiodiagnosis,
Sri Devaraj Urs Medical College,
Tamaka, Kolar.

Date:

Place: Kolar.

SRI DEVARAJ URS ACADEMY OF HIGHER EDUCATION AND RESEARCH, TAMAKA, KOLAR, KARNATAKA

CERTIFICATE BY THE GUIDE

This is to certify that the dissertation entitled **"DIAGNOSTIC POTENTIAL OF DIFFUSION WEIGHTED MRI IN DIFFERENTIATING BENIGN FROM MALIGNANT OVARIAN MASSES AND CORRELATING WITH HISTOPATHOLOGY"** is a bonafide research work done by **Dr. AMRUTHA RANGANATH,** under my direct guidance and supervision at Sri Devaraj Urs Medical College, Kolar**,** in partial fulfilment of the requirement for the degree of "**M.D. IN RADIODIAGNOSIS"**.

Dr. ANIL KUMAR SAKALECHA, M.D.,

Professor,

Department Of Radiodiagnosis,

Sri Devaraj Urs Medical College,

Tamaka, Kolar.

Date:

Place: Kolar.

SRI DEVARAJ URS ACADEMY OF HIGHER EDUCATION AND RESEARCH TAMAKA, KOLAR, KARNATAKA

CERTIFICATE BY THE HEAD OF DEPARTMENT

This is to certify that the dissertation entitled "**DIAGNOSTIC POTENTIAL OF DIFFUSION WEIGHTED MRI IN DIFFERENTIATING BENIGN FROM MALIGNANT OVARIAN MASSES AND CORRELATING WITH HISTOPATHOLOGY"** is a bonafide research work done by **Dr. AMRUTHA RANGANATH,** under direct guidance and supervision of **Dr. ANIL KUMAR SAKALECHA**, Professor, Department of Radiodiagnosis at Sri Devaraj Urs Medical College, Kolar**,** in partial fulfilment of the requirement for the degree of "**M.D. IN RADIODIAGNOSIS"**.

Dr. N. RACHEGOWDA, M.D., DMRD.,
Professor & HOD,
Department of Radiodiagnosis
Sri Devaraj Urs Medical College,
Tamaka, Kolar.

Date:

Place: Kolar.

SRI DEVARAJ URS ACADEMY OF HIGHER EDUCATION AND RESEARCH, TAMAKA, KOLAR, KARNATAKA

CERTIFICATE BY THE CO-GUIDE

This is to certify that the dissertation entitled **"DIAGNOSTIC POTENTIAL OF DIFFUSION WEIGHTED MRI IN DIFFERENTIATING BENIGN FROM MALIGNANT OVARIAN MASSES AND CORRELATING WITH HISTOPATHOLOGY"** is a bonafide research work done by **Dr. AMRUTHA RANGANATH,** under my co-guidance and supervision at Sri Devaraj Urs Medical College, Kolar**,** in partial fulfilment of the requirement for the degree of "**M.D. IN RADIODIAGNOSIS"**.

Dr. KALYANI.R, MD., FICP,

Professor & HOD
Department of Pathology
Sri Devaraj Urs Medical College and
Research Center, Tamaka
Kolar

Date:

Place: Kolar.

SRI DEVARAJ URS ACADEMY OF HIGHER EDUCATION AND RESEARCH TAMAKA, KOLAR, KARNATAKA

ENDORSEMENT BY THE HEAD OF THE DEPARTMENT AND PRINCIPAL

This is to certify that the dissertation entitled **"DIAGNOSTIC POTENTIAL OF DIFFUSION WEIGHTED MRI IN DIFFERENTIATING BENIGN FROM MALIGNANT OVARIAN MASSES AND CORRELATING WITH HISTOPATHOLOGY"** is a bonafide research work done by **Dr. AMRUTHA RANGANATH** under the direct guidance and supervision of **Dr. ANIL KUMAR SAKALECHA,** Professor, Department of Radiodiagnosis, Sri Devaraj Urs Medical College, Kolar, in partial fulfilment of University regulation for the award "**M.D. DEGREE IN RADIODIAGNOSIS**".

Dr. N. RACHEGOWDA,
Professor & HOD,
Department Of Radiodiagnosis,
Sri Devaraj Urs Medical College,
Tamaka, Kolar.

Date:
Place: Kolar.

Dr. P. N. SREERAMULU,
Principal,
Sri Devaraj Urs Medical College,
Tamaka, Kolar.

Date:
Place: Kolar.

SRI DEVARAJ URS ACADEMY OF HIGHER EDUCATION AND RESEARCH, TAMAKA, KOLAR, KARNATAKA

ETHICAL COMMITTEE CERTIFICATE

This is to certify that the Ethical committee of Sri Devaraj Urs Medical College, Tamaka, Kolar has unanimously approved

Dr. AMRUTHA RANGANATH,

Post-Graduate student in the subject of

RADIODIAGNOSIS at Sri Devaraj Urs Medical College, Kolar

to take up the Dissertation work entitled

"DIAGNOSTIC POTENTIAL OF DIFFUSION WEIGHTED MRI IN DIFFERENTIATING BENIGN FROM MALIGNANT OVARIAN MASSES AND CORRELATING WITH HISTOPATHOLOGY"

to be submitted to the

SRI DEVARAJ URS ACADEMY OF HIGHER EDUCATION AND RESEARCH, TAMAKA, KOLAR, KARNATAKA.

Member Secretary,

Sri Devaraj Urs Medical College,

Kolar – 563 101.

SRI DEVARAJ URS ACADEMY OF HIGHER EDUCATION AND RESEARCH, TAMAKA, KOLAR, KARNATAKA

COPY RIGHT

I hereby declare that Sri Devaraj Urs Academy of Higher Education and Research, Kolar, Karnataka shall have the rights to preserve, use and disseminate this dissertation/thesis in print or electronic format for academic/research purpose.

Dr. AMRUTHA RANGANATH

Date:

Place: Kolar.

Sri Devaraj Urs Academy of Higher Education and Research

Certificate of Plagiarism Check for Dissertation

Author Name	Dr. AMRUTHA RANGANATH
Course of Study	MD RADIODIAGNOSIS
Name of Major Supervisor	Dr. ANIL KUMAR SAKALECHA
Department	RADIODIAGNOSIS
Acceptable Maximum Limit	10%
Submitted By	librarian@sduu.ac.in
Paper Title	DIAGNOSTIC POTENTIAL OF DIFFUSION WEIGHTED MRI IN DIFFERENTIATING BENIGN FROM MALIGNANT OVARIAN MASSES AND CORRELATING WITH HISTOPATHOLOGY
Similarity	1%
Paper ID	187614
Submission Date	2020-11-26 14:49:57

Signature of Student

Signature of Major Advisor

Professor
Dept. of Radio-Diagnosis
R.L.J. Hospital & Reasearch Centre
Tamaka, Kolar-563 101

Head of the Department

Dept. of Radio Diagnosis,
R.L.J. Hospital & Research Centre
Tamaka, KOLAR-563 101

University Librarian

Library and Information Centre
Sri Devaraj Urs Medical College
Tamaka, KOLAR-563 101

Director OF Post Graduate Studies

Director
PG STUDIES
Sri Devaraj Urs Medical College
Tamaka, KOLAR-563 101

* This report has been generated by DrillBit Anti-Plagiarism Software

ACKNOWLEDGEMENT

I owe my debt and gratitude to my husband ***Dr. P. V. SUDHARSAN,*** *my parents* ***Dr. K. RANGANATH*** *and* ***Smt. D. PADMA,*** *my in laws* ***Dr. P.V. VIJAYARAGHAVAN*** *and* ***Dr. JAYA VIJAYARAGHAVAN*** *for their moral support and constant encouragement during the course of the study.*

With humble gratitude and great respect, I would like to thank my teacher, mentor and guide, ***Dr. ANIL KUMAR SAKALECHA****, Professor, Department of Radiodiagnosis, Sri Devaraj Urs Medical College and Research Institute, Kolar, for his able guidance, constant encouragement, immense help and valuable advices which went a long way in moulding and enabling me to complete this work successfully.*

I have great pleasure in expressing my deep sense of gratitude to ***Dr. N. RACHEGOWDA,*** *Professor and Head, Department of Radiodiagnosis, Sri Devaraj Urs Medical College and Research Institute, Kolar. Without his initiative and constant encouragement this study would not have been possible.*

I would also like to thank ***Dr. KALYANI. R****, Professor and Head, Department of Pathology, Sri Devaraj Urs Medical College for her wholehearted support, constant encouragement and guidance.*

I would like to thank ***Dr. NABAKUMAR SINGH*** *Associate Professor and* ***Dr. RAJESWARI, Dr. SHIVAPRASAD G. SAVAGAVE,*** *and* ***Dr. BUKKE RAVINDRA NAIK****, Assistant professors, Department of Radiodiagnosis, Sri Devaraj Urs Medical College and Research Institute, Kolar, for their constant support and encouragement during the study period.*

I would also like to thank ***Dr. ASHWATHNARAYANASWAMY, Dr. VARUN S, Dr. GAURAV YADAV, Dr. GOWTHAMI M, Dr. MADHUKAR M, Dr. DARSHAN A.V, Dr. RAHUL DEEP G, Dr. GNANA SWAROOP RAO POLADI*** *and all my teachers of Department of Radio-diagnosis, Sri Devaraj Urs Medical College, Kolar for their support.*

I am thankful to my seniors ***Dr. Parameshwar Keerthi B.H****,* ***Dr. Esakki Rajulu, Dr. Athira P.M, Dr. Hithishini H*** *and* ***Dr. Anshul Singh****, my fellow* ***postgraduates, Dr. E. Vineela, Dr. Sahana N Gowda , Dr. Thati Sai Soumya, Dr. Divya Teja Patil , Dr. Sushmitha Prasad*** *and all other* ***postgraduates*** *for having rendered all their co-operation and help to me during my study.*

I am extremely grateful to the patients and their families who volunteered to this study, without them this study would just be a dream.

I am also thankful to ***Mr. Ravi, Mr. Aleem, Mr. Chandrasekhar,*** *and* ***Mr. Mateen*** *along with other* ***technicians*** *of Department of Radio diagnosis, R.L Jalappa Hospital & Research Centre, Tamaka, Kolar for their help.*

*My sincere thanks to **Mr. Sunil, Mrs. Naseeba,** and **Mrs. Shobha,** along with rest of the computer operators.*

*I am also thankful to staff nurse **Mrs. Radha & Mr. Munipillappa, Mrs. Munivenkatamma** and other **technicians** of Department of Radiodiagnosis, R.L Jalappa Hospital & Research Centre, Tamaka, Kolar for their help.*

*Last but not the least I would be failing in my duty if I do not express my gratefulness to the **Almighty,** who helped me to successfully complete this study.*

Dr. AMRUTHA RANGANATH

LIST OF ABBREVIATIONS

ADC	- Apparent Diffusion Coefficient
Cm	- centimeter
CT	- Computed Tomography
CECT	- Contrast Enhanced Computed Tomography
DCE MRI	- Dynamic Contrast Enhanced Magnetic Resonance Imaging
DWI	- Diffusion Weighted Imaging
FDG-PET	- 18-Fluorodeoxyglucose- Positron Emission Tomography
GCTs	- Granulosa Cell Tumors
GRE	- Gradient Echo sequence
H & E	- Haematoxylin and Eosin stain
HE4	- Human Epididymis Protein 4
HPE	-Histopathological Examination
IOTA	- International Ovarian Tumor Analysis
mm	- millimeter
MRI	- Magnetic Resonance Imaging
MDCT	- Multidetector Computed Tomography
NPV	- Negative Predictive Value
OMGCT	- Ovarian Malignant Germ Cell Tumor
PPV	- Positive Predictive Value
RMI	- Risk of Malignancy Index
ROI	- Region of Interest
s-CA-125	- Serum Cancer Antigen 125

T1WI	- T1-Weighted Image
T2WI	-T2-Weighted Image
T1FS	- T1 Fat Saturated
T2FS	-T2 Fat Saturated
STIR	- Short Tau Inversion Recovery
USG	-Ultrasonography

ABSTRACT

Background: Ovarian masses are one of the rising causes of mortality among women worldwide and remains a cause for concern because of its poor outcomes. This warrants accurate pre-operative differentiation of benign and malignant ovarian masses. This can be achieved with diffusion weighted imaging (DWI) and Apparent diffusion coefficient (ADC) values, thereby aiding in planning of appropriate treatment strategies.

Aims and Objectives: Aims and objectives of this study were to evaluate morphology of the ovarian masses, to differentiate benign from malignant ovarian masses with DWI/ADC values and to correlate combined Magnetic Resonance Imaging (MRI) & DWI/ADC results with histopathological findings.

Material and Methods: This prospective observational study was conducted from January 2019 to June 2020 on 32 patients with clinically suspected or sonographically diagnosed ovarian masses who underwent MRI Pelvis. Baseline data, imaging findings on MRI & DWI/ADC were recorded and compared with histopathological diagnosis.

Results: A total of 32 patients were included in the study. Conventional MRI showed specificity of 84.2%, positive predictive value of 81.25% and overall diagnostic accuracy of 90.6% in characterising ovarian masses. Similarly, diffusion weighted imaging with corresponding ADC values showed specificity of 78.9%, positive predictive values of 76.47% and overall diagnostic accuracy of 87%.

Using an ADC cut off value of 1.23 x $10^{-3}$$mm^2$/s, the mean ADC values for benign and malignant ovarian masses showed statistical significance (p<0.001). Combined analysis of both Conventional MRI and DWI/ADC showed a significant increase in specificity, positive predictive value and diagnostic accuracy to 94.7%, 92.86% and 96.88% respectively.

Conclusion: Diffusion weighted imaging plays a pivotal role in characterizing benign and malignant ovarian masses with high diagnostic accuracy and should be added to the routine MRI protocol. We recommend an optimal ADC cut off of 1.23 x 10^{-3} mm^2/s to differentiate benign from malignant ovarian masses.

Keywords: Magnetic Resonance Imaging, Diffusion weighted imaging, Ovarian masses, Apparent diffusion coefficient, Histopathology.

TABLE OF CONTENTS

LIST OF TABLES

LIST OF FIGURES

INTRODUCTION

INTRODUCTION

Women belonging to various age groups manifest with a wide range of pelvic pathologies, from benign simple cysts to malignant ovarian masses. Ovarian cancer is the 7th most common malignancy worldwide and a notable cause of mortality among women in both developing and developed countries[1]. Incidence of ovarian cancer among Indian women is 36,170, accounting for 6.2% of overall malignancies and is ranked as 3rd most common malignancy[2]. Overall incidence of ovarian malignancy is 2.98% in Kolar[3].

Ovarian malignancies have high probability of recurrence inspite of aggressive treatment strategies[4]. The 5-year survival rate of early stage ovarian cancer is >90%, which drops significantly to 21% in advanced stages[1]. Accurate characterization of ovarian masses helps in optimizing treatment and improve patient care.

A combination of various radiological imaging modalities can be used to characterize the adnexal lesions and determine its nature. Ultrasonography (USG) is the first-line imaging modality for suspected adnexal masses. However, it is less accurate in characterizing indeterminate or complex ovarian masses. Computed Tomography (CT) has poor soft tissue resolution and an added risk of radiation exposure[5]. Magnetic Resonance Imaging (MRI) with excellent soft tissue resolution, and multiplanar imaging capability overcomes these limitations and plays a significant role in the work up of ovarian masses[4,6]. Based on varying signal intensities in different sequences, MRI can differentiate various types of tissues and

their malignant potential, thereby permitting better characterization of ovarian masses[6].

Diffusion weighted imaging (DWI) is one of the evolving MR imaging sequences based on Brownian movement, that is sensitive to changes in the microdiffusion of water molecule in both intracellular and extracellular spaces[7]. It improves tissue characterization when findings are interpreted together, than with conventional MR imaging sequences alone[4]. Quantitative analysis of diffusion is performed by employing Apparent Diffusion Coefficients (ADC).

Diagnostic challenge of ovarian masses is mainly attributed to imaging as biopsy is not applicable in the majority[8]. Diffusion weighted MRI is one such evolving imaging sequence that could be used in characterizing ovarian masses and has an additive value in distinguishing benign from malignant masses[9].

An increasing trend in the frequency of ovarian cancer among Indian women and lack of research work on early diagnostic modality for ovarian masses here, necessitates the need for establishing a non-invasive accurate pre-operative imaging modality. Thereby, reducing the need for unnecessary biopsies and surgical interventions.

The goal of this study is to accurately characterize the ovarian masses and distinguish benign from malignant masses by using DWI/ADC mapping and to correlate with the histopathological diagnosis which is the gold standard.

AIMS & OBJECTIVES

AIMS AND OBJECTIVES

The aims and objectives of the study were:

1. To assess the morphology of ovarian masses.
2. To differentiate benign from malignant ovarian masses using diffusion weighted imaging (DWI) and Apparent diffusion coefficient (ADC) values.
3. To correlate combined MRI and DWI/ADC findings with histopathology.

REVIEW OF LITERATURE

REVIEW OF LITERATURE

EMBRYOLOGY OF FEMALE REPRODUCTIVE SYSTEM

The reproductive system encompasses an array of organs responsible for generation of new off springs. Sex determination in mammals occurs at the same time as fertilization, on the basis of the chromosomal composition of the sperm, or in other words based on the existence or lack of 'Y chromosome'. In humans, the process of sexual differentiation starts by 4–5 weeks of gestational age, in the developing fetus, however it remains inapparent until the 12th week of gestation[10].

Initially, the genital system of both genders remains indistinguishable from each other, a period referred to as the 'indifferent stage of embryonic development' and the gonads are considered to be 'bipotential'. From here, the SRY gene decides the pathway of the genital system, the presence of which initiates the male differentiation and in its absence the fetus retains its initial embryology and further differentiates to form the female reproductive system[10].

Thus, the development of a female, forms the basic development path of the human embryo that calls for the lack of testosterone more than meagre existence of estrogen for its differentiation.

The development of the gonads occurs from three sources: the mesothelium (coelomic epithelium) lining the posterior abdominal wall, underlying mesenchyme (intermediate mesoderm), and the primordial germ cells.

Intermediate mesoderm forms a bulge knows as the ‘urogenital ridge’ along the ventromedial surface of the intermediate embryonic kidney - the mesonephros. At this stage the gonads contain mainly somatic cells,that form supporting, interstitial and steroid-producing cells and migrating germ cells which form the gametes. The mesonephros comprises of mesonephric and paramesonephric ducts which further grows and develops to form the male and female reproductive system respectively[11].

Development of ovaries

The development of ovary and ovum are interlinked, both of which begins early in embryogenesis and continues through birth, reproductive years and menopause. From the epithelium of urogenital ridge, arise the primary sex cord cells,that penetrate the underlying mesenchyme and form an indifferent gonad containing cortex and medulla. This undergoes differentiation to form the ovary in female fetus. The primitive ovaries migrate from the upper abdomen to the pelvis with the help of gubernaculum (mesenchymal cord attached to the infero-medial pole of the gonad) and by a processes of chemotaxis[12].

Descent of the Ovary

The ovaries originally develop in the lumbar region, following which they descend to the true pelvis. Like in males, a gubernaculum forms, continuing from the ovary to labium majus and attaches itself at junction of developing uterus with the uterine tube. Part of the gubernaculum persisting amidst the ovary and uterus forms the round ligament of the ovary and that persisting between the uterus and the labium majus forms the round ligament of the uterus[13].

Oogenesis

Gametes originate from the primordial germ cells during the 4th week of gestational life, which then migrate to the developing gonads and increase in number by their mitotic division during this migration. Here, they undergo further differentiation to form female gametes followed by mitotic (increases their number) and meiotic divisions (reduces the chromosomal content)[14]. The process of oogenesis, i.e. maturation and differentiation of primitive sex cells into oogonia (mitotic proliferation of primitive cells), primary oocytes (enlarged oogonia surrounded by epithelial cells) and finally into a mature ovum occurs in the ovarian cortex. It begins in utero and continues until menopause[14].

Proliferating primary oocytes roughly form 2 million primordial follicles. Each primordial follicle contains a single oocyte and single granulosa cell layer surrounding the oocyte. Continuous atresia of these follicles starts from before birth and continues throughout the reproductive phase such that 500000 of them remain at puberty and only about 400 mature ova are released during the span of entire reproductive phase in a female[15].

By the time, female reaches puberty, the oocyte completes its meiotic division and releases a secondary oocyte which remains arrested in second meiotic division. If fertilization occurs, second meiotic division is complete and an embryo is formed. In the absence of fertilization, the secondary oocyte regresses within 24 hours[14].

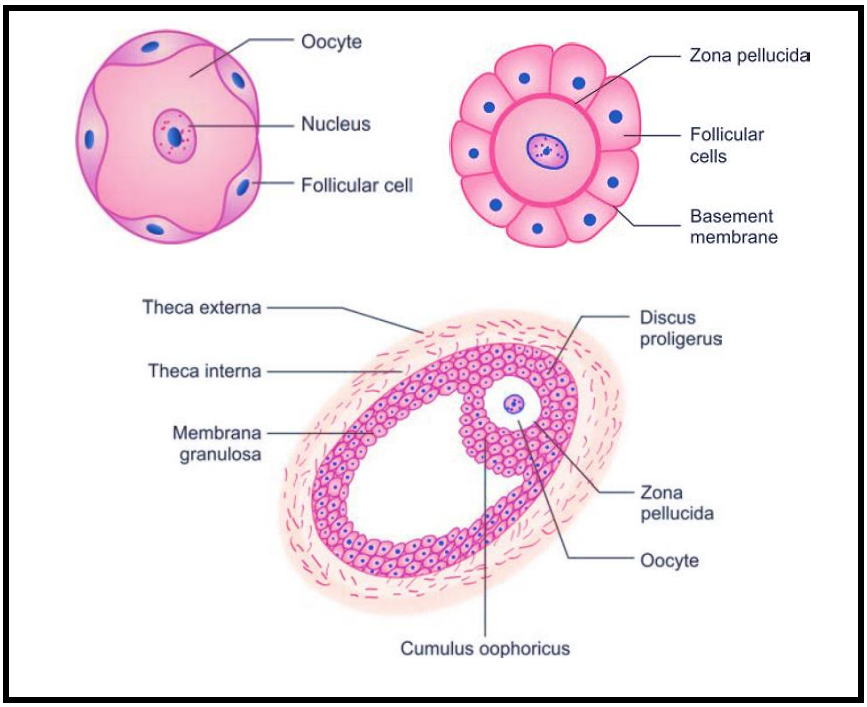

Figure 1. Different stages of ovarian follicular development

ANATOMY OF FEMALE PELVIS

The pelvis contains most of the reproductive tract in females and part of the reproductive tract in males. One ovary on each side, and a uterus, vagina, and clitoris in the midline form the major components of female reproductive system. The uterus is interposed in the midst of rectum and urinary bladder in the pelvic cavity. On each side, the fallopian tubes extend laterally to open near the ovary. Inferiorly, the vagina penetrates the pelvic floor and continues with the uterus in the pelvic cavity above[16].

Anatomy of ovaries

They are paired almond shaped gonadal structures that develop high in posterior abdominal wall, and descend inferiorly to be located amidst the uterus and pelvic wall. They remain suspended with their long axis in the vertical plane by utero-

ovarian ligament medially and infundibulopelvic ligament (suspensory ligament of ovary) laterally. In nulliparous women, it comes to lie in the ovarian fossa, that represents a depression in pelvic wall, anterior in relation to the ureters and below the external iliac vessels[16,17].

Inferiorly, the hilar surface, also known as its base is supported by the mesovarium that attaches the ovary to broad ligament, a double layered fold of peritoneum. This band of mesentery remains dorsal to the uterine tubes and the mesosalpinx. The primary neurovascular structures enter the ovaries through the hilum[17].

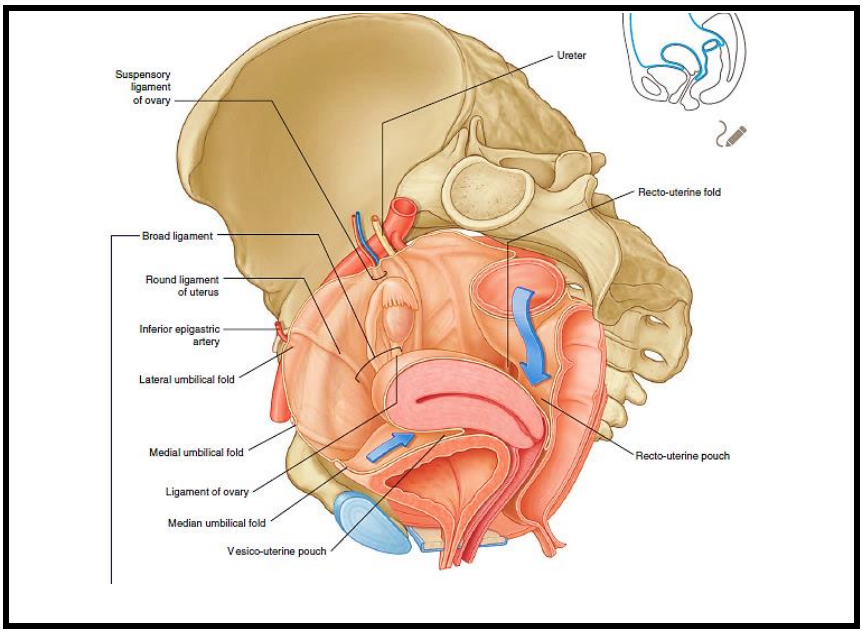

Figure 2. Anatomy of female pelvis

Their normal morphology depends on the age and reproductive status of a female. In a normal adult woman, they are approximately 2.5–5 cm long, 1.5–3 cm thick, and 0.7–1.5 cm wide, with a weight of 3–8 g[16,17]. Histologically, the ovary is composed of inner medulla and outer cortex and is enclosed by a single epithelial

covering. There is no peritoneal covering of ovary proper. The cortex consists of specialized connective tissue stroma and follicles in various stages of development or regression. The medulla primarily includes loose fibromuscular connective tissue and neurovascular structures. In some cases, hilum of ovary contains few hilus cells which are analogous to the Leydig cells of the testis[17].

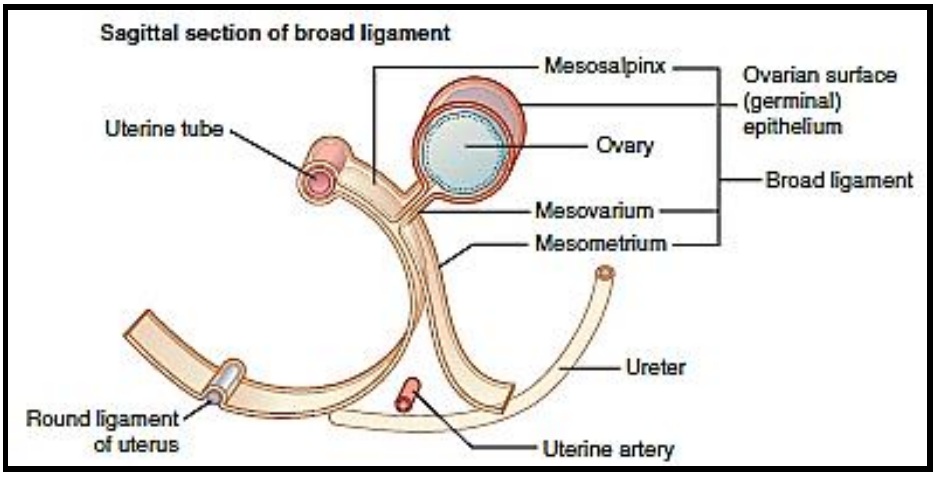

Figure 3. Ovarian ligaments

Blood supply of ovaries

The dominant blood supply to the ovary is by ovarian artery, a branch of abdominal aorta which anastomoses with the uterine artery[17]. Venous drainage follows the arteries. Ovarian veins on the right side flow into the inferior vena cava and on the left side into the left renal vein[16].

Innervation to the ovaries

The ovarian plexus and the uterovaginal plexus complete the innervation to the ovaries[17].

OVARIAN MASSES

Imaging of adnexal masses is diagnostically challenging, in terms of determination of the degree of suspicion for malignancy[18]. Majority of these adnexal masses are benign, and necessitates the need for confident exclusion of malignancy based on imaging appearance[19]. Of all the adnexal lesions, likely arising from ovary, the most common cysts that need to be considered and ruled out are functional cysts like simple cysts, corpus luteal cysts, hemorrhagic cysts, and benign cysts/cyst like conditions including endometriomas and polycystic ovarian changes.

Table 1. Ovarian Masses

Lesion type	Differential diagnosis
Benign	▪ Physiological/functional cysts: Simple or hemorrhagic ▪ Endometrioma ▪ Cystadenomas: serous or mucinous ▪ Mature cystic teratoma or dermoids ▪ Stromal tumors: fibroma or thecoma
Borderline & Malignant **I. Epithelial tumors**	▪ Serous cystadenocarcinoma ▪ Mucinous cystadenocarcinoma ▪ Clear cell carcinoma ▪ Endometrioid carcinoma ▪ Brenner's or transitional carcinoma

II. Non-epithelial tumors	▪ Germ cell tumors: dysgerminoma, yolk sac, embryonal tumors, immature teratomas etc. ▪ Sex-cord stromal tumors: granulosa cell tumor, Sertoli-Leydig tumor ▪ Metastasis: from breast, colon, gastric, pancreatic, appendiceal Other rare types: Primitive Neuroectodermal tumor, Lymphoma, Carcinosarcoma

I. BENIGN OVARIAN MASSES

Functional Cyst

Periodically, the appearance of ovaries changes, through the phases of ovarian follicular development, rupture, discharge of ovum, formation and regression of corpus luteum during their ovarian cycle[20].

Simple ovarian cyst/ follicular cyst

Simple cysts are unilocular, thin walled (wall thickness < 3 mm) and are less than 30 mm in size[18]. Usually a cyst of size, less than 25 mm is not significant in a premenopausal patient since the ovarian follicles, normally acquire a mean diameter of 20 - 24 mm at the time of ovulation. On MRI, most functional cysts demonstrate T1 hypointense and T2 hyperintense signal intensities. Post contrast images show thin peripheral rim enhancement[21].

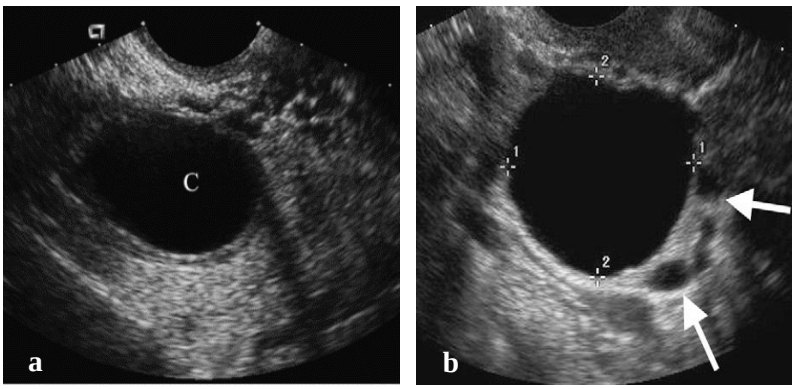

Figure 4. Trans-vaginal ultrasound images showing simple cyst (C) arising from the right ovary (a) with adjacent normal ovarian follicles (white arrows) (b).

Almost all the larger simple cysts (size > 5 cm, or change in shape and size during follow up) may develop into serous cystadenoma and necessitate surgical intervention[22]. The risk for malignant transformation in simple ovarian cysts was found to be 0.7% in premenopausal phase and 1.6% in postmenopausal phase[23].

Hemorrhagic cyst:

These are common functional cysts in the premenopausal women, derived from follicular or corpus luteal cysts[24]. Usually they are unilateral and regress within 6-8 weeks.

Wide spectrum of imaging appearances in hemorrhagic cyst, depends on the maturity of clot, the most common being well defined, regular, thin walled cyst with internal echoes and fine interdigitating or lacelike fibrin strands within, giving a ‘‘fishnet appearance’’ on sonography. Sometimes, they may present with fluid-fluid levels or appear like solid lesions due to internal subacute clot formation[25].

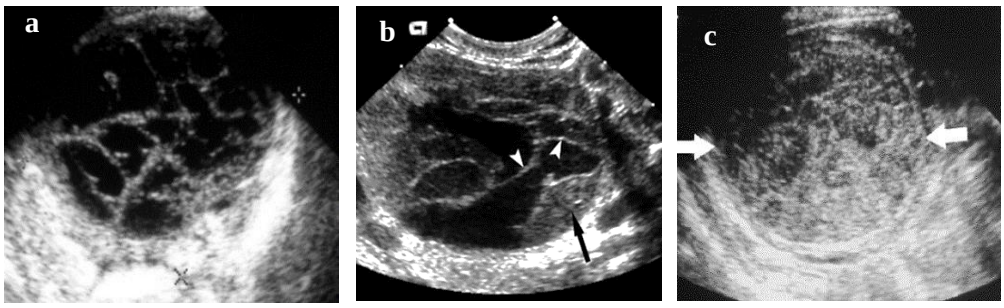

Figure 5. Transvaginal ultrasound images showing spectrum of imaging appearances of hemorrhagic cyst a) lacelike reticular pattern, b) retracted clot formation (arrowheads) and c) apparent solid lesion (white arrows).

On MRI, these cysts show relatively high signal intensity on T1WI and intermediate to high signal intensity on T2WI[21,24].

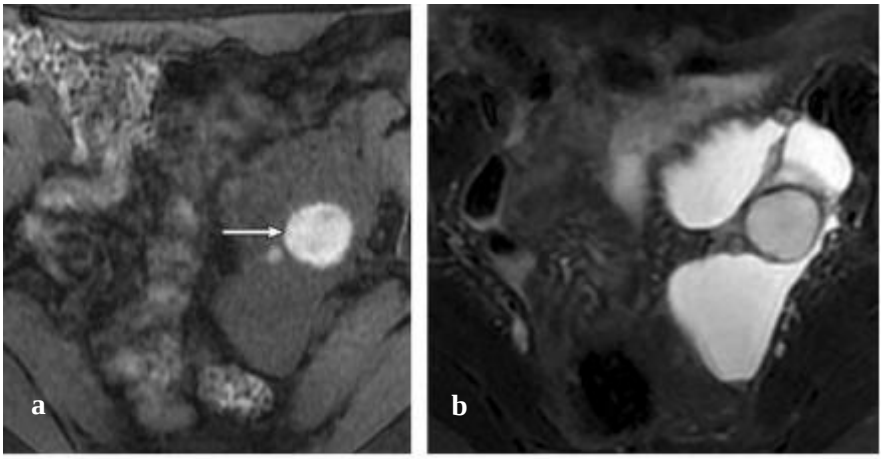

Figure 6. MRI Pelvis showing hemorrhagic cyst a. Axial T1FS image in 40-year-old female shows hyperintense left ovarian cyst (white arrow) b. Corresponding axial T2FS images of the cyst shows intermediate signal intensity

Corpus luteum

Corpus luteum is an endocrine organ in itself within the ovary that maintains and regulates menstruation and early pregnancy. It can grow upto a maximum size of 25-40 mm, especially during the luteal phase of ovarian cycle[26]. Sonographically seen as a cyst with internal echoes and collapsed, crenated wall, demonstrating ring vascularity on colour Doppler[27].

Endometrioma

Extra-uterine implantation of endometrial tissue, commonly involving the ovaries in reproductive age group is termed as endometriosis[21]. They commonly present as

cystic mass with diffuse internal echoes. Additionally, multilocularity and presence of hyperechoic wall foci in the lesion favors its diagnosis[24].

On MRI, endometriomas are seen as homogenously hyperintense cystic mass on T1WI with intermediate-low signal on T2WI, representing the various stages of hemoglobin degradation products, classically termed as '*T2 shading sign*'[21,24]. Presence of discrete intracystic hypointense spots on T2WI, known as '*T2 dark spots*' (more specific than T2 shading sign) and adhesion/tethering to adjacent structures aid in the diagnosis of endometriosis[21,28]. Sometimes chronic endometriomas may present as a solid mass[19]. Less than 1% of endometriomas undergo malignant transformation[24].

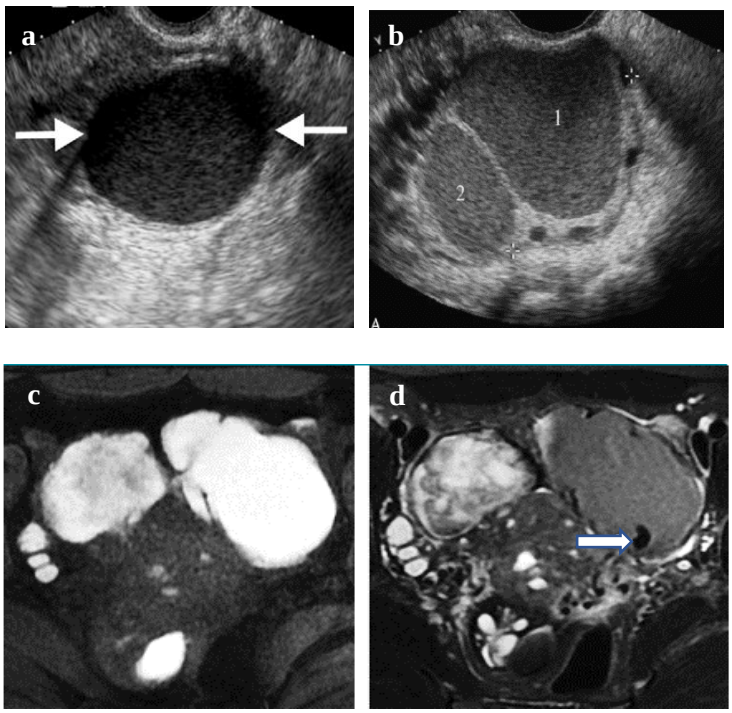

Figure 7. USG & MRI images for ovarian endometrioma (a & b). Transvaginal ultrasound image demonstrating unilocular (white arrows) and bilocular (1 & 2) ovarian cyst with diffuse homogenous low-level internal echoes. (c) Axial T1FS

image shows bilateral hyperintense adnexal lesions. d. T2FS image shows T2 dark spot (thick white arrow) and shading sign.

Cystadenomas

Epithelial ovarian tumors constitute 60% of entire ovarian neoplasms and 85% of malignant ovarian neoplasms, with a peak incidence at around sixth or seventh decade[29]. Serous and mucinous variety are the most common histological subtype of epithelial tumors[24,29].

Serous cystadenoma

They constitute approximately 20% to 25% of all benign ovarian tumors[24]. On imaging, they are predominantly unilocular (rarely multilocular), bilateral, thin walled (< 3 mm), cystic lesions that demonstrate homogenous T2 hyperintense signal and T1 hypointense signal with no significant post contrast enhancement. Pelvic lymphadenopathy, ascites or peritoneal deposits are usually absent[21,30].

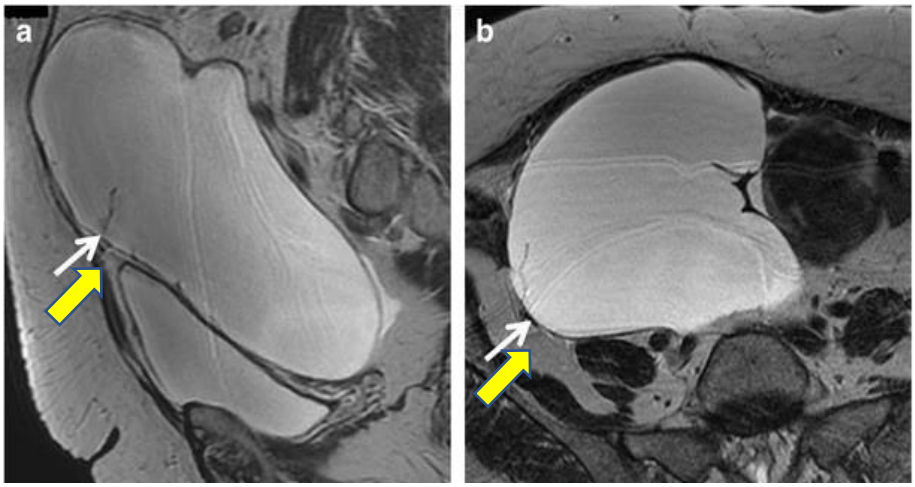

Figure 8. MR images in a 64-year-old female a) T2 sagittal, b) T2 axial images shows large unilocular hyperintense cystic mass (yellow arrows).No solid nodules/papillary projections present.

Mucinous cystadenoma

They are second most common epithelial tumors after serous cystadenomas and constitute 20% to 25% of all benign ovarian neoplasm[24].

They are usually larger in size than serous cystadenomas and are multiloculated, with thin regular walls, multiple internal septations without vegetations/papillary projections. On MRI, they demonstrate variable T1 and high T2 signal intensity based on the mucin content with no significant post contrast enhancement[21,24].

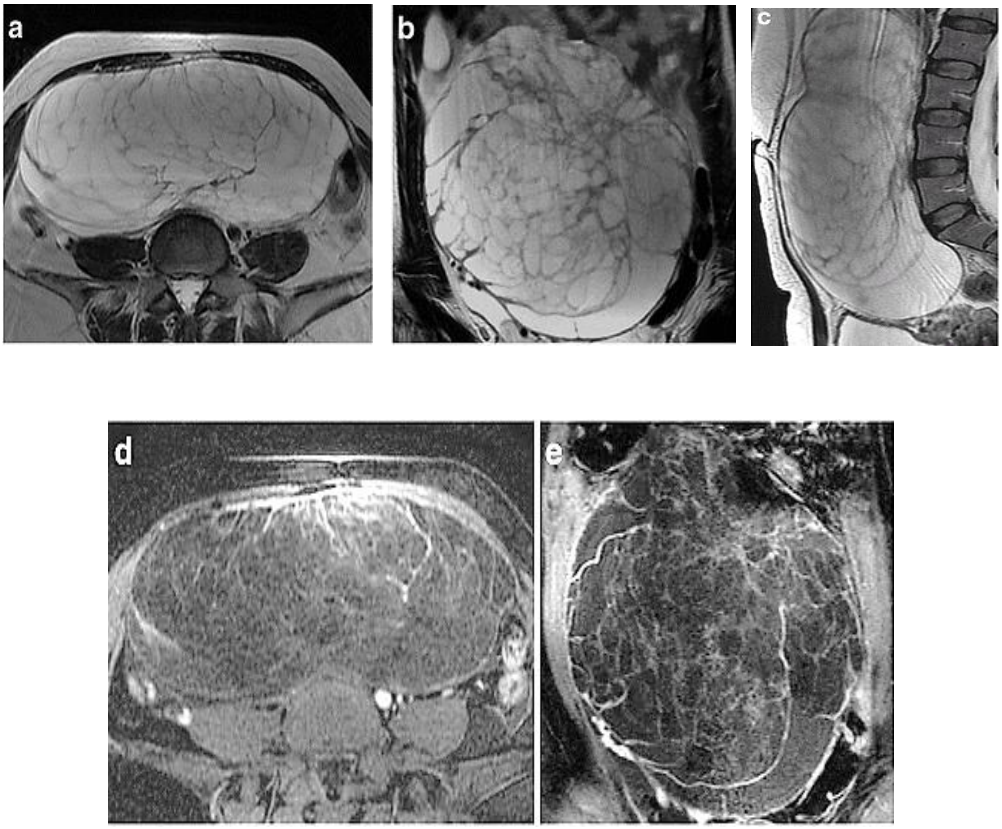

Figure 9. MRI Pelvis demonstrating mucinous cystadenoma in 44-year female. a) axial, b) coronal & c) sagittal T2WI shows a large multiloculated hyperintense lesion. d) axial and e) coronal T1FS post contrast images show no significant enhancement of mass.

Benign Teratoma

Ovarian teratomas are most frequently encountered benign ovarian tumors and accounts for 20% of all ovarian neoplasms, especially in females of age less than 45 years[20,21]. They are derived from all three germ layers and are sub-classified as, mature cystic teratomas, immature teratomas, monodermal and fetiform teratomas, among which mature cystic teratomas are the most common form, constituting 99% of them[20,31].

Mature cystic teratomas

Mature cystic teratomas, also known as dermoids, are derived from at least two well-differentiated, germ cell layers. They are most often asymptomatic and evolve slowly[20,31]. They possess a spectrum of imaging appearances from purely cystic masses to a purely solid form[24].On sonography, their imaging appearance has been described to have 'virtually limitless combinations' of echogenicity. Most commonly present as cystic masses with intraluminal echogenic protrusion representing the 'dermoid plug/Rokitansky nodule'[31]. They may present as partially echogenic masses with posterior shadowing obscuring the rest of the mass, due to fat content, calcifications and hair, known as the '*tip of ice berg sign*' or with diffuse/regional high amplitude echoes depending on its sebaceous content admixed with hair. A combination of hair and non-fatty fluids in dermoids gives a classical 'dermoid mesh pattern', seen as hyperechoic lines and dots[21,32,33].

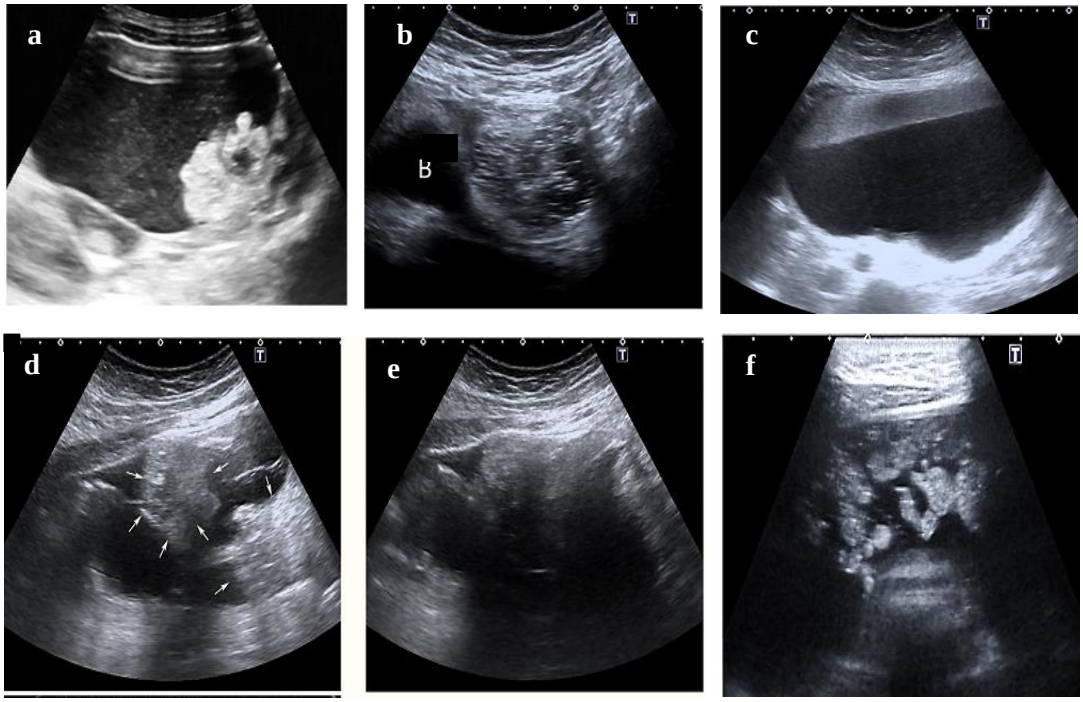

Figure 10. Transvaginal ultrasound images demonstrating imaging spectrum of mature cystic teratoma. a) Cystic mass with Rokitansky protuberance, b) dermoid mesh appearance c) fat fluid levels d) tip of ice berg sign e) echogenic lesion with posterior acoustic shadowing and f) meat ball sign.

They seldom present with fat fluid levels or as cystic mass with floating hyperechoic spherules/globules known as the 'meat ball sign'[34,35].Malignant transformation occurs in about 1% to 3% of dermoids[36] and is probably higher in postmenopausal women, with a reported occurrence of upto 15% in a study[37].

On MRI, the lipid-laden cyst fluid reveals T1-hyperintense signal with signal drop on fat-suppression sequences, intermediate signal intensity on T2WIs and is considered diagnostic for a dermoid[18,30]. T1 and T2 hypointense signal intensity could represent soft tissue protuberances and calcifications[21].

Imaging features of both endometrioma and mature cystic teratoma overlap as both demonstrate T1 hyperintense signal, however, 62% - 87% of teratomas demonstrate chemical shift artefact at fat-fluid interface represented as bright band on T2WI at fat fluid interface with dark bands on the opposite side of tumor[18,31].

Some other classical imaging features of teratoma include intratumoral palm tree like protrusions (desquamated epithelial tissue admixed with tufts of hair) of variable signal intensity, floating globules (nidus of debris, desquamated epithelial cells and hair shafts) of T2 hyperintense and T1 hypointense signal intensity encapsulated by sebaceous material showing opposite signal intensity to that of nidus on corresponding sequences and variable post contrast enhancement of Rokitansky protuberances. Some lesions may also have variable keratinoid material that demonstrates restricted diffusion on DWI/ADC[31].

Monodermal teratoma

Monodermal teratomas, constitute the less common category of mature teratomas that are predominantly composed of one type of tissue including struma ovarii, carcinoid tumors and tumors with neural differentiation[19,38].

Struma Ovarii

It is mainly composed of mature thyroid tissue that contains acini filled with colloid material forming approximately 3% of all mature teratomas[38].

They present as complex, heterogenous solid cystic mass on sonography. On MRI, it may be seen as a complex or multiloculated cystic mass with some locules

demonstrating high and some of them showing low signal intensity on T1 & T2 weighted images due to the presence of thick gelatinous colloid[19,38].

Carcinoid Tumors

They are uncommon, and are mostly seen in post-menopausal females as predominantly solid masses, with likely malignant transformation, hence remain a close differential for solid ovarian malignancies[38].

Benign Sex Cord Stromal Tumors

Sex cord stromal tumors make up for 8% of all ovarian neoplasms, affect all age groups and are derived from granulosa cells, sertoli cells, leydig cells and fibroblasts[29]. Fibrotic tumors are further sub-grouped as fibromas, fibrothecomas, cystadenofibromas and Brenner's tumor.

Fibroma and fibrothecomas

They are typically unilateral, solid, benign sex cord ovarian tumors forming 3-4% of total ovarian neoplasms with its highest incidence in peri-menopausal age group[18,19].They are made of fibrous tissue and theca cells with abundant intracytoplasmic lipid. These tumors are known for their hormonal, especially estrogenic effects, owing to the presence of theca cells[18].

Ultrasound remains non-specific for its imaging, and requires MRI for further differentiation from solid ovarian malignancies and uterine leiomyomas[29,39.]They typically demonstrate low signal intensities on T1 & T2 images due to its high collagen content. Few heterogenous T2 signal changes may be present in larger

tumors if associated with cystic changes/edema[39]. Typically, these lesions with fibrous components show delayed enhancement which becomes a useful feature to characterize them[18]. Ascites may be present, even in large quantities in upto 40% of cases and some with pleural effusion (Meig's syndrome) but is not indicative of malignancy[18,20].

Brenner's tumor

They are rare, mostly benign, ovarian neoplasms forming 1-3% of them, presenting at about 50 years of age. They mostly present as a small unilateral solid mass with dense amorphous calcification[20].

They present as homogenous T2 low signal solid lesion, with signal intensity similar to fibromas and may be seen in association with other ovarian tumors in the same ovary, most often mucinous cystadenoma in 30% of cases[40].

Sclerosing stromal tumor of ovary

It is a rare form of benign sex cord stromal tumor, seen in women less than 30 years presenting with most common complaint of menstrual irregularity, as a well encapsulated multiloculated lesion[41]. Capsule is seen as T1 & T2 hypointense rim and rest of the tumor is a heterogenous solid cystic tumor demonstrating T2 hypointense pseudonodules against a background of hyperintense stroma.

Spoke wheel pattern on Doppler ultrasonography represented as large peripheral vessels with centripetal flow and early peripheral enhancement followed by

delayed centripetal enhancement seen on dynamic MR studies are some characteristic features of this lesion[20,41].

Table 2. Signal intensities of benign ovarian masses on MRI

Ovarian masses	T2WI	T1WI	Fat suppressed T1WI
Serous cystadenoma	High	Low	Low
Mucinous cystadenoma	High	Intermediate - High	High
Mature Cystic Teratoma	Intermediate	High	Low
Endometrioma	High	High	High
Fibroma	Low to intermediate	Intermediate	Intermediate

II. BODERLINE AND MALIGNANT OVARIAN MASSES

The presence of irregular solid components/vegetations which show variable post contrast enhancement, thick irregular wall (> 3 mm), large soft tissue component with variable necrotic areas, presence of ascites, lymphadenopathy, peritoneal deposits and intra-abdominal metastases are some of the universally accepted imaging findings used to demarcate benign and malignant tumors. These findings hold true for the various modalities[18,20,24].

Most malignancies show these features and a mention on few salient features for specific groups such as epithelial tumours, germ cell tumours and sex-cord stromal tumors have been described below.

a) Epithelial Tumors

These tumors constitute 60% of overall, and 85% of all malignant ovarian malignancies and have been classified as benign, borderline and malignant surface epithelial tumors[18].

Serous and mucinous tumors

They are the most common form of ovarian epithelial tumors. Serous cystadenocarcinomas represent 40% to 50% and mucinous cystadenocarcinomas account for 5% to 10% of overall malignant ovarian neoplasms[24].

Papillary projections (solid, nonfatty, nonfibrous tissue), seen as T2 hypointense structures are single best predictor and distinctive pathologic feature of serous epithelial tumors that may correlate with tumor aggressiveness[18,21,24]. They may depict restriction of diffusion on DWI with heterogeneous enhancement on post contrast study[42]. Bilaterality, heterogeneity, psammomatous calcifications (in about 30% cases) and peritoneal carcinomatosis are common associations with serous carcinoma.

Mucinous carcinomas are usually unilateral multiloculated lesions that may possess papillary projections and solid enhancing components. These tumors have imaging features comparable with their benign counterpart, but with mural thickening,

more solid components, heterogenous enhancement, and restricted diffusion indicating their aggressive nature. Signal intensities on T1 and T2WI depends on mucin content. Tumor rupture resulting in pseudomyxoma peritonei (characterized by diffuse mucinous implants in the abdomen) may be an established complication of mucinous carcinomas[21].

Endometrioid carcinomas

Endometrioid carcinomas form 10-15% of malignant ovarian lesions and are almost always malignant, usually presenting with synchronous endometrial hyperplasia/carcinoma in 15-30% of these cases. They are known to be the commonest malignancy arising from preexisting endometriomas. Bilaterality is a feature in 15-30% of endometrioid carcinoma. Nonspecific imaging features include complex solid cystic mass associated with endometrial thickening[29].

Clear cell carcinoma

It constitutes 5% of all malignancies and is the second most frequent malignancy to arise from endometriomas after endometrioid carcinoma[29].

Commonly presents as a unilateral large, ovoid, smooth walled, unilocular cyst with solid protrusions. The mural nodules of clear cell carcinoma are focal, eccentric, and polypoidal in nature as compared to endometrioid carcinomas in which the solid protrusions are multifocal, concentric, and broad-based[43].

b) Non epithelial Tumors

Germ cell tumors

Ovarian malignant germ cell tumors (OMGCTs), constituting 2.6% of all ovarian malignancies arise from primitive gonadal germ cells and usually present in adolescent age group in association with elevated serum tumor markers[44]. Some of the important germ cell tumors have been briefly described below.

Ovarian dysgerminoma are the most prevalent malignant germ cell tumors & approximately form 1-2% of all malignant tumors, predominantly seen in young women. Hence, requires a confident pre-operative diagnosis to ensure fertility sparing surgeries, irrespective of the stage of disease[45].

They characteristically present as multilobulated solid mass with fibrovascular septae and possible speckled calcification in some. Some of them present with low signal intensity/low attenuation areas representing necrosis[29]. On MRI, they typically present as a solid, lobulated mass with fibrovascular septae. They show hypointense signal on T1WI, iso-hyperintense T2 signal and avid post contrast enhancement. The septae are better appreciated on T2WI as hyperintense[44].

Figure 11. Ovarian dysgerminoma in 17-year-old girl. Coronal T2WI shows a lobulated solid hypointense mass in left ovary with intervening hyperintense septae (white arrows).

Immature teratomas are the second most prevailing malignant germ cell tumors with peak incidence between 15 to 19 years and is responsible for 30% of mortality due to ovarian cancers in females less than 20 years of age[44]. 10% of the cases present with immature teratomas in contralateral ovary and coexisting ipsilateral mature cystic teratomas are seen in 26% of cases[46].

They usually present as well encapsulated solid lesions or as predominantly solid lesions with cystic components (solid components represent the immature elements), wherein the cystic components may contain either serous or mucin or fatty sebaceous material and is associated with capsule rupture. Areas of calcification, fat and hemorrhage may be present[46,47.]

Many times cysts in immature teratomas contain serous fluid in comparison with mature teratomas wherein the cyst contains predominantly fatty sebaceous material. Also calcification in immature teratomas appear small and irregular,

distributed diffusely in the tumors, as opposed to those in mature teratoma appearing tooth-like or coarse and is usually within the mural nodule or attached to wall of the cyst[44]. However, there is no specific diagnostic criteria for immature teratoma and is many times indistinguishable from mature cystic teratomas[46,46].

Yolk sac tumors, previously known as *endodermal sinus tumors* are third most common tumors belonging to malignant germ cell tumors and are commonly seen in women of 2nd and 3rd decade. Presents commonly as unilateral, smooth solid cystic mass with hemorrhagic areas.

Some characteristic imaging features, though not pathognomic include the '*bright dot sign'* referring to the contrast enhanced foci in solid components on contrast enhanced computed tomography (CECT)/post contrast sequences on MRI signifying areas of dilated vessels and the '*capsular tears'* [44].

Malignant transformation of mature cystic teratoma refers to origin of malignancy denovo in a pre-existing mature teratoma, most common (~ 80%) being squamous cell carcinoma with the most probable site of occurrence being the Rokitansky's nodule. Malignant transformation of benign teratoma can be suspected in an elderly lady (usually > 45 years old) presenting with a large lesion, measuring more than 10 cm and an associated elevation in serum squamous carcinoma antigen to > 2 ng (seen in 81.3% of cases). At this stage, they present with heterogeneously enhancing irregular solid components with transmural spread and infiltration into adjacent viscera, further aiding in diagnosis of malignant potential of the benign teratoma[44].

No specific imaging features of *malignant mixed ovarian germ cell tumors* have been described. They most commonly present as unilateral large solid masses with cystic components, hemorrhage and necrosis. Calcification and fat components may be present if associated with teratomatous elements[44].

Rest of the germ cell tumors include embryonal tumors, polyembryomas and tumors with mixed germ cell components.

Sex cord stromal tumors

These are rare neoplasms arising from primitive sex cord or stromal cells (7% of all ovarian tumors). Sex cord cells include the granulosa cells and Sertoli cells, while theca cells, fibroblasts, and Leydig cells constitute the stromal cells[48].

Table 3. WHO classification of sex cord stromal tumors of ovary

Pure stromal tumors	▪ Fibroma ▪ Thecoma ▪ Fibrosarcoma ▪ Luteinized thecoma with sclerosing peritonitis ▪ Leydig cell tumor ▪ Steroid cell tumor ▪ Sclerosing stromal tumor ▪ Signet-ring stromal tumor ▪ Microcystic stromal tumor
Pure sex cord tumors	▪ Adult granulosa cell tumor ▪ Juvenile granulosa cell tumor ▪ Sertoli cell tumor ▪ Sex cord tumor with annular tubules

Mixed sex cord stromal tumors	▪ Sertoli-Leydig cell tumors o Well-differentiated o Moderately differentiated with heterologous elements o Poorly differentiated with heterologous elements o Retiform with heterologous elements ▪ Sex cord-stromal tumors, Not otherwise specified.

Benign tumors have been briefly described previously, some of the important malignant forms of the sex cord stromal tumors will be described below.

Ovarian fibrosarcomas are rare malignant tumors of the ovary, having a malignant clinical course demonstrating severe nuclear atypia and mitotic figures. They present as large unilateral masses with T1 and T2 diffuse hypointense signals showing variable degree of edema/cystic changes, necrosis and hemorrhage[48].

Steroid cell tumors are rare ovarian neoplasm arising from cells secreting steroid hormone, presenting commonly in 5^{th} and 6^{th} decade of life. They are further categorized into three types, Leydig cell tumor (from Leydig cells), stromal luteoma (from stromal cells), and steroid cell tumors not otherwise specified, when the lineage remains unknown[49,50]. Most of them are virilizing and also can be a rare cause of Cushing's syndrome[51]

They are usually small (with no significant ovarian enlargement), unilateral nodules (< 3 cm in size) that demonstrates T1 hyperintense signal due to excessive

intracellular lipids and avid post contrast enhancement due to its vascularity[50]. Rarely, they are seen as larger, solid, lobulated masses that alter the dimensions of the ovary[51].

Granulosa cell tumors of the ovary (GCT) are a part of the pure sex cord stromal tumors, accounting for less than 5% of all ovarian malignancies. It is the most common sex cord stromal tumor and is also known as the most common clinically estrogenic tumor[50].

They have been sub-classified into adult (95% of GCTs) and juvenile forms, however their gross appearance and radiological morphology remain the same and can be considered together. Juvenile granulosa cell tumors are sometimes associated with Olliers disease and Maffucci syndrome and forms a prime differential for an ovarian mass in young females with Olliers/Mafucci syndrome[51].

They usually present in the adolescent age group, with common occurrence at an age of 13 years and are rarely seen in women above 30 years of age. Due to its hyperestrogenic effect, they present in association with endometrial changes such as endometrial hyperplasia, polyps and carcinoma in 3-25% of cases[52].

On imaging, they present with a spectrum of features from solid or predominantly solid masses to completely cystic masses, with many of them showing multilocular cystic areas, hemorrhage, fibrotic changes. Unlike most epithelial tumors, they remain confined to the ovary at the time of diagnosis and rarely present with peritoneal deposits[50].

On CT and ultrasonography, they present as multilocular solid cystic masses with thick irregular septations. Calcifications are usually rare[51].Heterogenous, multilocular, sponge-like cystic mass on MRI with blood products are typical imaging appearance of GCTs. They are T1 heterogeneously hyperintense (due to hemorrhagic components) and T2 intermediate signal intensity lesion with multiple cystic spaces, giving a characteristic 'spongy appearance' (due to macrofollicular growth pattern). They lack intracystic papillary projections and show moderate post contrast enhancement[51,52,].

Unlike epithelial neoplasms, they present as low-grade tumors at the time of diagnosis, with rare incidences of peritoneal deposits and recurrence and hence carry an overall favorable prognosis[51].

*Sertoli-Leydig cell tumors***,** previously known as androblastomas /arrhenoblastomas, are tumors composed of a mixture of sertoli cells, leydig cells and fibroblasts. They are rare (< 0.5%) tumors but are the most common virilising tumor[51].

They are rare tumors in young women which often present with clinical manifestations of androgenic activity. They may be unilateral, solid/solid-cystic/cystic or papillary lesions and have a high recurrence rate. They are small solid hypoechoic masses on USG , are commonly are seen as solid enhancing masses with intralesional cystic areas on CT and as T1 hypointense lesions and T2 moderate intensity (based on amount of fibrous component) with T2 hyperintense cysts, thickened wall and

septae, solid components all of which show avid post contrast enhancement on MRI[50,53].

Ovarian metastasis

Metastasis to the ovaries constitute 10% of total ovarian malignancies. The most common primaries in decreasing order of frequency includes gastrointestinal, pancreatic, breast, and uterine tumors. Hematogenous, transperitoneal, lymphatic or direct tumor extension can all be modes of spread of the disease.

Ovarian metastasis are not so easily distinguishable from primaries, however features such as smaller size, bilaterality, more uniform locules and moderate to intense post contrast enhancement of solid areas favour diagnosis of metastasis over primary ovarian malignancy. Also, they are usually associated with lesser elevation of CA 125 & HE4 than with primary tumors[24,54].

Other rare histological varieties

Some of the rare varieties of ovarian tumors can represent lymphomas, leukemias, neuroectodermal tumors and carcinosarcomas.

Lymphomas of ovary are rare (< 2% of cases) and can be seen as unilateral/bilateral predominantly solid masses with avid post contrast enhancement and variable T2 signal intensity[55].

Carcinosarcomas, representing 1-4% of ovarian cancers, commonly present in the $6^{th}/7^{th}$ decade of life and clinically present with ascites and para-aortic

lymphadenopathy at the time of diagnosis. On imaging, they are large heterogenous T2 hyperintense and T1 hypointense lesions with laminar or stripe like post contrast enhancement pattern[56,57]

ROLE OF IMAGING IN OVARIAN MASSES

Role of Ultrasonography

Pelvic ultrasound forms the first line imaging modality for any suspected adnexal or ovarian mass with sensitivity of more than 90% and specificity of 51–97% for malignancy[58].

Most adnexal masses are benign and have typical sonological appearances which thus can aid in confident diagnosis of the lesion. A practical approach to its characterization on ultrasonography was provided by Douglas L. Brown wherein a four-point approach to diagnose masses was outlined – the extra-ovarian location, identifying it as one among the 5 common ovarian lesions (simple cyst, haemorrhagic cyst, corpus luteum, endometrioma and mature cystic teratoma), correlating with the patient's clinical history and differentiating between a complex-cystic and a solid mass[59].

Recognition of the normal ovary, distinctly from the suspected adnexal mass confirms the extra-ovarian nature of the lesion. Likewise, visualization of the ovarian follicles and normal ovarian stroma in its periphery, provides a clue that lesion is arising from the ovaries. However, the utility of these concepts is limited in large adnexal masses and in post-menopausal women in whom visualization of normal ovary or its follicles is difficult[59].

Morphologic scoring system on ultrasound, Risk of Malignancy Index (RMI scoring system) for discriminating benign from malignant ovarian masses was established that had a sensitivity of 100% and specificity of 83%. This is calculated with a simplified equation calculated from the product of menopausal status score (M), ultrasonographic score (U), and absolute value of serum CA-125 (s- CA-125)[60].

Table 4. Ultrasound criteria	
Multilocular cyst	1
Solid area	1
Bilateral lesions	1
Ascites	1
Intraabdominal metastasis	1
None of the above features	0
2 or more features	3

Table 5. Menopausal Status (M)	
Premenopausal	1
Postmenopausal	3

Ultrasound score (U)

- Score 0–1: U=1
- Score 2–5: U=3

s-CA-125 (u/ml) (the actual value is used)

A **RMI Score > 200**

highly suggestive of malignacy

'The International Ovarian Tumor Analysis (IOTA)' criteria has given some simple rules to categorise the lesions into three categories based on the morphological appearances as benign, malignant or indeterminate lesions as follows[58].

Table 6. Features of benignancy and malignancy based on IOTA scoring	
Benign features	• Simple unilocular cysts of any size • Smooth multilocular cyst with largest dimension < 100 mm • Cyst with solid component of maximum dimension less than 7 mm • Presence of posterior acoustic shadowing • No significant Doppler flow
Malignant features	• Irregular multilocular solid tumor with largest dimension > 100 mm • Irregular solid tumor • Presence of at least four papillary projections • Ascites • Strong Doppler flow in the solid component

Table 7. Criteria for assessing nature of lesion based on IOTA simple rules		
Malignant	Benign	Indeterminate
If one or more malignant features is present in the absence of any benign features, the lesion is malignant	If one or more benign features is present in the absence of any malignant features, the lesion is benign	If both benign and malignant features are present, the lesion is indeterminate

Although, ultrasound is a fundamental imaging modality for adnexal lesions and can be reasonably used to categorise them as benign or malignant, it has its limitations in staging the ovarian tumors, and has a low sensitivity of 69% in picking up intra-abdominal deposits. It is also operator dependent and the findings might get obscured in the presence of bowel shadows[60].

Role of Computed Tomography

Most often, the advanced stages of abdominal malignancies present with non-specific clinical findings, in which case the role of multidetector computed tomography (MDCT) becomes crucial in identifying occult abdominal malignancies including those arising from ovary, colon, stomach or pancreas[30].

Spiral CT as an imaging modality is widely available, easily performed, feasible and is less time consuming. Ability of CT to differentiate bowel from peritoneal deposits following oral contrast administration proves more advantageous than ultrasound or MRI[18].

CT provides adequate information of clinical relevance including size of the primary tumor, size and location of any peritoneal deposits, and the lymph node status. Hence becoming the imaging modality of choice for staging of ovarian malignancies and deciding on its resectability or cytoreduction[60].

Features suggestive of malignancy on CT include cysts with thick walls, septations, and papillary projections that are more apparent on post contrast images.

Presence of ancillary findings like gross ascites, peritoneal implants and lymphadenopathy increase the probability of malignancy[30].

Additionally, CT can also be used to look for persistent or recurrent ovarian tumors, monitor treatment response, and predict the outcome of cytoreductive surgeries in advanced ovarian carcinomas. Presence of peritoneal thickening, implants > 2 cm, mesenteric involvement, suprarenal para-aortic lymphadenopathy, pelvic side wall infiltration, hydroureter, involvement of diaphragmatic surfaces all indicate a poor surgical outcome. Thus, playing a significant role in reducing unnecessary surgical intervention[60].

There have been various studies assessing the accuracy of CT in predicting malignant nature of adnexal masses, maximum reported was found to be as high as 89%. However, it can easily overlook small peritoneal deposits. The sensitivity in diagnosing peritoneal implants > 1 cm is 85–93%, which significantly drops to about 25–50% when the size of the deposit is 1 cm or less[60].

Though CT is the preferred modality for women with advanced ovarian malignancy for its staging, recognition of peritoneal deposits and lymph node status, some studies still consider MRI as more effective in staging. There have not been sufficient data to prove its superiority over the use of MRI in assessing ovarian lesions[18].

Role of Magnetic Resonance Imaging (MRI)

MRI, as an imaging modality combines some of the best features of ultrasound and CT and is highly recommended for evaluation of masses found indeterminate on ultrasound or CT. The sensitive and specificity of contrast enhanced MRI in diagnosing malignancy is 100% and 94%, respectively. Therefore, this proves beneficial for those women with radiologically indeterminate mass posing low risk for malignancy[30].

MRI provides excellent soft tissue resolution, tissue characterization and is useful in assessing the internal architecture, especially following contrast administration. It not only is sensitive in diagnosing malignancies, but can also definitely confirm the benign nature of some adnexal lesions such as mature cystic teratomas, leiomyomas, endometrioma based on their MR imaging characteristics, which could otherwise have overlapping imaging features on other imaging modalities[18].

Features suggesting malignancy on MRI is comparable to those found on CT or ultrasound such as large size, complex masses containing solid and cystic components, cyst wall irregularity, septations, intramural nodules, papillary projections and early enhancement on dynamic contrast-enhanced MR images.

The overall accuracy in distinguishing malignant from benign ovarian lesions is as high as 83-91% for MRI with an accuracy for staging, comparable to that of CT as previously stated. MRI has sensitivity of 95%, specificity of 70%, and accuracy of 88% for predicting tumor resectability, as compared to 55%, 86%, and 63%, respectively, for CT[60].

It also has a good sensitivity and accuracy in looking for recurrent ovarian lesions. In those patients with raising s-CA 125 levels, and indeterminate imaging findings on CT or ultrasound, MRI has a reported sensitivity and accuracy of 84% and specificity of 100%[60]. Thus, contrast enhanced MR studies have become a problem solving tool especially in cases classified as indeterminate lesions on other imaging modalities, due to its excellent tissue characterization and soft tissue contrast, finally aiding in a comprehensive pre-operative assessment of ovarian masses.

Diffusion weighted imaging (DWI)

Diffusion weighted MRI, an in-vivo functional sequence works on the principle of Brownian motion and helps in noninvasive assessment of diffusion of water molecules at the microstructure level in biological tissues. This aids in comprehensive understanding of the cell organization, cellular density, altered cell membrane permeability, microstructure and microcirculation of water molecules and thus analyses the tissue character[61].

Assessment of restricted diffusion quantitatively, can be done by calculating the corresponding ADC values which are lower in malignant than benign lesions. Overlapping values might be noticed between some benign and malignant lesions, however these lesions are easily identifiable with the help of other conventional sequences as benign. High signal intensity with low ADC values is considered to be a useful criteria to predict malignancy[5].

Thus, diffusion weighted imaging augments the morphological details provided by the conventional MR sequences and when interpreted in combination with

conventional sequences, adds to the sensitivity and accuracy of MRI in differentiating benign from malignant ovarian/adnexal masses[61].

Role of Positron Emission Tomography/Computed Tomography (PET/CT)

The use of 18 FDG-PET imaging, has limited role in tissue characterization and is not routinely recommended for detection of primaries, however has found its place in treatment planning and follow up. A sensitivity of 52–58% and specificity of 76–78% have been recorded. False negative results have been recorded with borderline tumors and false positive results with hydrosalpinx, endometriosis, pedunculated fibroids and physiological gastrointestinal activity[30,60].

FDG-PET when combined with contrast enhanced CT, has proved beneficial in suspected recurrences or for tumor staging. Together it forms the most reliable method of detecting tumor recurrence with a sensitivity of 91% and specificity of 88%, a value higher than with CT or MRI alone. In addition, lack of tracer uptake in post treatment phase, reduces the false positive rates. Thus, FDG PET plays a major role in staging, treatment planning and follow up[30].

CLINICAL STUDIES

Emad-Eldin S et al, conducted a study in 2018 to evaluate the diagnostic potential of diffusion weighted imaging and dynamic contrast enhanced MRI in characterizing complex ovarian masses. They observed a significant difference in ADC values between benignancy & malignancy with a cut off of $0.95 \times 10^{-3} mm^2$ /s and also concluded that the addition of DWI and DCE MRI to conventional sequences improved the diagnostic value in characterizing complex ovarian masses[4].

A hospital based prospective observational study by Mittal M and Mannan N was performed to establish the relationship between ADC values of benign and malignant ovarian masses. They observed that, though there was some overlie in ADC values for benign and malignant lesions, the comprehensive average ADC values in the malignant lesions was lower than in benign ones and was statistically significant ($p < 0.001$). They also suggested an optimal cut off, of $\geq 1.23 \times 10^{-3} mm^2$ /s to discern benign and malignant ovarian masses and this cut off gave them a sensitivity of 82.4%, a specificity of 95.2%, a PPV 81.4%, and a NPV of 82.1%[9].

A study conducted in Mansoura University, Egypt on 30 women with complex cystic ovarian masses with 17 biopsy proven benign and 13 malignant masses found no statistical significance in ADC values obtained from solid components of benign and malignant masses. Also, the sensitivity of MRI was comparable to that of DWI (92.3%), however DWI showed higher specificity of 88.2% compared to conventional MRI sequences that was around 64.7% and hence concluded that addition of DWI to MRI can augment the specificity of imaging[8].

An article published in the World journal of surgical oncology establishes role of diffusion imaging in pre-operative characterization of ovarian masses in a group of 191 patients and stated that, detection of T2 hyperintensity in solid components of these masses with low ADC values (cut off of 1.2) proved to be effective in discriminating benign against malignant masses[5].

A meta-analysis by Yuan et al, that included 12 studies with 1142 lesions in total, acknowledged a pooled sensitivity of 86% and pooled specificity of 81% for diagnostic accuracy of DWI. They also observed that mean ADC value ranges from 0.8 to 2 mm^2/s for malignant and from 1.13 to 1.9 mm^2/s for benign lesions respectively. However, values for malignant lesions still remained lower than those seen in benign lesions. Hence concluded that DWI is an accurate non-invasive technique that can be adjunctive to conventional sequences in augmenting the diagnostic accuracy[62].

A case control study published in the internal journal of clinical and experimental medicine in 2015 acknowledged that both CT and DWI/MRI were of diagnostic value to distinguish benign from malignant masses, however DWI was contemplated to be more advanced than CT in terms of its specificity, sensitivity and diagnostic accuracy[63].

Another compressive meta-analyses based on 21 studies concluded that using DWI alone to interpret the nature of ovarian mass might have some pitfalls as some benign masses such as teratomas and endometriomas can exhibit lower ADC values as would be expected in malignant masses. This was reasoned due to the content in these lesion such as keratin deposits in teratomas and hemosiderin/blood products in

endometriomas. However, these lesions could be easily identified as benign on conventional sequences without the need for DWI. Similarly, there were a few malignant masses exhibiting high ADC values attributed to degree of necrosis/cystic areas. Hence concluding that combined approach is better than using either alone[64].

Kitajima K, et al, in their study had investigated the effectiveness of DWI in evaluating intrapelvic recurrence of gynecological malignancies and showed that a combination of T2 weighted imaging and DWI provided comprehensive assessment of recurrent gynecological malignancies[65].

A recent study published in 2020, stated that the average ADC values for ovarian, nodal and peritoneal malignancies was lower than that of benign masses, non-metastatic lymph nodes and benign peritoneal lesions. It was concluded that addition of DWI/ADC to routine MRI sequences improved quantitative and qualitative analysis of the ovarian masses, lymph nodes, and peritoneal deposits thereby contributing to diagnosis, staging and planning of treatment in ovarian malignancies[66].

MATERIALS AND METHODS

MATERIALS AND METHODS

Source of data:

This hospital based observational study was conducted over a period of 18 months from January 2019 to June 2020 on 32 patients who were referred for MR imaging of pelvis to Department of Radio-Diagnosis at R.L. Jalappa Hospital and Research Center attached to Sri Devaraj Urs Medical College, Tamaka, Kolar. Informed consent was taken from patients in the language understandable by them, for their willingness to participate in the study.

Study design: Hospital based observational study.

Sample size: A sample size of 30 patients was selected using n masters' software. Sample size estimated by using the proportion of subjects with benign and malignant ovarian masses detected by DWI from the study by Mittal M, et al[9] using the formula

$$\text{Sample size} = \frac{Z_{1-\alpha/2}{}^2\, p(1-p)}{d^2}$$

Here

Z1-α/2 = 1.96 at 5% alpha error. Since in majority of studies, p values below 0.05 is considered significant, 1.96 is used in formula.

p = Expected proportion in population based on previous studies or pilot studies.

d = Absolute error or precision – Has to be decided by researcher.

p = 0.82

1 – p = 0.18

d = 14%

Considering 10% non-responsiveness, an estimation of a sample size of $27 + 2.7 \approx 30$ was done for the study. A total of 32 patients with ovarian masses were included in the final analysis. The patients were involved in the study if they fulfilled the inclusion/exclusion criteria listed below:

Inclusion Criteria:

- All patients with clinically suspected pelvic mass / sonographically diagnosed ovarian mass referred for MRI.

Exclusion criteria:

- Patients with congenital uterine anomalies.
- Ovarian torsion.
- All patients having cardiac pacemakers, prosthetic heart valves and cochlear implants.
- Claustrophobic patients.

Method of collection of data:

Informed consent was taken. Baseline information of the patients participating in the study were recorded along with pertinent clinical history and relevant lab investigations.

MRI of pelvis was performed on patients fulfilling the inclusion/exclusion criteria on 1.5 Tesla, 18 channel, MR Scanner (Siemens® Magnetom Avanto®).

Sequences used for MRI

The patients were positioned supine and following sequences were performed:

Conventional sequences include:

1. Sagittal and axial T1-weighted fast spin echo,
2. Sagittal, axial and coronal T2-weighted fast spin echo,
3. Sagittal and Coronal Short Tau Inversion Recovery (STIR),
4. Gradient Echo sequence (GRE)
5. T1 Fat Saturated sequence (T1FS)

Advanced sequences:

1. Single-shot echo-planner diffusion weighted image was acquired in axial plane with b values of 50, 400 and 800 s/mm ^{2}.
2. Corresponding ADC maps were obtained to calculate the ADC values.

Patients with normal renal function, underwent contrast study as and when required.

Data analysis:

The following morphological parameters were assessed on MRI:

i. Size of the lesion
ii. Morphology of the lesion, in terms of presence of solid components, fat content, internal septations and hemorrhagic areas.
iii. Papillary projections
iv. Regional lymphadenopathy and
v. Presence of ascites, peritoneal deposits and regional metastasis.

Figure 12: Siemens Magnetom Avanto® 1.5 T MRI scanner.

Placement of ROI and calculation of ADC

Diffusion weighted images were obtained using the b values of 50, 400 and 800 s/mm². The ADC maps were reconstructed from diffusion weighted images using plugin of ADC map calculation version 2.3 in OsiriX MD version 2.7 of 64-bit DICOM viewer software.

The ROIs were positioned in the sections of ovarian lesions so as to include maximum area of restricted diffusion in solid components, to calculate the ADC values. In order to ensure standardization, the largest possible regions of interest (ROIs) were manually placed and varied from 15 to 150 mm^2. In some cases, that showed irregular/heterogenous solid components and multiple vegetations, 2 to 3 ROIs were placed and the average of those values was utilized for statistical analysis.

In predominantly cystic ovarian masses, the ROIs were placed in areas of tissue homogeneity, away from the septations or wall of the lesion. The ADC values obtained were used for statistical analysis.

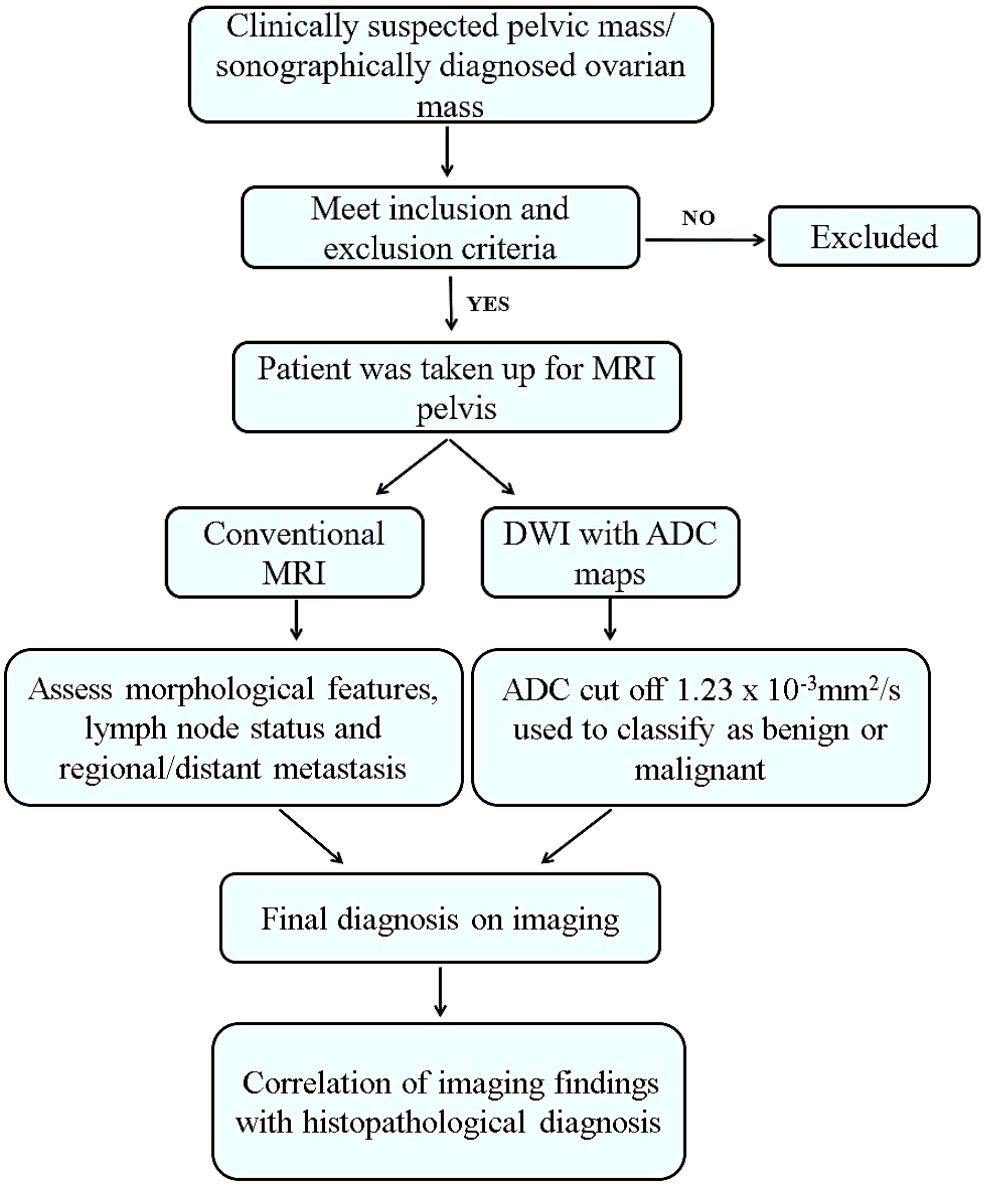

Figure 13: Schematic representation of the study design

Statistical analysis

The statistical data analysis was done using the SPSS 22.0 for windows and Microsoft Excel 2010 program. The ordinal and categorical variables between them were interpreted by Chi- square (χ^2) test. The t-test was used for the comparison of the mean ADC values. *P* value less than 0.05 ($p < 0.05$) was considered as statistically significant.

The sensitivity, specificity, diagnostic accuracy, positive predictive value (PPV) & negative predictive value (NPV) for conventional MRI & DWI/ADC values for characterising benign and malignant ovarian lesions was computed individually and compared with values obtained when both were interpreted together. The final imaging diagnosis was compared with the histopathological diagnosis, which is considered gold standard.

RESULTS

RESULTS

The study included 32 ovarian lesions, belonging to varying age groups. Mean age of presentation in this study was 49.81 ± 4.46 years (Mean ± SD) with a range of 23-70 years.

Age group distribution

Table 8: Age group distribution.

Age in years	Number of cases	Percentage (%)
≤ 19	0	0
20-29	4	13
30-39	2	6
40-49	10	31
50-59	5	16
60-69	10	31
≥ 70	1	3
TOTAL	**32**	**100**

Patients were classified into 7 groups, each of 10 years age interval, ranging from under 19 years to more than 70 years as represented in Table 8. Two of these age groups accounted for majority of the study population (62%) i.e. 40-49 years (n=10; 31%) and 60-69 years (n=10;31%) thus sharing a common highest age distribution. There was a single case of 70-year-old woman presenting with ovarian mass and no cases were recorded in females of age less than 19 years.

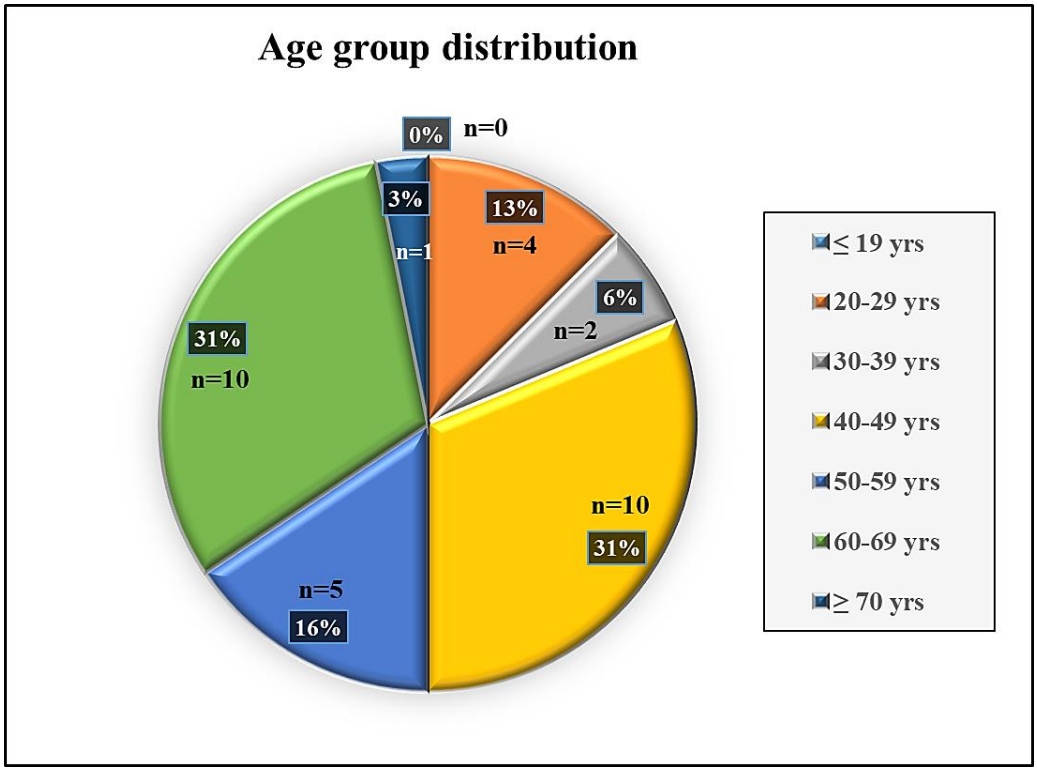

Figure 14: Age group distribution

There was no statistical significance in the mean age of presentation, which in our study was 48.7 ± 13.89 years (mean ± SD) for benign and 51.38 ± 11.69 years (mean ± SD) for malignant ovarian masses, with a *p* value of .582 ($p > 0.05$; not significant).

Table 9: Average age for types of ovarian mass

Types of ovarian mass	**Average age (in years) ± SD**	***P* value**
Benign	51.38 ± 11.69 years	*P* = **.582** (> 0.05)
Malignant	48.7 ± 13.89 years	Insignificant

Distribution based on menstrual status of patients

Table 10: Distribution based on menstrual status of patients

Menstrual status of patient	Number of patients (n)	Percentage (%)
Premenopausal	12	37
Post-menopausal	20	63
Total	**32**	**100**

A good number of patients i.e. n=20, forming 63% of the study population, were belonging to the post-menopausal age group while only 12 females were of pre-menopausal age group, accounting for 37% of the population.

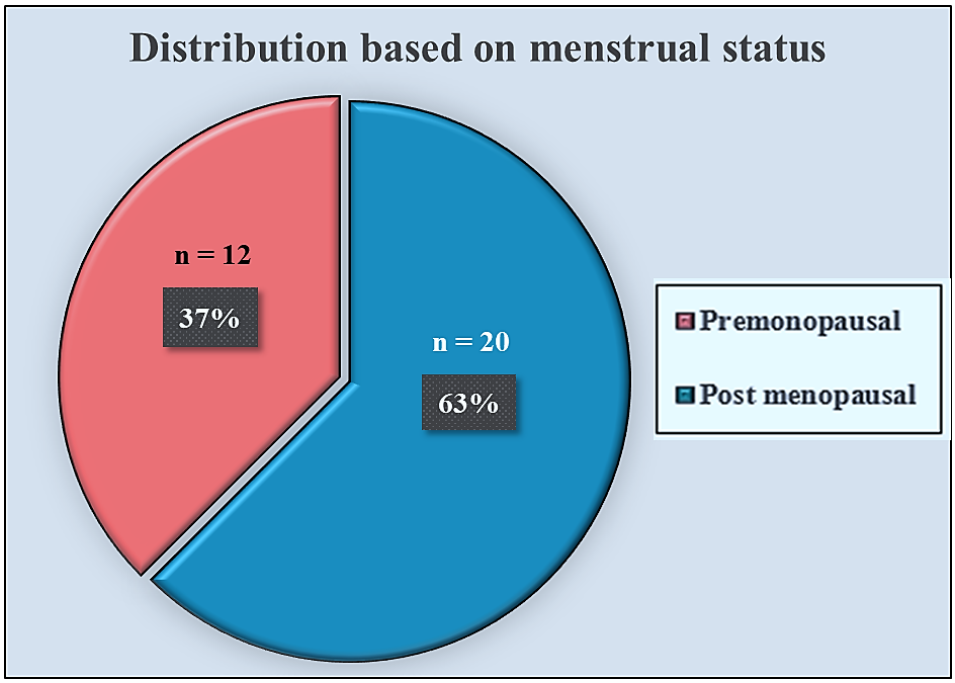

Figure 15: Distribution based on menstrual status

Distribution of lesions based on menstrual status

Table 11: Distribution of lesions based on menstrual status

Menstrual status of patient	Types of lesion			Percentage (%)	
	Benign	Malignant	Total	Benign	Malignant
Premenopausal	7	5	**12**	58.3%	41.6%
Postmenopausal	12	8	**20**	60%	40%
***P* = .95; not significant**					

In women, belonging to premenopausal age group (n=12), 7 out of the 12 ovarian masses were benign (58.3%) and remaining 5 were malignant (41.6%). Likewise, among those who attained menopause (n=20), 12 masses were benign (60%) and 8 of them were diagnosed malignant on histopathology (40%) as demonstrated in the Table 11.

In this study, we noticed that the menstrual status of the patient was not a significant risk factor for development of ovarian malignancies with a *p* value of .95 ($p > 0.05$; insignificant).

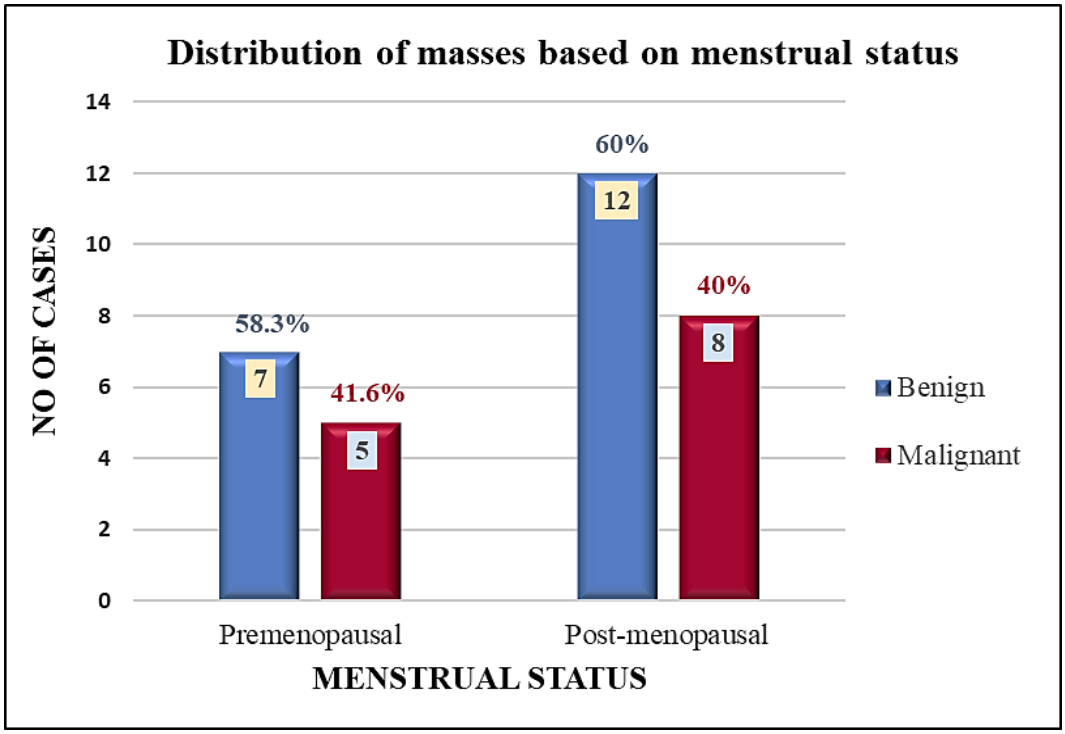

Figure 16: Distribution of masses based on menstrual status

Distribution based on clinical symptoms at the time of presentation

Table 12: Distribution of clinical symptoms at the time of presentation

Clinical symptoms	No of cases	Percentage (%)
Pain abdomen	16	50
Mass per abdomen	8	25
Abdominal distension	4	12.5
Pain abdomen & Distension	2	6.3
Pain abdomen and mass per abdomen	1	3.1
Irregular cycles	1	3.1

Most commonly encountered clinical symptom in this study was pain abdomen (n=16;50%) followed by mass per abdomen (n=8;25%) and abdominal distension

(n=4;12.5%). There were three cases presenting with combinations of the above symptoms and only 1 woman presented with irregular cycles.

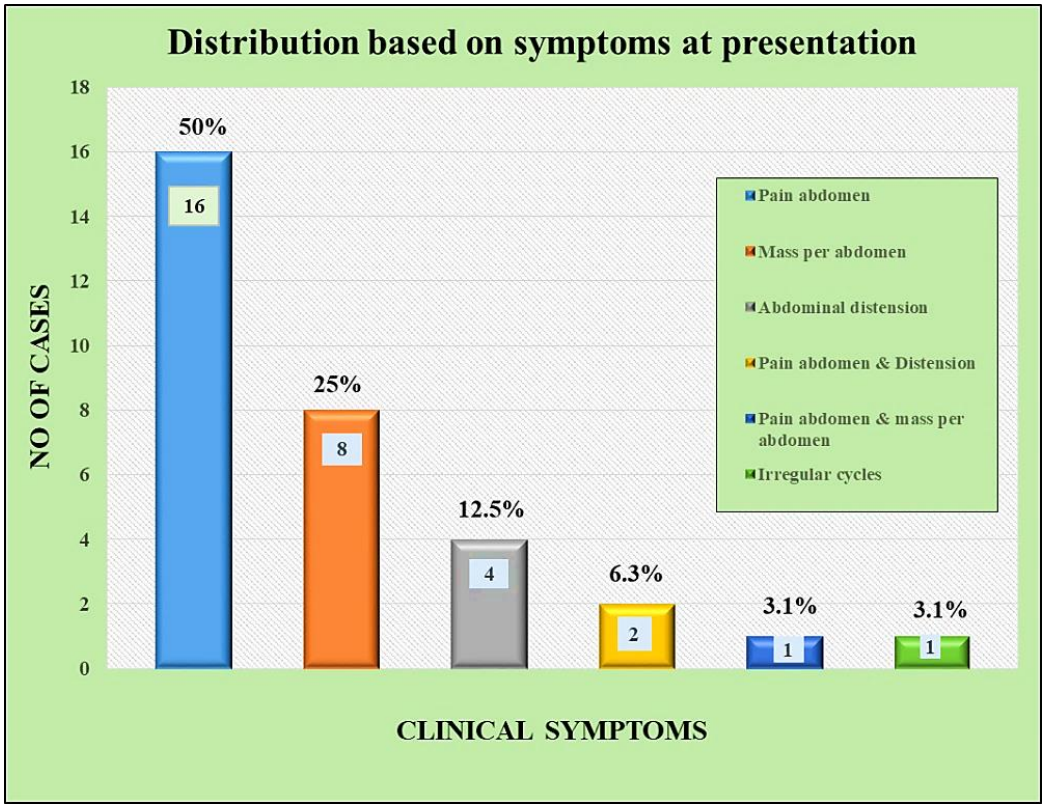

Figure 17: Distribution based on symptoms at presentation

Histopathological distribution

Based on the histopathological diagnosis, 19 of the ovarian masses (59%) were proven benign and 13 of them (41%) were malignant, thus having a small majority of benign ovarian masses in our study group.

Table 13: Histopathological distribution

Histopathological type	No of ovarian masses	Percentage (%)
Benign	19	59
Malignant	13	41

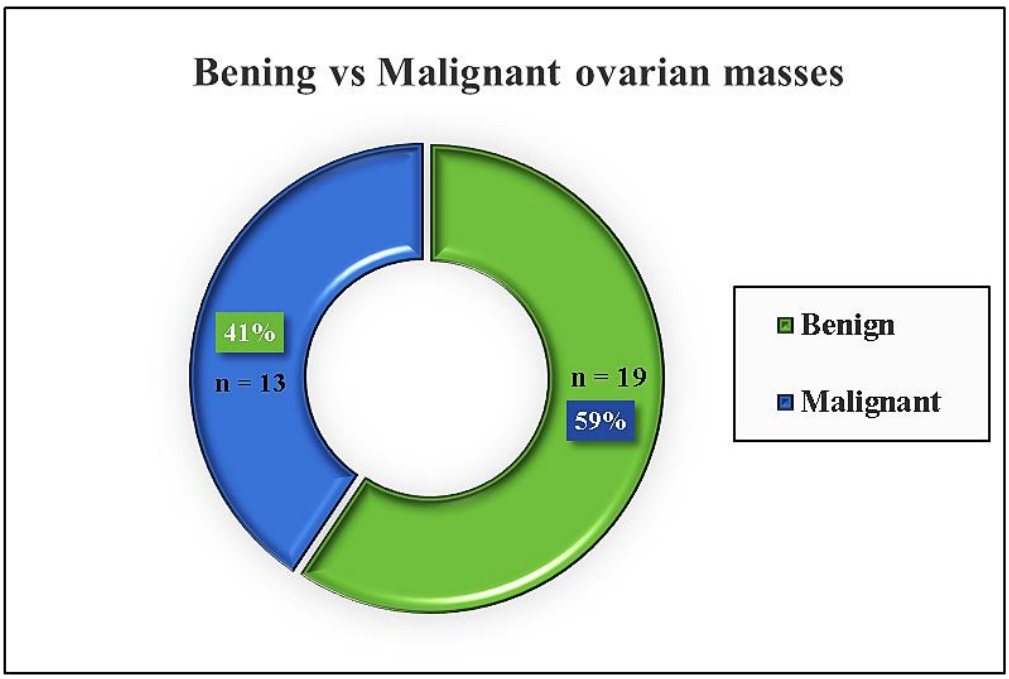

Figure 18: Histopathological distribution

Histopathological types of benign ovarian masses

Table 14: Histopathological types of benign ovarian masses

Histopathological type	No of cases (n)	Percentage (%)
Serous cystadenoma	4	21
Mucinous cystadenoma	6	32
Seromucinous cystadenoma	1	5
Mature teratoma	5	26
Endometrioma	1	5
Simple cyst	1	5
Haemorrhagic cyst	1	5

Most common benign ovarian mass identified here was mucinous cystadenoma (n=6;32%), followed by mature teratoma (n=5;26%) and serous cystadenoma (n=4;21%). Single cases each of seromucinous cystadenoma, endometrioma, simple cyst and haemorrhagic cyst were also present.

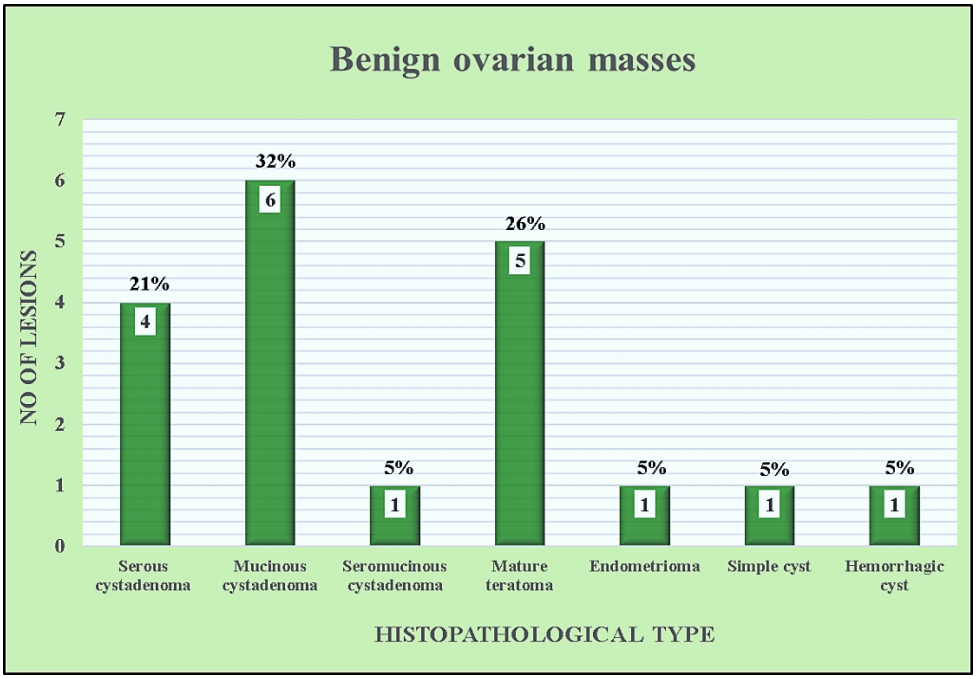

Figure 19: Histopathological types of benign ovarian masses

Histopathological types of malignant ovarian masses

Table 15: Histopathological types of malignant ovarian masses

Histopathological type	No of cases (n)	Percentage (%)
Serous cystadenocarcinoma	9	70
Mucinous cystadenocarcinoma	3	23
Granulosa cell tumour	1	7

Most commonly identified malignant ovarian mass was serous cystadenocarcinoma of the ovary (n=9;70%) followed by mucinous cystadenocarcinoma (n=3;23%) and a single case of granulosa cell tumour. One case of mucinous cystadenocarcinoma and two cases of serous cystadenocarcinomas presented with peritoneal deposits. None of the cases showed regional lymph node metastasis or distant metastasis in our study.

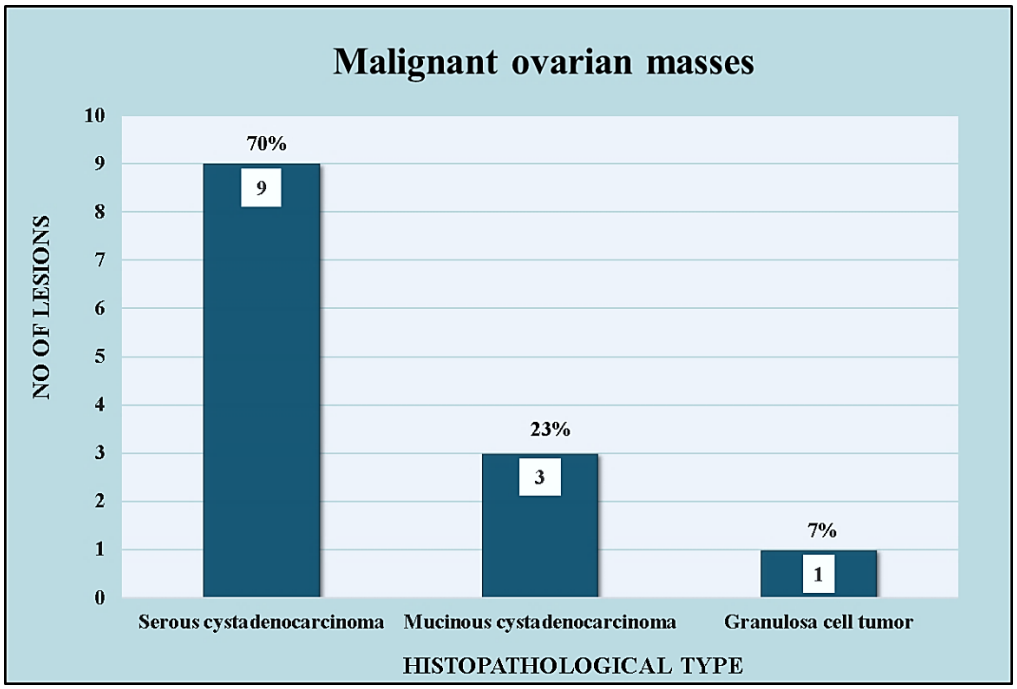

Figure 20: Histopathological types of malignant ovarian masses

Correlation between Conventional MRI and Histopathological diagnosis

Based on the imaging findings on conventional MRI, these 32 ovarian masses were categorised into benign (n=16;50%) and malignant (n=16;50%) masses. Following surgery, they were subjected for histopathological examination which identified 19 benign and 13 malignant ovarian masses.

Table 16: Correlation between Conventional MRI and Histopathological diagnosis

Modality	Benign	Malignant
Conventional MRI	16	16
Histopathological findings	19	13

Table 17: Analysis of the diagnosis on Conventional MRI

Parameters	Conventional MRI
Sensitivity	100%
Specificity	84.2%
Accuracy	90.6%
PPV	81.25%
NPV	100%

All the malignant ovarian masses were accurately picked up as malignancies with conventional sequences of MRI, thus resulting in a sensitivity and negative predictive value of 100% each. However, there were 3 cases of pathologically proven benign masses that were over-diagnosed as malignant on conventional MR imaging. With these findings, the specificity for conventional sequences was found to be 84.2%, and overall diagnostic accuracy was 90.6%. It was also observed that, this modality had a PPV of 81.25%, which implies that in 18.75% of the times, the malignancies can be missed on conventional MR imaging.

Distribution based on pattern of diffusion

There were 24 ovarian masses (75%) demonstrating restricted diffusion while the remaining 8 (25%) of them showed free diffusion with no significant restricting solid components within.

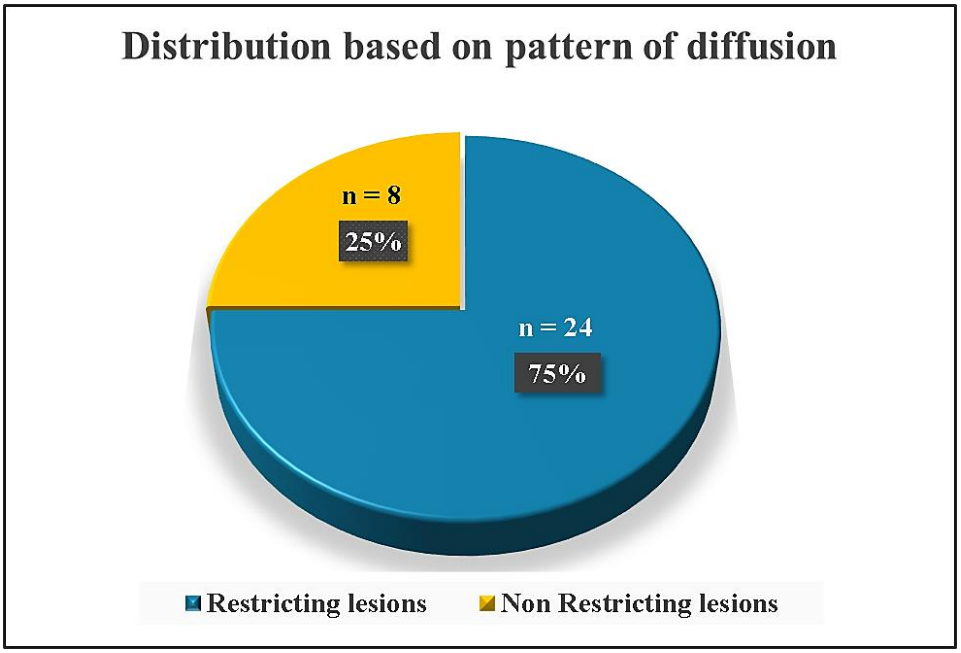

Figure 21: Patterns of diffusion

Correlation between DWI/ADC and HPE diagnosis

Among the 32 ovarian masses, 15 (46.8%) of them demonstrated an ADC value > 1.23 x $10^{-3}$$mm^2$/s, suggesting a benign value and the remaining 17 (53.1%) of them had values < 1.23 x 10^{-3} mm^2/s, suggesting that the masses were malignant.

Table 18: Correlation between DWI/ADC and HPE diagnosis

Modality	Benign	Malignant
DWI/ADC*	15	17
HPE	19	13

DWI/ADC – Diffusion weighted Imaging/Apparent diffusion coefficient

HPE - Histopathological Examination

* ADC value < 1.23 x 10^{-3} mm^2/s was considered malignant & > 1.23 x 10^{-3} mm^2/s as benign.

Totally, there were 17 masses with low ADC values (i.e. ADC < 1.23 x $10^{-3}$$mm^2$/s), out of which 13 cases were proven as malignant on histopathology and thus were correctly diagnosed on DWI/ADC. However, there were 4 benign ovarian masses which were incorrectly diagnosed to be malignant based on the DWI/ADC findings.

The overall mean ADC value for all the 32 ovarian masses included in our study was 1.36 ± 0.705 x $10^{-3}$$mm^2$/s. The mean value for ADC in benign ovarian masses (n=19) was 1.73 ± 0.66 x $10^{-3}$$mm^2$/s, and that for malignant ovarian masses (n=13) was 0.786 ± 0.21 x 10^{-3} mm^2/s with a statistical significance of < 0.001 (i.e. $p < 0.05$; significant).

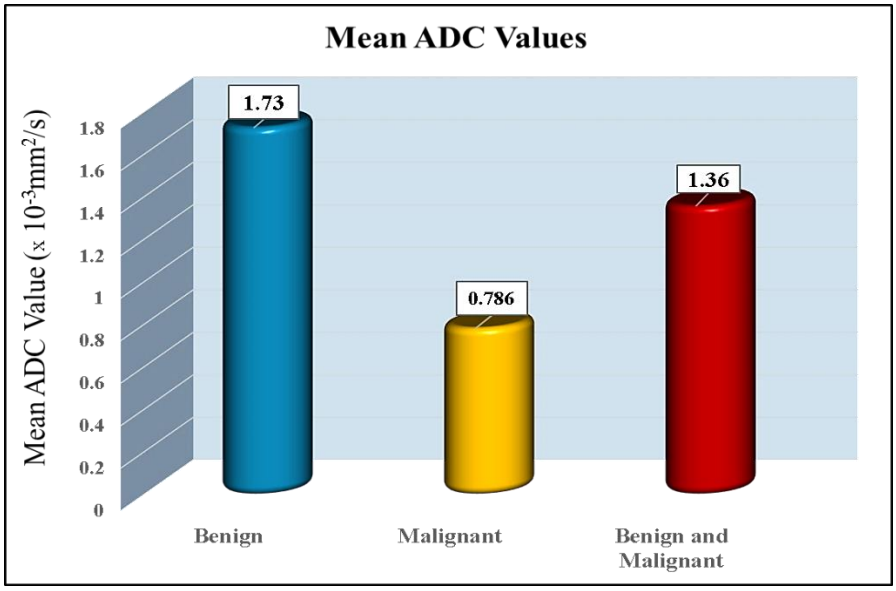

Figure 22: Mean ADC values

Table 19: Analysis of the diagnosis on DWI/ADC

Parameters	DWI/ADC
Sensitivity	100%
Specificity	78.9%
Accuracy	87%
PPV	76.47%
NPV	100%

All the malignant ovarian masses were correctly diagnosed with ADC values < 1.23 x 10^{-3} mm^2/s, thus sensitivity and negative predictive value for DWI/ADC remains a perfect score of 100%. The specificity of this test was 78.9% and had an overall diagnostic accuracy of 87%. This was found to be lower than what was previously seen with conventional MRI sequences. DWI/ADC when used independently, can successfully predict the malignancy in only 76.47% of the cases (i.e. PPV = 76.47%).

Correlation between combined MRI and DWI/ADC diagnosis with HPE diagnosis

Table 20: Correlation between combined MRI and DWI/ADC interpretation with HPE diagnosis

	Benign	Malignant
MRI and DWI/ADC	18	14
HPE	19	13

MRI - Magnetic Resonance Imaging

DWI/ADC – Diffusion weighted Imaging/Apparent diffusion coefficient

HPE - Histopathological Examination

When findings of both conventional MRI sequences and DWI/ADC were interpreted together, all histopathology proven ovarian malignancies as expected were correctly diagnosed to be malignant and thus there were no false negative cases. There was only one false positive result with this approach. On statistical analysis of this data, the following results were obtained.

Table 21: Analysis of the combined MRI and DWI/ADC diagnosis.

Parameters	Combined MRI with DWI/ADC
Sensitivity	100%
Specificity	94.7%
Accuracy	96.88%
PPV	92.86%
NPV	100%

The specificity, diagnostic accuracy and positive predictive values of using combined MRI and DWI/ADC for image interpretation were calculated and was found to be 94.7%, 96.88% and 92.86% respectively. The sensitivity and negative predictive value remains 100 % each.

Comparative analysis for diagnosis on MRI, DWI/ADC and combined MRI with DWI/ADC

Table 22: Comparative analysis for diagnosis on MRI, DWI/ADC and combined MRI with DWI/ADC

Parameters	Conventional MRI	DWI/ADC	Combined MRI with DWI/ADC
Sensitivity	100%	100%	100%
Specificity	84.2%	78.9%	94.7%
Accuracy	90.6%	87%	96.88%
PPV	81.25%	76.47%	92.86%
NPV	100%	100%	100%

On comparing the above statistical parameters for conventional MRI, DWI/ADC and combined use of MRI with DWI/ADC for diagnostic evaluation of ovarian masses, the following observations were made. Conventional MRI showed a good diagnostic accuracy of 90.6%, specificity of 84.2% and a PPV of 81.25%. When only DWI/ADC was used for image interpretation with an ADC cut off of 1.23 x $10^{-3}$$mm^2$/s to classify ovarian masses as benign or malignant, the diagnostic accuracy, specificity, and PPV was lowered to 87%, 78.9% and 76.47% respectively.

This was because of the fact that, there were 4 benign ovarian masses, which had ADC values >1.23 x $10^{-3}mm^2/s$, thus reducing the specificity and the overall diagnostic accuracy. However, when conventional sequences and DWI/ADC were combined for assessment of ovarian masses, there was an increase in the specificity from 84.2% to 94.7%, diagnostic accuracy from 90.6% to 96.88% and PPV from 81.25% to 92.86%, which indirectly implies, that the chances of missing a malignancy with this method of image interpretation is reduced further.

IMAGES

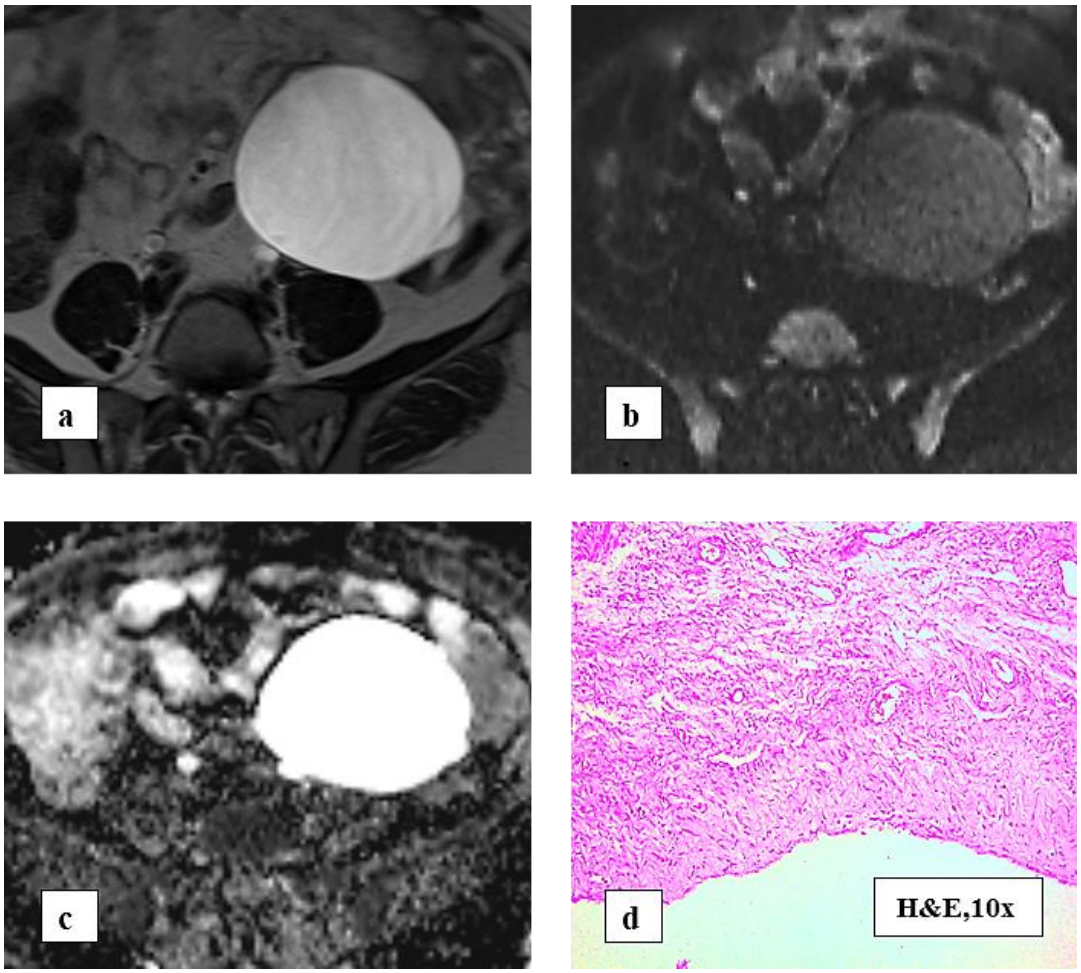

Figure 23: MRI pelvis in 35-year-old lady with left ovarian simple cyst. There is a well-defined ovoid left adnexal cyst with uniform T2 hyperintense signal and no solid components/septations (a). There is no restriction of diffusion on DWI/ADC with an ADC value of 2.3 x $10^{-3}mm^2/s$ (b & c). The left ovary was not seen separately from the mass. Microphotograph shows fibrocollagenous cyst wall lined by flat benign cells (d).

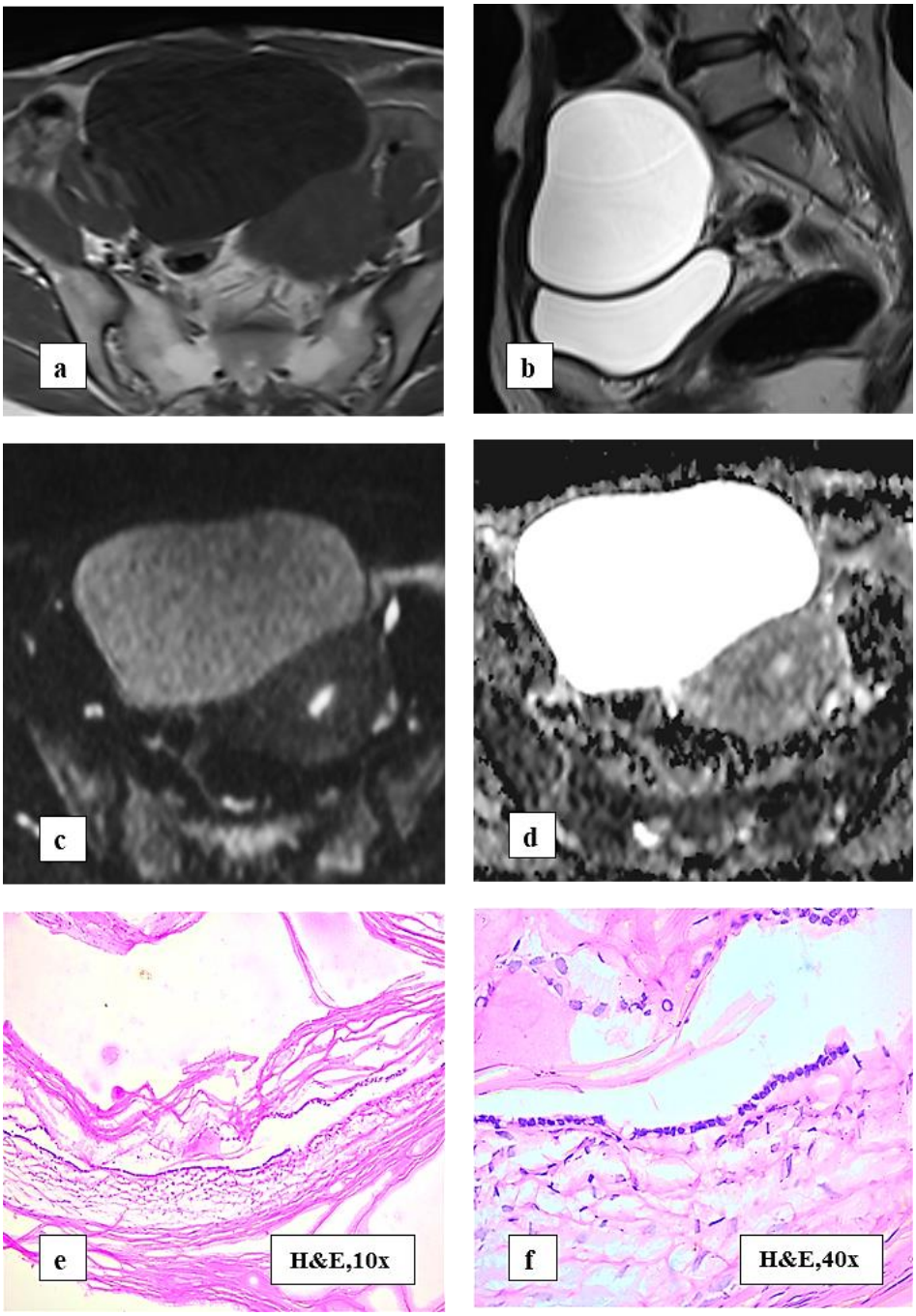

Figure 24: MRI Pelvis in a lady aged 45 years shows right ovarian serous cystadenoma. Axial T1WI reveals a well-defined hypointense right adnexal lesion (a) with uniform hyperintense signal on sagittal T2WI (b). It demonstrates free diffusion on DWI/ADC (c & d) with ADC value of 3.0 x $10^{-3}mm^2/s$. No septations/solid components/papillary projections seen within the lesion. Microphotographs (e & f) shows fibrocollagenous cyst wall lined by cuboidal/low columnar cells.

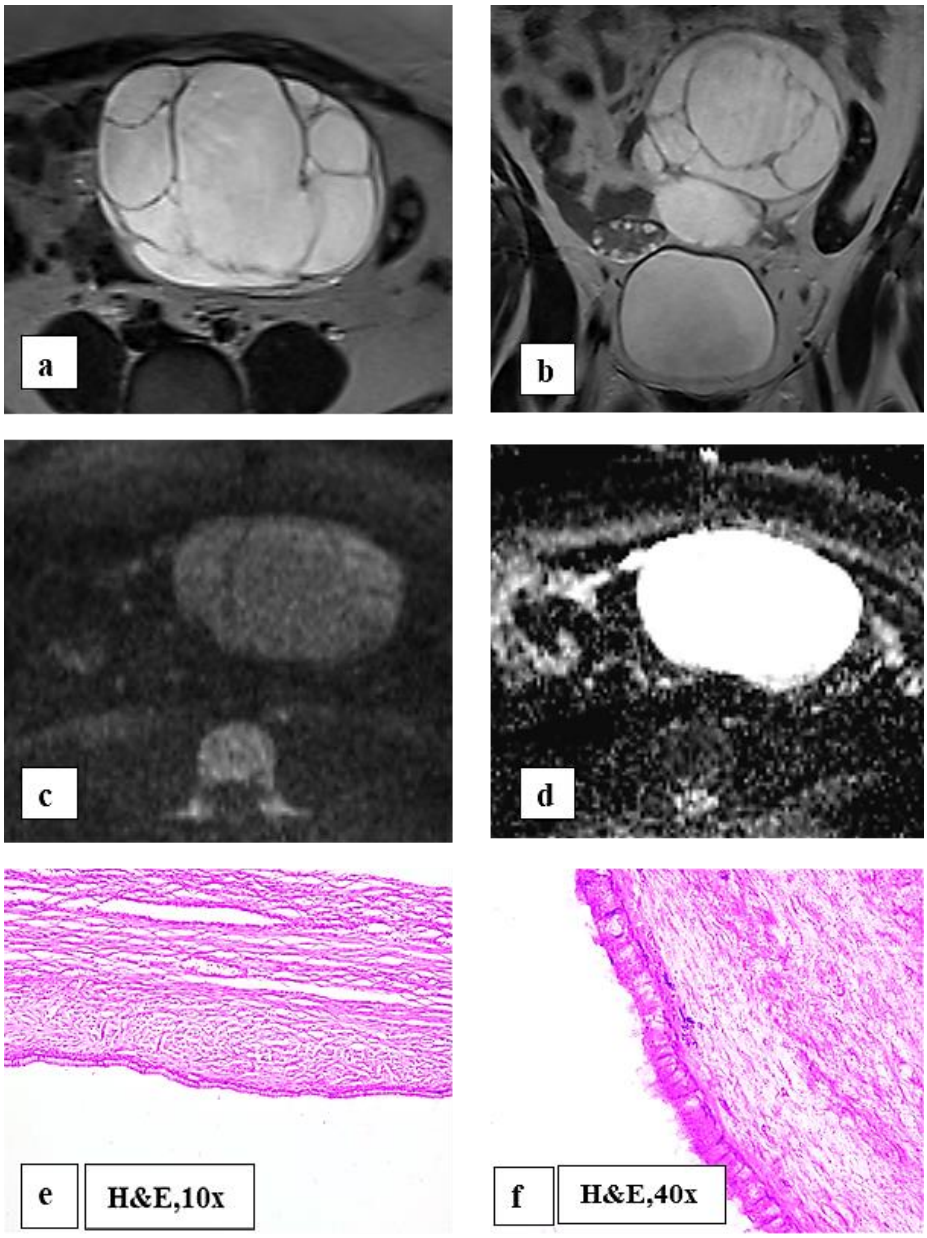

Figure 25: MRI Pelvis in a 29 year old women shows a well defined multiloculated cystic lesion in left adnexa with hyperintense signal intensity as seen in T2 axial and coronal images (a & b) with intervening hypointense septae (~ 2.6 mm). Left ovary is not seen separately. Right ovary appears normal (b). DWI/ADC images show no restricted diffusion with an ADC value of 1.7 x $10^{-3}$$mm^2$/s (d & e). Microphotographs shows fibrocollagenous cyst wall lined by mucinous columnar cells (e & f).

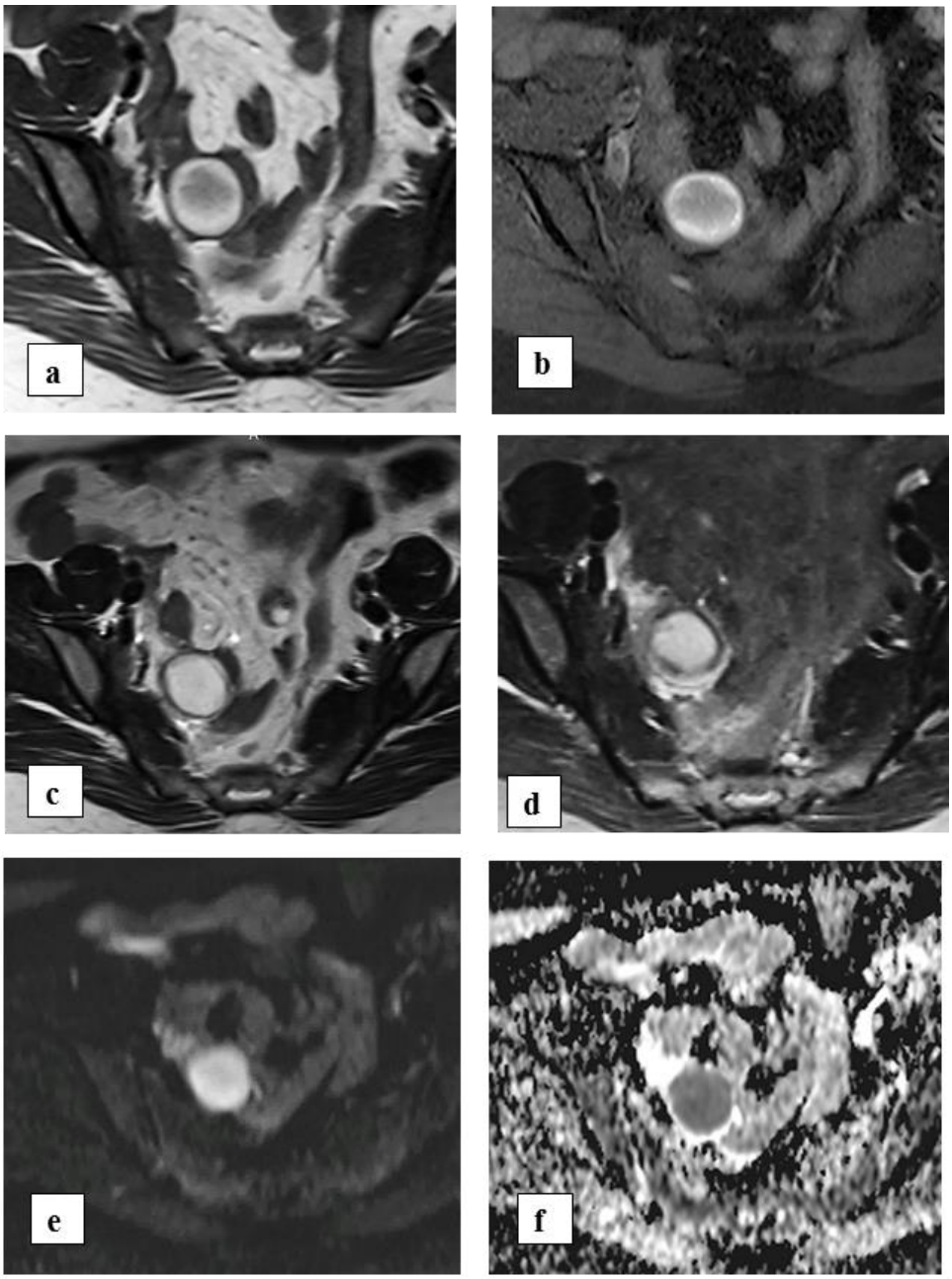

Figure 26: MRI of 55-year-old lady presenting with pelvic pain shows right ovarian hemorrhagic cyst. Well defined, round ovarian mass with T1 hyperintense signal (a) that does not suppress on T1FS (b) and shows hyperintense signal on T2 (c) & STIR images (d). It demonstrates restricted diffusion on DWI (e & f) with ADC value of 0.9 x 10^{-3} mm^2/s.

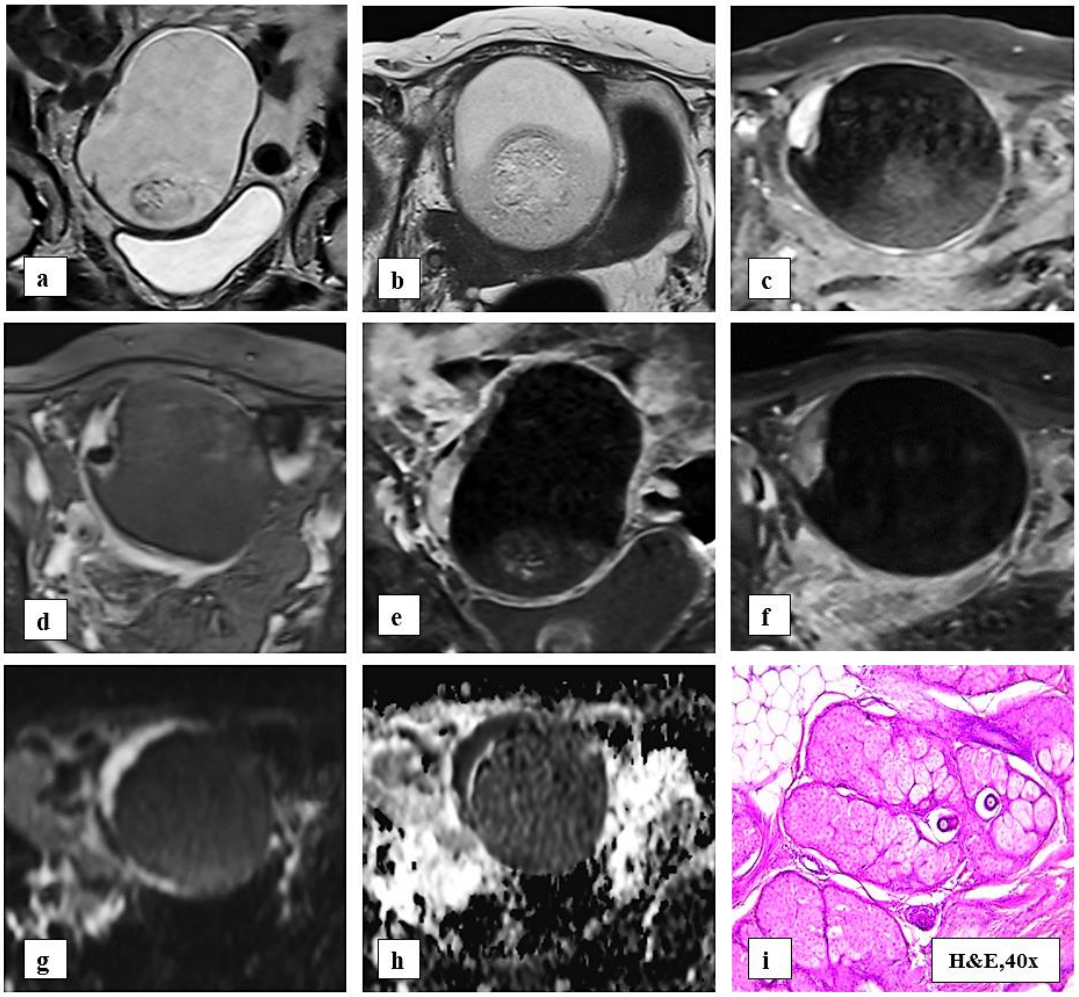

Figure 27: MRI Pelvis in 60-year-old women shows large left ovarian mature teratoma. T2 coronal image (a) shows a well-defined, ovoid mass with intermediate signal intensity. T1 axial image (b) demonstrates fat fluid level seen as hypointense fluid in dependent portion and hyperintense fat above, with fat suppression on T1FS (c). Peripheral blooming seen on GRE (d), representing calcification. The lesion shows heterogenous enhancement of solid components and cyst wall as shown on TIFS coronal & axial post contrast images (e & f) and peripheral areas of restriction on DWI/ADC images (g & h) with ADC value of 1.1 x 10^{-3} mm^2/s. Microphotograph shows benign sebaceous glands with hair follicle and chondroid tissue consistent with mature teratoma (i).

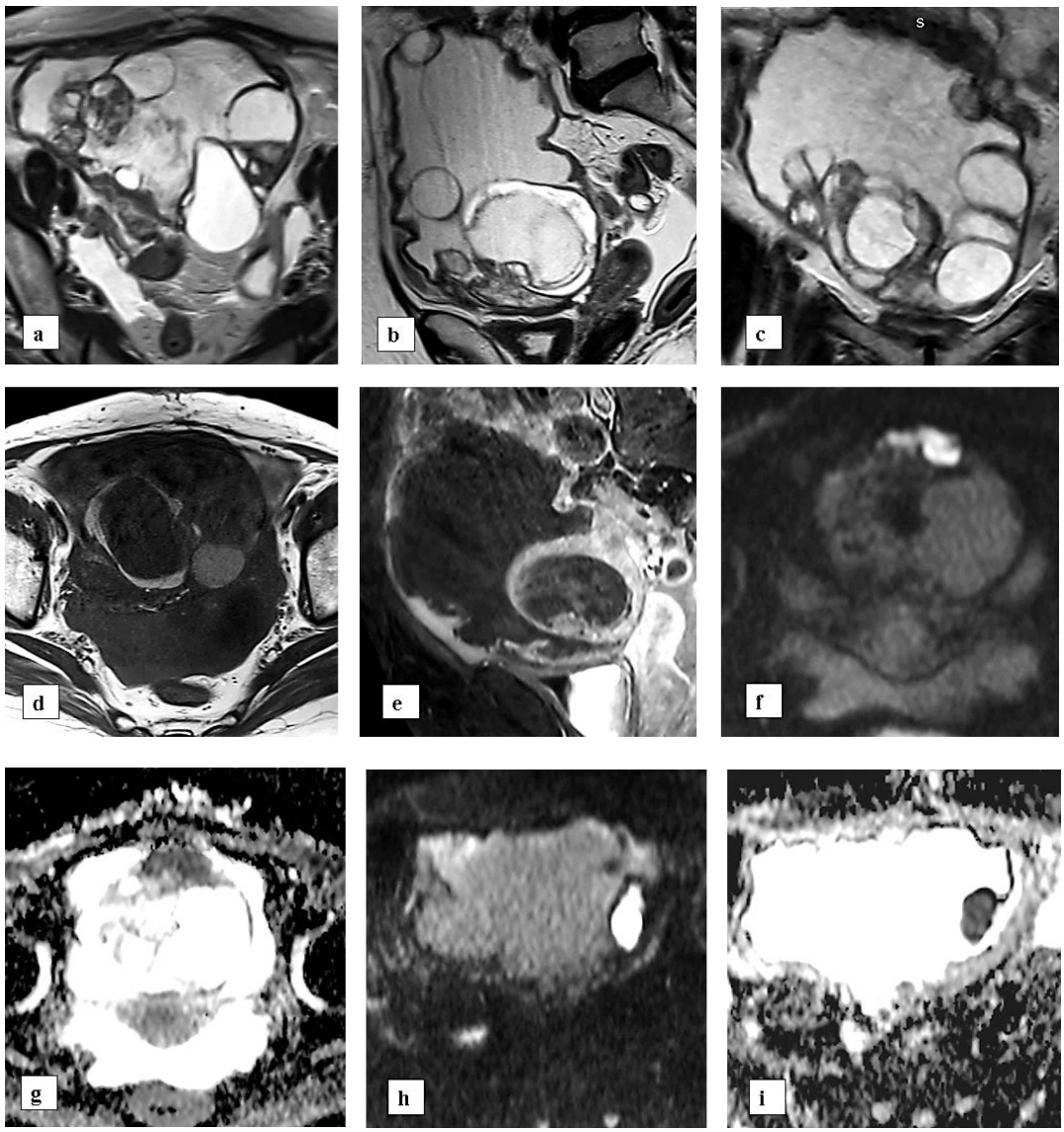

Figure 28: MRI Pelvis in 65-year-old lady shows benign seromucinous cystadenoma of right ovary. T2 axial, sagittal & coronal images (a,b,c) shows a heterogenous solid cystic pelvo-abdominal mass with T2 hyperintense signal intensity. Areas of T1 hyperintense signals also noted on T1 axial section (d). T1 post contrast sagittal image shows heterogenous enhancement of walls and solid components (e). Multiple patches of restricted diffusion seen with ADC value of 1.38 x $10^{-3}mm^2/s$ on DWI/ADC images (f,g,h,i).

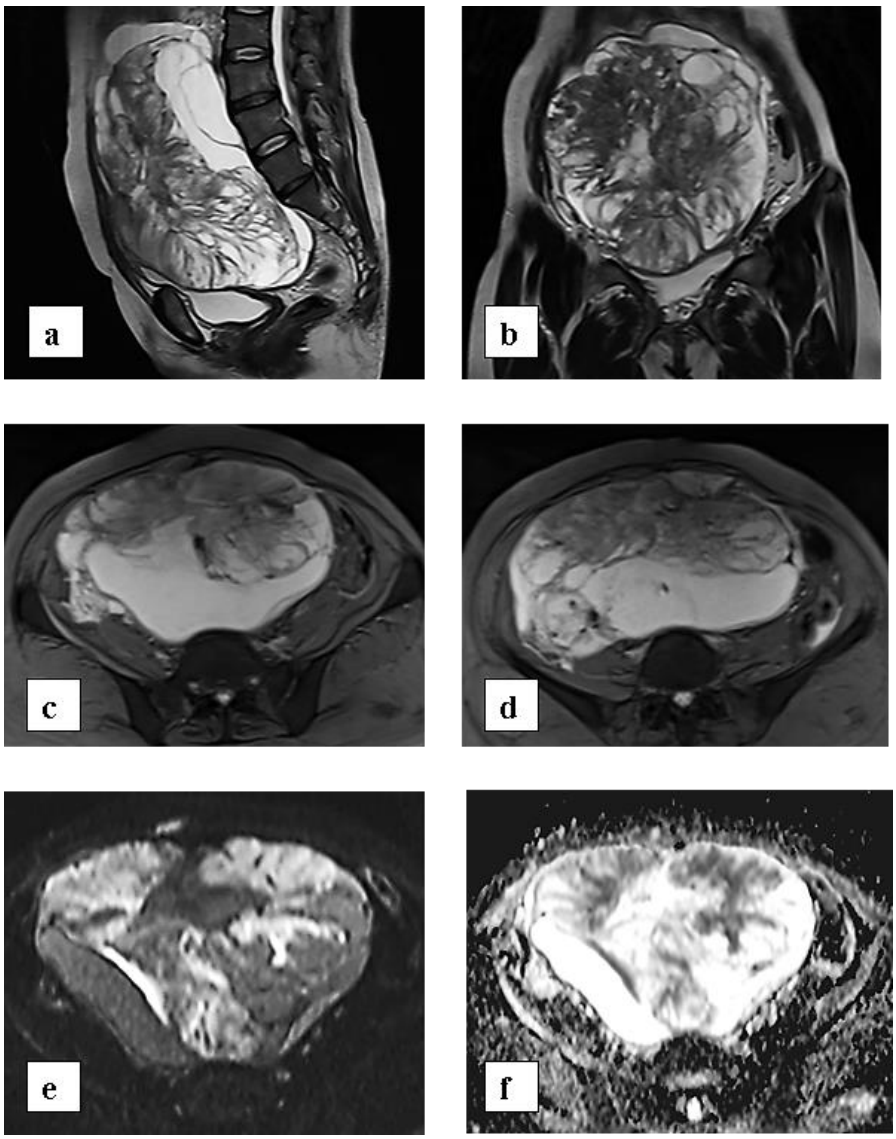

Figure 29: Pelvic MRI in 60 year old lady presenting with abdominal distention shows large pelvo-adominal solid cystic mass in midline with thick septations (~ 4 mm) on T2 sagittal and coronal images (a & b).Few intratumoral blooming foci suggesting areas of intratumoral hemorrhage seen on GRE (c & d). Solid components show patchy areas of restricted diffusion on DWI and corresponding ADC image (e & f) with ADC value of 0.8 x 10^{-3} mm^2/s . This was a case of right ovarian serous cystadenocarcinoma.

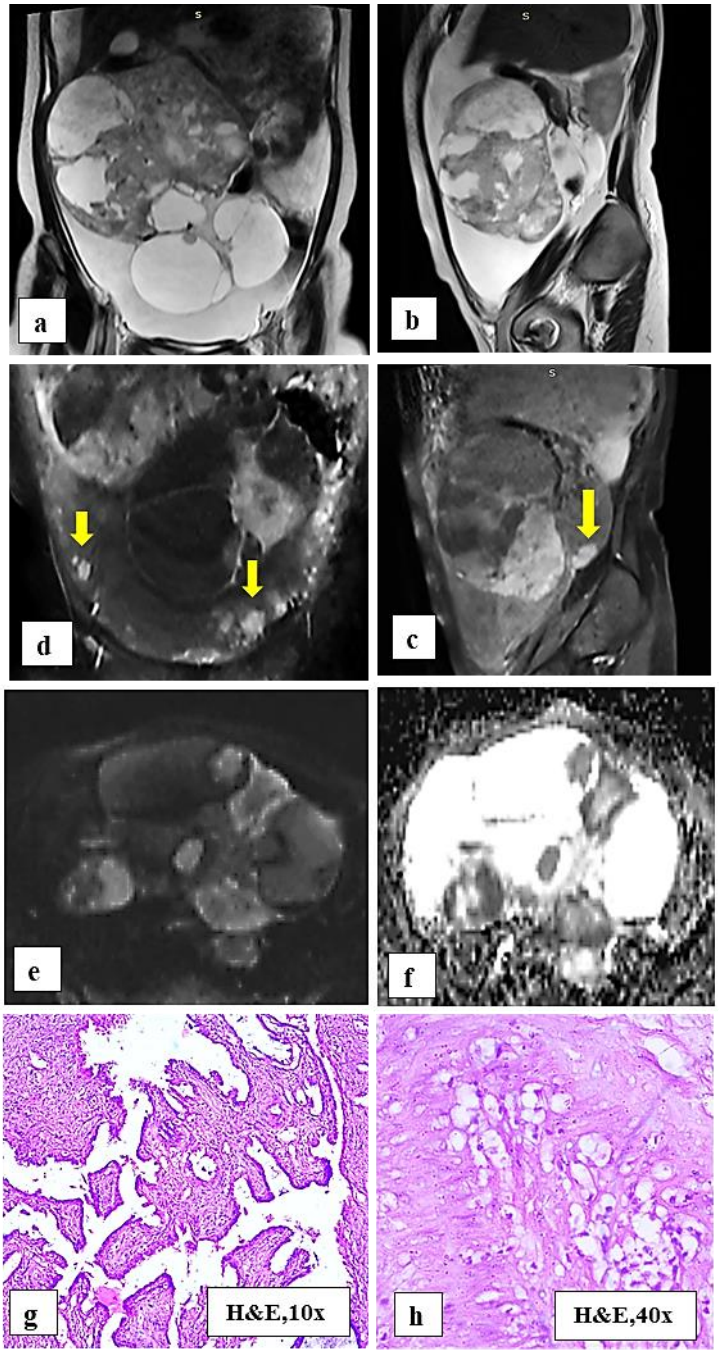

Figure 30: MRI pelvis in 23-year-old women. T2 coronal & sagittal images shows a large pelvo-abdominal solid cystic mass with heterogenous T2 signal intensity and gross ascites (a & b). On T1 post contrast study, heterogenous enhancement (c & d) and few peritoneal deposits (yellow arrows) are seen. Patches of restricted diffusion are seen (e & f) with ADC value of 0.8 x 10^{-3} mm^2/s. Microphotographs shows papillary structures (g) covered by malignant mucinous cells, which are infiltrating the stroma as shown (h) – features consistent with mucinous cystadenocarcinoma of ovary.

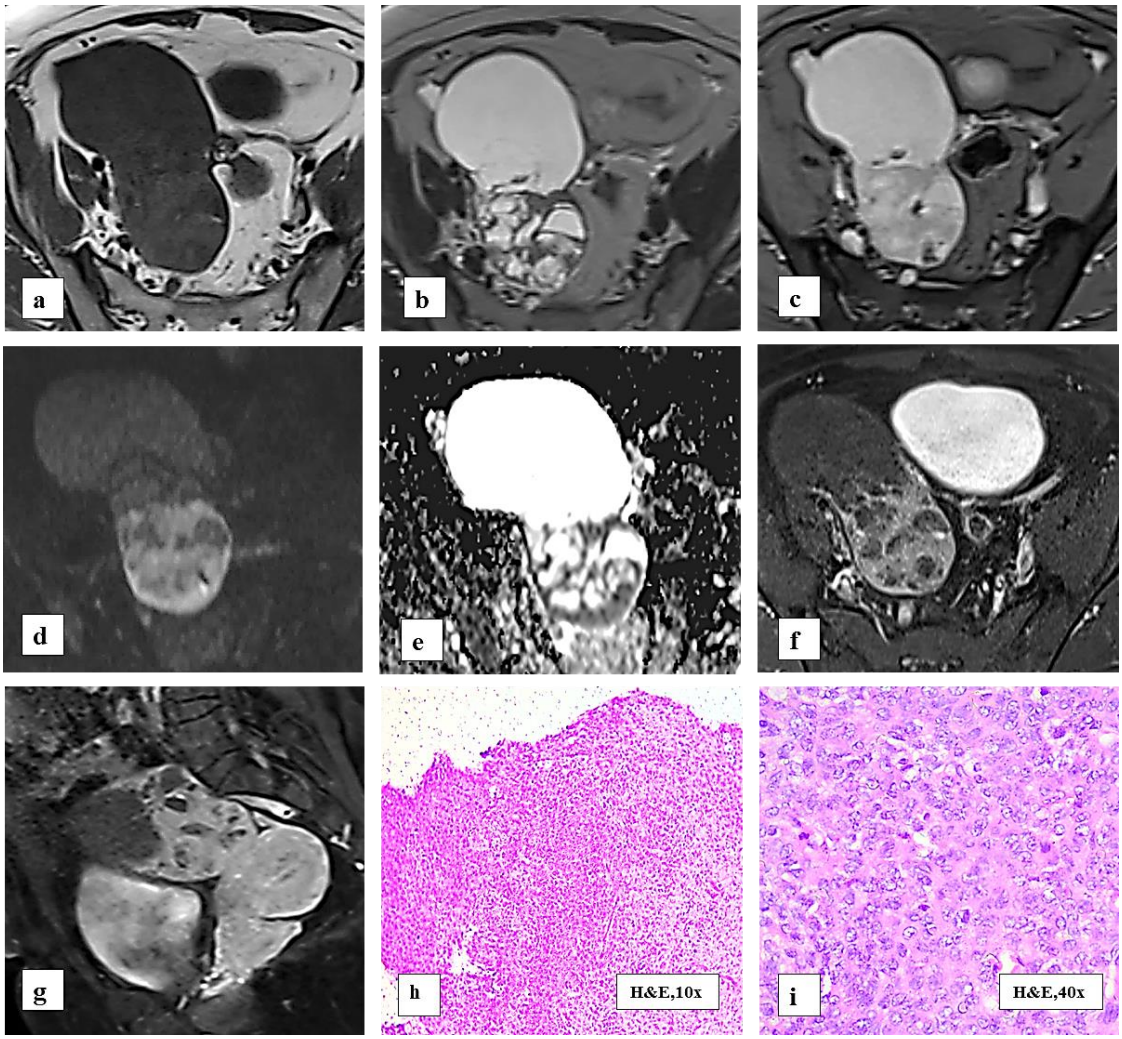

Figure 31: MRI Pelvis in 68 year old lady shows left ovarian granulosa cell tumor. T1 axial image shows a large, well defined solid cystic mass with intermediate signal intensity (a) and heteregenously hyperintense signal on T2 axial section (b). The lesion demonstrates few blooming areas on GRE (c) and restricted diffusion on DWI/ADC (d & e). ADC value was 0.7 x 10^{-3} mm^2/s. T1FS post contrast axial and sagittal images (f & g) demonstrates hetergenously enhancing solid components of the mass. Microphotographs show round to ovoid cells in sheets or ill-defined lobules (h) and longitudinal nuclear grooves in tumor cells (i).

DISCUSSION

DISCUSSION

Ovarian cancer is one of the prominent causes of mortality among women in developed and developing countries. In Kolar, the overall incidence of ovarian malignancies is about 2.98%[3]. Diagnosis of ovarian mass as benign or malignant represents a diagnostic challenge and is clinically important as it can avoid unnecessary surgical interventions and optimize the treatment strategy. Women with suspected ovarian malignancies may require referral to tertiary care centers for cytoreductive surgery and aggressive chemoradiotherapy, while those with benign masses can be conservatively managed and may require simple surgical interventions.

Ultrasonography has always been used as the first line investigation for pelvic imaging. Adnexal lesions may sometimes be an incidental finding on ultrasonography and in 5-25% of the cases it remains inconclusive even after performing ultrasound. Some studies even suggest that in 22% of cases, the diagnosis on ultrasonography can remain indeterminate even after applying the International Ovarian Tumor Analysis (IOTA) principles[67]. CT, carries a risk of radiation exposure and has poor soft tissue resolution, resulting in a wide range of sensitivity (35.5%-100%), specificity (73.7%-92.5%) and overall diagnostic accuracy (34%-82%) and hence cannot be reliably used[68].

MRI, because of its multiplanar imaging capabilities and remarkable soft tissue resolution, is the preferred imaging method for pre-operative characterization of ovarian masses. DWI is an upcoming, non-invasive, advanced imaging sequence that works on the principle of Brownian movement and assesses the cellular organization, cellular density and pattern of diffusivity at the tissue microstructure level[7].

Likewise, the quantitative assessment of diffusion, expressed as apparent diffusion coefficient values (ADC), shows higher values for benign lesions and lower values in malignancies. Addition of DWI with ADC can complement the routine MRI protocols in differentiating benign from malignant masses.

In the present study, we evaluated the diagnostic efficacy of DWI/ADC in characterizing ovarian masses in the 32 females referred for MRI. The most commonly identified age groups in our study was between 40-49 years (31%), and 60-69 years (31%) together accounting for 62% of the cases, with an average of 49.81 ± 12.88 years (mean ± SD) and range of 23 to 70 years. Our results closely resemble a study done by Emad-Eldin S *et al*[4] in 2018, who reported the mean age of 44.15 ± 15.08 years (mean ± SD) (range 16-80 years) in women presenting with ovarian masses.

There was no significance for the average age of presentation in our study, that would influence the nature of ovarian mass. The average age for benign masses was 48.7 ± 13.89 years (mean ± SD) and that for malignant masses was 51.38 ± 11.69 years (Mean ± SD), with *p* value of .58. This was comparable to another study on Asian population by Zhang *et al*[7] in 2012, who reported mean age for benign and malignant masses to be 48.2 ± 30.0 years (mean ± SD) and 50.2 ± 28.5 years (mean ± SD) respectively.

About 63% (n=20) of women in our study, had attained menopause and remaining 37% (n=12) were of pre-menopausal age group. Among post-menopausal group of patients, 60% of the masses were benign and 40% were malignant. Similarly,

among women of reproductive age, 58.3% of cases were benign and 41.6% were malignant. As such, menopause was not a significant confounding factor for malignancy in this study (p = .95). This is supported by a study conducted by Titus-Ernstoff L *et al*[69] who assessed the reproductive and menstrual factors in relation to risk for ovarian cancers and concluded that there was no association between overall risk for ovarian malignancy and natural age of menopause.

Most frequent symptom at presentation was pain abdomen, in 50% of cases followed by mass per abdomen in 25% cases and abdominal distension in 12.5% of cases. There was a slight predominance of benign ovarian masses (n=19;59.3%) as compared to malignancies (n=13;40.62%) in our study.

In our study, most common benign ovarian mass was mucinous cystadenomas (n=6;32%) followed by mature teratoma (n=5;26%) and serous cystadenomas (n=4;21%). This was contrary to the results declared by Jha *et al*[70], in which the most commonly encountered benign tumor was serous cystadenoma (32.6%) followed by mucinous cystadenoma (15.6%). Likewise, another study by Sharadha *et al*[71] who assessed the changing clinico histopathological trend in ovarian cancers reported the incidence of serous cystadenoma (67%) to be highest, superceding those of mucinous cystadenoma (19%) and mature teratoma (11.6%).

We also noticed in our study that, ovarian serous cystadenocarcinoma (n=9;70%) was the most common ovarian malignancy followed by mucinous cystadenocarcinoma (n=3;23%). Jha *et al*[70] had similar findings and stated that, the incidence of serous cystadenocarcinomas of ovary (46.2%) was more than that of

mucinous cystadenocarcinomas (23%). Similarly, observations made by Sharadha *et al*[71] in her study, were in concordance with our results, showing that the incidence of serous cystadenocarcinomas (42.9%) superceded those of mucinous cystadenocarcinomas (28.6%).

Our study included solid, cystic as well as complex solid cystic ovarian masses. Based on conventional MR imaging features, such as presence or absence of thick septations (> 3 mm), heterogenous solid components, papillary projections, ascites, regional lymph node involvement, contrast enhancement, peritoneal deposits and regional metastasis, these lesions were classified as benign or malignant. There were 16 benign (50%) and 16 malignant (50%) ovarian masses. On histopathological examination, 13 of these were confirmed to be malignant, thereby giving 3 false positive cases with conventional MRI. One such case was that of a 60-year-old lady presenting with pain abdomen. On imaging, a large (> 10 cm) solid cystic left adnexal mass with fat fluid level, solid components and calcifications, demonstrating fat suppression on T1FS, restricted diffusion of peripherally located solid components and heterogenous post contrast enhancement of solid components and cyst wall was recorded. Though a rare phenomenon, a possible malignant transformation of the teratoma was considered[44]. However, this turned out to be benign teratoma on histopathology.

Similarly, there were two other cases of 55-year-old (presenting with pain abdomen) and 66-year-old women (presenting with suspicious mass per abdomen), both of which showed multiloculated T1 intermediate-high signal intensity solid cystic adnexal masses with thick heterogeneously enhancing septations/solid

components and mild to moderate ascites. Based on these morphological findings, they were diagnosed to be mucinous cystadenocarcinomas on MRI. However, they were histopathologically proven cases of seromucinous cystadenoma and mucinous cystadenoma respectively.

Comparing the findings on conventional MRI with HPE diagnosis, we observed the specificity, PPV and the overall diagnostic accuracy to be 84.2%, 81.25% and 90.6% respectively. These values obtained in our study are consistent with findings in a prospective study done by Taalab SE *et al*[72] published in 2020 on 'role of MRI in evaluating ovarian masses' that showed a specificity of 89.5%, PPV of 84.6% and a diagnostic accuracy of 93.3% respectively for conventional MRI.

We also evaluated these masses on diffusion weighted images at b 50,400 and 800 for its signal intensity and calculated the ADC values from b 800 image. We observed that, there were 24 masses (75%) with heterogenous solid components demonstrating restricted diffusion while in the remaining 8 masses (25%) there was no restricted diffusion. Using the ADC cut off, of 1.23 x $10^{-3}$$mm^2$/s, we had 17 cases with low ADC values and 15 cases with higher ADC values. Of the 17 cases with low ADC values, we had 13 histopathologically proven malignancies, each demonstrating values less than 1.23 x $10^{-3}$$mm^2$/s. Remaining 4 cases with ADC value < 1.23 x $10^{-3}$$mm^2$/s were proven benign. These included one case of hemorrhagic cyst and 3 cases of mature teratomas. The ADC values obtained in our study for these benign masses are as follows:

Table 23: ADC values of benign restricting lesion

Ovarian mass	ADC Value
Hemorrhagic cyst	0.9 x $10^{-3}mm^2/s$
Mature teratoma	1.0 x $10^{-3}mm^2/s$
	1.1 x $10^{-3}mm^2/s$
	1.1 x $10^{-3}mm^2/s$

These findings in our study are in accordance with various studies that have come across such benign ovarian lesions showing restricted diffusion with low ADC values. It is a known fact that, tumors with high cellularity will show restricted diffusion as expected in malignancies. However, some tissue substances like blood, pus, necrosis and keratin may also show restriction on diffusion imaging even though they indicate a benign etiology[73]. Therefore, benign ovarian lesions such as mature cystic teratomas (keratin content and Rokitansky nodule), haemorrhagic cyst, endometriomas (blood products), fibromas & thecomas (rich collagen content) and tubo-ovarian abscess (pus) can show restricted diffusion and have low ADC values[73].

Zhang *et al*[5] in his study on 191 ovarian masses, observed that 83.3% of fibrothecomas, 80% of Brenner's tumor and 100% of cystadenofibromas had low ADC values and reasoned it to be due to the abundance of collagen elements restricting the diffusivity. Similarly, studies by Fujii *et al*[5], Thomassin-Naggara I *et al*[74], and Bazot M *et al*[9], have reported that cystic teratomas and endometriomas show low ADC values. Benign composition of our study did not include fibromas,

thecomas or Brenner's tumor, however we had one case of hemorrhagic cyst with low ADC value and 5 teratomas in which 3/5 teratomas showed low ADC values (as shown in table 23). Excluding these lesions could have been a potential selection bias for deriving an optimal ADC cut off value to differentiate benign from malignant ovarian masses in our study. Moreover, in more than 90% of cases, these tumors are correctly diagnosed on conventional MRI as mentioned by Takeuchi *et al*[9] and Mittal M *et al*[9] in their studies. Therefore, including them in our study did not impose any diagnostic challenge.

With this cut off value of 1.23 x $10^{-3}mm^2/s$ for ADC mapping, there was a statistically significant difference (p value < 0.001) in the mean ADC values for benign (1.73 ± 0.66 x $10^{-3}mm^2/s$) and malignant (0.786 ± 0.21 x $10^{-3}mm^2/s$) ovarian masses. This was comparable to the results obtained by Zhang *et al*[5] who also reported significant difference in mean ADC values i.e. 1.22 ± 0.46 x $10^{-3}mm^2/s$ and 0.91 ± 0.20 x $10^{-3}mm^2/s$ for benign and malignant masses respectively. Similarly, Mittal M *et al*[9] in his study established a mean ADC value of 1.45 ± 0.15 x $10^{-3}mm^2/s$ and 0.96 ± 0.16 x $10^{-3}mm^2/s$ in benign and malignant ovarian masses respectively. However, some studies such as that done by Fujii *et al*[4] assessing role of DWI in 123 ovarian lesions (42 malignant & 81 benign masses) differ in their observations by stating that, there was no statistical significance for mean ADC values between benign and malignant masses. This they suggested was due to inclusion of various benign restricting tumors such as sex cord stromal tumors, and Brenner's tumors in their study.

This also explains a declining trend in the statistical parameters (specificity, PPV and overall accuracy of 78.9%, 76.47% and 87% respectively) obtained in our study when findings on only DWI/ADC were compared with histopathological diagnosis. Zhang *et al*[5] observed in his study that, after excluding benign restricting ovarian masses, the statistical analysis improved as described: sensitivity from 66.7% to 97.7%, PPV from 91.4% to 96.6% & NPV from 82.1% to 99.1%. There was no statistical significance in the specificity which was 90.9% and 90.1% respectively. Thus, it is important to keep in mind the pitfalls with diffusion weighted imaging while establishing the final diagnosis.

When the final diagnosis was made combining the morphological features on MRI and the ADC values on DWI, the following observations were made. Among two of the three cases that were falsely diagnosed to be malignant on conventional MRI, the ADC values were high ($1.38 \times 10^{-3} mm^2/s$ & $1.30 \times 10^{-3} mm^2/s$ respectively) suggesting benign etiology and only in one benign mass the ADC value was low ($1.10 \times 10^{-3} mm^2/s$). Likewise, among the 4 benign lesions which demonstrated low ADC values on diffusion weighted imaging, morphological features on conventional MRI clearly ruled out a possibility of malignancy. For this combined approach of imaging, specificity, PPV and overall diagnostic accuracy significantly increased to 94.7%, 92.86% and 96.88% respectively. A study by Taalab SE *et al*[72] observed a specificity of 89.5%, PPV of 84.6% and an accuracy of 93.3% when image interpretation was done with routine MRI. The same increased to a specificity of 94.7%, PPV of 91.7% and an accuracy of 96.7% when DWI/ADC was applied for final diagnosis, therefore suggesting that the addition of DWI to routine MRI would ensure accurate pre-operative diagnosis. A combined interpretation of findings on both conventional MRI

and DWI/ADC helps in overcoming the limitations of each individual modalities, thereby reducing the false positive results and increasing the overall diagnostic accuracy.

This study had some limitations. Firstly, our study population was relatively small and requires larger sample volume to validate the results obtained in this study. Second, we did not find a wide spectrum of benign and malignant ovarian masses among the 32 cases. Inclusion of different types of benign and malignant masses such as fibromas, thecomas, fibrothecomas, ovarian metastasis could influence or alter the efficacy of diffusion imaging in differentiation of ovarian masses. However, since our study included both simple as well as complex masses, and has a comparable contribution by both benign and malignant types of ovarian masses, the results and outcomes derived are reliable.

CONCLUSION

CONCLUSION

In the current study, it was concluded that diffusion weighted imaging with corresponding ADC values is an adjunct to conventional MRI in differentiating benign from malignant ovarian masses. Though the sensitivity and negative predictive value remained consistent, the specificity, positive predictive value and the overall diagnostic accuracy showed an increasing trend when both conventional MRI and DWI/ADC were used in combination for characterisation of ovarian masses.

Mean ADC values for benign and malignant ovarian masses showed statistical significance (p <.001) when an optimal ADC cut off value of 1.23 x $10^{-3}mm^2/s$ was used. Mean age of presentation for benign masses was 51.38 ± 11.69 years (mean ± SD) and that for malignancies was 48.7± 13.89 years (mean ± SD) respectively with no statistical significance. DWI/ADC has an adjunctive role in accurate preoperative characterisation of ovarian masses, especially in sonographically inconclusive cases.

We therefore recommend the addition of a non-invasive, less time consuming, advanced sequence such as DWI/ADC mapping to routine MRI protocols as a problem solving tool for characterisation of complex/indeterminate ovarian masses. The use of an optimal ADC cut off (1.23 x $10^{-3}mm^2/s$) as concluded in our study can effectively distinguish benign and malignant masses thereby avoiding unnecessary and erroneous treatment strategies.

SUMMARY

SUMMARY

Ovarian cancers are becoming one of the leading causes of mortality among women in both developing and developed countries. Accurate and early diagnosis of these cases can help streamline the treatment protocols and thereby reduce the overall mortality rates. Though ultrasound is the favoured primary imaging modality for pelvic pathologies, it remains inconclusive for complex adnexal masses. CT, with its poor soft tissue resolution and risk of radiation exposure fails to satisfy the need. MRI, with excellent soft tissue contrast and multiplanar imaging capabilities, in combination with advanced sequences like diffusion weighted imaging has a potential role in characterising ovarian masses, thereby reducing unwanted surgical interventions. This study was taken up to emphasise the role of diffusion weighted imaging and ADC mapping in solving the diagnostic challenge posed by these ovarian masses.

The aims and objectives of the study were to evaluate morphology of the ovarian mass on MRI, to differentiate benign from malignant ovarian masses with DWI/ADC values and to correlate the MRI & DWI/ADC findings with histopathology.

This prospective observational study was conducted from January 2019 to June 2020 on 32 patients with suspected pelvic mass who underwent MRI of Pelvis at the Department of Radio-Diagnosis at R. L. Jalappa Hospital and Research Center attached to SDUMC, Kolar. Prior informed consent was taken from the patients for their willingness to participate in the study. The inclusion criterion was all patients with clinically suspected pelvic mass or sonographically diagnosed ovarian mass

referred for MRI. Those with congenital uterine anomalies, ovarian torsion, cardiac pacemakers, prosthetic heart valves, cochlear implants and with history of claustrophobia were eliminated from this study.

Baseline data of the patients were recorded along with pertinent clinical history and relevant lab investigations. MRI of pelvis was performed on patients fulfilling the inclusion/exclusion criteria on 1.5 Tesla, 18 channel, MR Scanner (Siemens® Magnetom Avanto®). Patient was positioned supine and the following sequences were applied : Sagittal and axial T1 and T2-weighted fast spin echo, sagittal and coronal STIR sequence; Gradient echo sequence, advanced sequences like single-shot echo-planner diffusion weighted image in axial plane with b values of 50, 400 and 800 s/mm^2. Patients with normal renal function underwent contrast study as and when required. Morphological parameters such as presence or absence of thick septations (> 3mm), papillary projections, heterogenous solid components, contrast enhancement, ascites, regional lymph node involvement, peritoneal deposits and regional metastasis were assessed on conventional MR sequences. Suitable ROIs (15-150 mm^2) were placed on b 800 diffusion weighted image to calculate the ADC values. ADC cut off value of 1.23 x 10^{-3} mm^2/s was utilized to differentiate benign (> 1.23 x 10^{-3} mm^2/s) and malignant (< 1.23 x 10^{-3} mm^2/s) masses. Both conventional MRI and DWI/ADC findings were recorded and interpreted for the final diagnosis. The ovarian masses were subjected to histopathological examination. The pathological results were compared with conventional MRI and DWI/ADC findings.

The data was entered in Microsoft excel sheet. The measurable variables were analyzed and interpreted between them by the student's t test and the ordinal and

categorical variables between them were interpreted by Chi-square (χ^2) test. The statistical procedures were performed with the help of an SPSS statistical package (ver 21) and OpenEpi ver 3.01. *P* value < 0.05 was treated as statistically significant.

The study included 32 cases of ovarian masses. The mean age of patients was 49.81 ± 4.46 years (mean ± SD) with a range varying from 23-70 years. Most of them were in post-menopausal age group (n=20;63%), while the remaining were in the reproductive age group (n=12;37%). The average age for benign [48.7± 13.89 years (mean ± SD)] and malignant [(51.38 ± 11.69 years (mean ± SD)] lesions was comparable, with no significant difference (*p=.58*). The average age at presentation and the menstrual status of the patient did not determine the pathological type of the mass. Overall, there was a slight majority of benign lesions (n=19;59.37%) as compared to ovarian malignancies (n=13;40.63%).

Of the benign masses, mucinous cystadenoma (n=6;32%) was most common, followed by mature teratoma (n=5;26%) and serous cystadenoma (n=4;21%). On the malignant spectrum, we had a clear majority by serous cystadenocarcinoma (n=9;70%) followed by mucinous cystadenocarcinoma (n=3;23%) and one case of granulosa cell tumour of ovary (7%). MRI findings were correlated with HPE diagnosis and specificity, PPV and the overall diagnostic accuracy were found to be 84.2%, 81.25% and 90.6% respectively. There were no false negative results, hence both sensitivity and NPV was 100%.

There were three cases that were falsely diagnosed to be malignant on conventional MRI, that were histopathologically proven as benign masses. They

included, one case of a 60-year lady presenting with suspected mass per abdomen and diagnosed as teratoma with possible malignant transformation. The histopathological diagnosis made was mature teratoma. Two other cases, one of 65-year-old lady with abdominal distention and another 55-year-old with suspected mass per abdomen, both of whom were falsely diagnosed to have mucinous cystadenocarcinoma. On histopathology, they turned out to be seromucinous cystadenoma and mucinous cystadenoma respectively. Analysing the ADC values in these cases, following observations were made. The ADC values in mature teratoma was 1.10×10^{-3} mm^2/s. This can be explained by the fact that teratomas are one among the benign restricting ovarian lesions that are well- known to show low ADC values. In the other two cases, ADC values were $1.38 \times 10^{-3} mm^2/s$ and $1.30 \times 10^{-3} mm^2/s$ respectively ($> 1.23 \times 10^{-3}$ mm^2/s), both matching the histopathological diagnosis of benign etiology.

ADC cut off value of $1.23 \times 10^{-3} mm^2/s$ was used for DWI/ADC mapping. There were no false negative cases which explains the perfect score of 100% for sensitivity and negative predictive value. However, 4 benign masses demonstrated restricted diffusion and had low ADC values, thereby reducing the specificity, positive predictive value and overall diagnostic accuracy of DWI/ADC to 78.9%, 76.47% and 87% respectively.

Among the 4 benign lesions that demonstrated areas of restriction, one was a case of hemorrhagic cyst in 35-year-old lady and 3 cases were of mature teratomas in middle aged ladies with ADC values lower than $1.23 \times 10^{-3} mm^2/s$ (malignant value). In these cases, the classical morphological features were distinct enough to be correctly diagnosed as benign ovarian masses on conventional MRI therefore

overcoming this limitation with diffusion imaging. Thus, when both imaging techniques were analysed together, the limitations and pitfalls of each individual modality was overcome thereby reducing the number of false positive cases. This justifies the significant increase in the statistical parameters such as specificity, positive predictive value and overall diagnostic accuracy to 94.7%, 92.86% and 96.88% respectively.

We concluded that diffusion weighted imaging with corresponding ADC values is accurate in pre-operative diagnosis of ovarian masses. We advocate an optimal ADC cut off value of 1.23×10^{-3} mm^2/s for the quantitative assessment of diffusion and differentiation of benign from malignant ovarian masses with high diagnostic accuracy. Thus DWI/ADC should be incorporated into routine MRI protocols for imaging in ovarian masses to ensure appropriate treatment strategies.

BIBLIOGRAPHY

BIBLIOGRAPHY

1. Zhang Y, Luo G, Li M, Guo P, Xiao Y, Ji H et al. Global patterns and trends in ovarian cancer incidence: age, period and birth cohort analysis. BMC Cancer 2019;19:984.

2. Ferlay J, Ervik M, Lam F, Colombet M, Mery L, Piñeros et al. Global Cancer Observatory: Cancer Today. [Internet]. Gco.iarc.fr. 2018 [cited 29 October 2018]. Available at: https://gco.iarc.fr/today/data/factsheets/populations/356-india-fact-sheets.pdf

3. Kalyani R, Das S, Bindra Singh MS, Kumar H. Cancer profile in the Department of Pathology of Sri Devaraj Urs Medical College, Kolar: a ten years study. Indian J Cancer 2010;47:160-5.

4. Emad-Eldin S, Grace MN, Wahba MH, Abdella RM. Diagnostic potential of diffusion weighted and dynamic contrast enhanced MR imaging in the characterisation of complex ovarian lesions. Egypt J Radiol Nucl Med 2018;08:884-91.

5. Zhang P, Cui Y, Li W, Ren G, Chu C, Wu X. Diagnostic accuracy of diffusion-weighted imaging with conventional MR imaging for differentiating complex solid and cystic ovarian tumours at 1.5T. World J Surg Oncol 2012;10:237.

6. Kochiyil J, Vernekar J. Utility of MRI in uterine and adnexal lesions. Int J Med Res Rev 2016;4:655-63.

7. Meng XF, Zhu SC, Sun SJ, Guo JC, Wang X. Diffusion weighted imaging for the differential diagnosis of benign vs malignant ovarian neoplasms. Oncol Lett 2016;11:3795-802.

8. Tantawy MS, Elrakhawy M, Saleh G, El-morsv A, Saleh GA.DWI in characterization of complex ovarian masses, would it help?. Egypt J Radiol Nucl Med 2018;49:878-83.

9. Mittal M, Mannan N. Evaluation of Diffusion Weighted MRI findings and ADC Values within the solid component According To Histological Types of Ovarian Masses. Int J Med Res Prof 2016;2:33-8.

10. Yao HH. The pathway to femaleness: current knowledge on embryonic development of the ovary. Mol Cell Endocrinol 2005;230:87-93.

11. Pask A. The Reproductive System. Adv Exp Med Biol 2016;886:1-12.

12. Sokkary N, Dietrich JE. Ovarian embryology, anatomy, and physiology including normal menstrual physiology. Endocrine Surgery in Children. Chapter 23. 1st edition. Springer Berlin Heidelberg 2018: Pg 319–26.

13. Singh I. Urogenital System. In: Devi VS, editor. Inderbir Singh's Human Embryology. Chapter 16. 11th edition. Jaypee Brothers Medical Publishers 2018: Pg 283-4.

14. Singh I. Reproductive System, Gametogenesis, Ovarian and Menstrual Cycles. In: Devi VS, editor. Inderbir Singh's Human Embryology. Chapter 3. 11th edition. Jaypee Brothers Medical Publishers 2018: Pg 27-44.

15. Macklon NS, Fauser BC. Follicle development during the normal menstrual cycle. Maturitas 1998;30:181-8.

16. Drake RL, Vogl AW, Mitchell AWM. Pelvis and Perineum. Gray's Anatomy For Students. Chapter 5. 4th edition. Elsevier Limited 2020: Pg 415-95.

17. Berek JS. Anatomy and Embryology. Berek & Novak's Gynecology. Chapter 5. 15th edition. Lippincott Williams & Wilkins 2012: Pg 177-8.

18. Jeong YY, Outwater EK, Kang HK. Imaging evaluation of ovarian masses. Radiographics 2000;20:1445-70.

19. Brown DL, Dudiak KM, Laing FC. Adnexal masses: US characterization and reporting. Radiology 2010;254:342-54.

20. Forstner R, Kinkel K. Adnexal masses: Characterisation of Benign Ovarian Lesions. In: Hamm B, Forstner R, editors. MRI and CT of the Female Pelvis. Chapter 9. 1st edition. Springer Science & Business Media 2007: Pg 197-232.

21. Wasnik AP, Menias CO, Platt JF, Lalchandani UR, Bedi DG, Elsayes KM. Multimodality imaging of ovarian cystic lesions: Review with an imaging based algorithmic approach. World J Radiol 2013;5:113-25.

22. Oyelese Y, Kueck AS, Barter JF, Zalud I. Asymptomatic postmenopausal simple ovarian cyst. Obstet Gynecol Surv 2002;57:803-9.

23. Granberg S. Preoperative assessment of unilocular adnexal cysts by transvaginal ultrasonography: a comparison between ultrasonographic morphologic imaging and histopathologic diagnosis. Am J Obstet Gynecol 2001;184:48-54.

24. Park SB, Lee JB. MRI features of ovarian cystic lesions. J Magn Reson Imaging 2014;40:503-15.

25. Jain KA. Sonographic spectrum of hemorrhagic ovarian cysts. J Ultrasound Med 2002;21:879-86.

26. Baerwald AR, Adams GP, Pierson RA. Form and function of the corpus luteum during the human menstrual cycle. Ultrasound Obstet Gynecol 2005;25:498-507.

27. Swire MN, Castro-Aragon I, Levine D. Various sonographic appearances of the hemorrhagic corpus luteum cyst. Ultrasound Q 2004;20:45-58.

28. Corwin MT, Gerscovich EO, Lamba R, Wilson M, McGahan JP. Differentiation of ovarian endometriomas from hemorrhagic cysts at MR imaging: utility of the T2 dark spot sign. Radiology 2014;271:126-32.

29. Jung SE, Lee JM, Rha SE, Byun JY, Jung JI, Hahn ST. CT and MR imaging of ovarian tumors with emphasis on differential diagnosis. Radiographics 2002;22:1305-25.

30. Iyer VR, Lee SI. MRI, CT, and PET/CT for ovarian cancer detection and adnexal lesion characterization. AJR Am J Roentgenol 2010;194:311-21.

31. Sahin H, Abdullazade S, Sanci M. Mature cystic teratoma of the ovary: a cutting edge overview on imaging features. Insights Imaging 2017;8:227-41.

32. Bronshtein M, Yoffe N, Brandes JM, Blumenfeld Z. Hair as a sonographic marker of ovarian teratomas: improved identification using transvaginal sonography and simulation model. J Clin Ultrasound 1991;19:351-5.

33. Malde HM, Kedar RP, Chadha D, Nayak S. Dermoid mesh: a sonographic sign of ovarian teratoma. AJR Am J Roentgenol 1992;159:1349-50.

34. Owre A, Pedersen JF. Characteristic fat-fluid level at ultrasonography of ovarian dermoid cyst. Acta Radiol 1991;32:317-9.

35. Tongsong T, Wanapirak C, Khunamornpong S, Sukpan K. Numerous intracystic floating balls as a sonographic feature of benign cystic teratoma: report of 5 cases. J Ultrasound Med 2006;25:1587-91.

36. Pantoja E, Rodriguez-Ibanez I, Axtmayer RW, Noy MA, Pelegrina I. Complications of dermoid tumours of the ovary. Obstet Gynecol 1975;45:89-94.

37. Wei F, Jiang Z, Yan C. Analysis of 20 mature ovarian cystic teratoma cases in postmenopausal women. Chin Med J 2001;114:137-8.

38. Outwater EK, Siegelman ES, Hunt JL. Ovarian teratomas: tumor types and imaging characteristics. Radiographics 2001;21:475-90.

39. Shinagare AB, Meylaerts LJ, Laury AR, Mortele KJ. MRI features of ovarian fibroma and fibrothecoma with histopathologic correlation. AJR Am J Roentgenol 2012;198:W296-303.

40. Outwater EK, Siegelman ES, Kim B, Chiowanich P, Blasbalg R, Kilger A. Ovarian Brenner tumors: MR imaging characteristics. Magn Reson Imaging 1998;16:1147-53.

41. Kim JY, Jung KJ, Chung DS, Kim OD, Lee JH, Youn SK. Sclerosing stromal tumor of the ovary: MR-pathologic correlation in three cases. Korean J Radiol 2003;4:194-9.

42. Park SB, Kim MJ, Lee KH, Ko Y. Ovarian serous surface papillary borderline tumor: characteristic imaging features with clinicopathological correlation. Br J Radiol 2018;91:20170689.

43. Morioka S, Kawaguchi R, Yamada Y, Iwai K, Yoshimoto C, Kobayashi H. Magnetic resonance imaging findings for discriminating clear cell carcinoma and endometrioid carcinoma of the ovary. J Ovarian Res 2019;12:20.

44. Shaaban AM, Rezvani M, Elsayes KM, Baskin Jr H, Mourad A, Foster BR et al. Ovarian malignant germ cell tumors: cellular classification and clinical and imaging features. Radiographics 2014;34:777-801.

45. Tsuboyama T, Hori Y, Hori M, Onishi H, Tatsumi M, Sakane M et al. Imaging findings of ovarian dysgerminoma with emphasis on multiplicity and vascular architecture: pathogenic implications. Abdom Radiol 2018;43:1515-23.

46. Outwater EK, Siegelman ES, Hunt JL. Ovarian teratomas: tumor types and imaging characteristics. Radiographics 2001;21:475-90.

47. Saba L, Guerriero S, Sulcis R, Virgilio B, Melis G, Mallarini G. Mature and immature ovarian teratomas: CT, US and MR imaging characteristics. Eur J Radiol 2009;72:454-63.

48. Horta M, Cunha TM. Sex cord-stromal tumors of the ovary: a comprehensive review and update for radiologists. Diagn Interv Radiol 2015;21:277-86.

49. Jiang W, Tao X, Fang F, Zhang S, Xu C. Benign and malignant ovarian steroid cell tumors, not otherwise specified: case studies, comparison, and review of the literature. J Ovarian Res 2013;6:53.

50. Jung SE, Rha SE, Lee JM, Park SY, Oh SN, Cho KS et al. CT and MRI findings of sex cord-stromal tumor of the ovary. AJR Am J Roentgenol 2005;185:207-15.

51. Outwater EK, Wagner BJ, Mannion C, McLarney JK, Kim B. Sex cord-stromal and steroid cell tumors of the ovary. Radiographics 1998;18:1523-46.

52. Zhang H, Zhang H, Gu S, Zhang Y, Liu X, Zhang G. MR findings of primary ovarian granulosa cell tumor with focus on the differentiation with other ovarian sex cord-stromal tumors. J Ovarian Res 2018;11:46.

53. Cai SQ, Zhao SH, Qiang JW, Zhang GF, Wang XZ, Wang L. Ovarian Sertoli-Leydig cell tumors: MRI findings and pathological correlation. J Ovarian Res 2013;6:73.

54. Xu Y, Yang J, Zhang Z, Zhang G. MRI for discriminating metastatic ovarian tumors from primary epithelial ovarian cancers. J Ovarian Res 2015;8:61.

55. Heo SH, Kim JW, Shin SS, Jeong SI, Lim HS, Choi YD et al. Review of ovarian tumors in children and adolescents: radiologic-pathologic correlation. Radiographics 2014;34:2039-55.

56. Ling Y, Feng CY, Xia SM, Shen LH, Luo LQ, Zhang HY. Magnetic resonance imaging of ovarian carcinosarcoma: correlation to the clinicopathological findings. J South Med Univ 2010; 30:1648-50.

57. Makris GM, Siristatidis C, Battista MJ, Chrelias C. Ovarian carcinosarcoma: a case report, diagnosis, treatment and literature review. Hippokratia 2015;19:256-9.

58. Patel-Lippmann KK, Sadowski EA, Robbins JB, Paroder V, Barroilhet L, Maddox E et al. Comparison of International Ovarian Tumor Analysis Simple Rules to Society of Radiologists in Ultrasound Guidelines for Detection of Malignancy in Adnexal Cysts. AJR Am J Roentgenol 2020;214:694-700.

59. Brown DL. A practical approach to the ultrasound characterization of adnexal masses. Ultrasound Q 2007;23:87-105.

60. Javadi S, Ganeshan DM, Qayyum A, Iyer RB, Bhosale P. Ovarian Cancer, the Revised FIGO Staging System, and the Role of Imaging. AJR Am J Roentgenol 2016;206:1351-60.

61. Ali H, El-Sayed E, Abdullah M. The role of diffusion-weighted MRI on the differentiation of complex adnexal masses. Menoufia Medical Journal 2019;32:881.

62. Yuan X, Guo L, Du W, Mo F, Liu M. Diagnostic accuracy of DWI in patients with ovarian cancer: A meta-analysis. Medicine 2017;96:e6659.

63. Fan X, Zhang H, Meng S, Zhang J, Zhang C. Role of diffusion-weighted magnetic resonance imaging in differentiating malignancies from benign ovarian tumors. Int J Clin Exp Med 2015;8:19928-37.

64. Kim HJ, Lee SY, Shin YR, Park CS, Kim K. The Value of Diffusion-Weighted Imaging in the Differential Diagnosis of Ovarian Lesions: A Meta-Analysis. PLoS One 2016;11:e0149465.

65. Kitajima K, Tanaka U, Ueno Y, Maeda T, Suenaga Y, Takahashi S et al. Role of diffusion weighted imaging and contrast-enhanced MRI in the evaluation of intrapelvic recurrence of gynecological malignant tumor. PLoS One 2015;10:e0117411.

66. Ali R, Nassef H, Ibrahim A, Chalabi N, Mohamed A. The Role of Diffusion Weighted Imaging in suspected cases of ovarian cancer.Egypt J Radiol Nucl Med 2020;51:1-11.

67. Forstner R, Thomassin-Naggara I, Cunha TM, Kinkel K, Masselli G, Kubik-Huch R et al. ESUR recommendations for MR imaging of the sonographically indeterminate adnexal mass: an update. Eur Radiol 2017;27:2248-57.

68. Michielsen K, Dresen R, Vanslembrouck R, De Keyzer F, Amant F, Mussen E et al. Diagnostic value of whole body diffusion-weighted MRI compared to computed tomography for pre-operative assessment of patients suspected for ovarian cancer. Eur J Cancer 2017;83:88-98.

69. Titus-Ernstoff L, Perez K, Cramer DW, Harlow BL, Baron JA, Greenberg ER. Menstrual and reproductive factors in relation to ovarian cancer risk. Br J Cancer 2001;84:714-21.

70. Jha R, Karki S. Histological pattern of ovarian tumors and their age distribution. Nepal Med Coll J 2008;10:81–5.

71. Sharadha S, Sridevi TA, Renukadevi TK, Gowri R, Binayak D, Indra V. Ovarian masses: changing clinico histopathological trends. J Obstet Gynaecol India 2015;65:34-8.

72. Taalab SE, Reffat MM, Elshazly IM. Diffusion-weighted magnetic resonance imaging for the characterization of ovarian tumors in the reproductive age group. Benha Med J 2018;35:401-6.

73. Agostinho L, Horta M, Salvador JC, Cunha TM. Benign ovarian lesions with restricted diffusion. Radiol Bras 2019;52:106-11.

74. Thomassin-Naggara I, Daraï E, Cuenod CA, Fournier L, Toussaint I, Marsault C et al. Contribution of diffusion-weighted MR imaging for predicting benignity of complex adnexal masses. Eur Radiol 2009;19:1544-52.

ANNEXURES

ANNEXURE I

PROFORMA

DIAGNOSTIC POTENTIAL OF DIFFUSION WEIGHTED MRI IN DIFFERENTIATING BENIGN FROM MALIGNANT OVARIAN MASSES AND CORRELATING WITH HISTOPATHOLOGY

Demographic Details:

Name:

Age:

Address:

UHID:

Clinical History:

Local Examination:

-Per abdomen Findings (if any):

Size of lesion:

Location:

Consistency of lesion:

Tenderness on Palpation:

MRI FINDINGS:

<table>
<tr><td colspan="3">MRI FINDINGS</td></tr>
<tr><td rowspan="6"></td><td>Size (cm)</td><td colspan="2"></td></tr>
<tr><td rowspan="2">Septations</td><td>< 3mm</td><td>> 3mm</td></tr>
<tr><td colspan="2"></td></tr>
<tr><td>Papillary projection</td><td colspan="2"></td></tr>
<tr><td rowspan="4">Character of mass
- Solid
- Solid & cystic
- Cystic</td><td colspan="2"></td></tr>
<tr><td colspan="2"></td></tr>
<tr><td colspan="2"></td></tr>
<tr><td rowspan="3"></td><td>Fat</td><td colspan="2"></td></tr>
<tr><td>Calcification</td><td colspan="2"></td></tr>
<tr><td>Hemorrhagic components</td><td colspan="2"></td></tr>
<tr><td rowspan="2">DWI</td><td>Restricted diffusion</td><td colspan="2"></td></tr>
<tr><td>No Restricted diffusion</td><td colspan="2"></td></tr>
<tr><td rowspan="2">ADC Value</td><td>< 1.23 x $10^{-3}mm^2/s$</td><td colspan="2"></td></tr>
<tr><td>>1.23 x $10^{-3}mm^2/s$</td><td colspan="2"></td></tr>
<tr><td>OTHER FINDINGS</td><td colspan="3"></td></tr>
<tr><td>LYMPH NODES</td><td colspan="3"></td></tr>
<tr><td>ASCITES</td><td colspan="3"></td></tr>
<tr><td>REGIONAL METASTASIS</td><td colspan="3"></td></tr>
</table>

MRI diagnosis:

Histopathological Diagnosis:

ANNEXURE II

INFORMED CONSENT

Study title: DIAGNOSTIC POTENTIAL OF DIFFUSION WEIGHTED MRI IN DIFFERENTIATING BENIGN FROM MALIGNANT OVARIAN MASSES AND CORRELATING WITH HISTOPATHOLOGY

Chief researcher/ PG guide's name: Dr. ANIL KUMAR SAKALECHA

Principal investigator: Dr. AMRUTHA RANGANATH

Name of the subject:

Age :

a. I have been informed in my own language that this study involves MRI as part of procedure. I have been explained thoroughly and understand the procedure.

b. I understand that the medical information produced by this study will become part of institutional record and will be kept confidential by the said institute.

c. I understand that my participation is voluntary and may refuse to participate or may withdraw my consent and discontinue participation at any time without prejudice to my present or future care at this institution.

d. I agree not to restrict the use of any data or results that arise from this study provided such a use is only for scientific purpose(s).

e. I confirm that Dr. AMRUTHA RANGANATH / Dr. ANIL KUMAR SAKALECHA (chief researcher/ name of PG guide) has explained to me the purpose of research and the study procedure that I will undergo and the possible risks and discomforts that I may experience, in my own language.

I hereby agree to give valid consent to participate as a subject in this research project.

Participant's signature/thumb impression

Signature of the witness: Date:

1)

2)

I have explained to _____ (subject) the purpose of the research, the possible risk and benefits to the best of my ability.

Chief Researcher/ Guide signature

ಸಮ್ಮತಿ ಪತ್ರ:

ಈ ಕೆಳಗೆ ಸಹಿ ಮಾಡಿರುವ ---------- ಆದ ನಾನು ಈ ಅಧ್ಯಯನದಲ್ಲಿ ಪಾಲ್ಗೊಳ್ಳುವ ಸಲುವಾಗಿ ವೈದ್ಯಕೀಯ ಪರೀಕ್ಷೆಗೆ ಒಳಪಡಲು ನನ್ನ ವೈಯ್ಯಕ್ತಿಕ ವಿವರಗಳನ್ನು ನೀಡಲು ಸಮ್ಮತಿಸಿರುತ್ತೇನೆ.

ಈ ಅಧ್ಯಯನದ ಉದ್ದೇಶ, ಅಧ್ಯಯನದ ಸಂದರ್ಭದಲ್ಲಿನೀಡುವ ಮತ್ತು ಸಂಗ್ರಹಿಸುವ ಮಾಹಿತಿಯ ಗೋಪ್ಯತೆಯ ಬಗ್ಗೆ ನನಗೆ ನನ್ನ ಸ್ಥಳೀಯ ಭಾಷೆಯಲ್ಲಿ ಓದಿ ಹೇಳಲಾಗಿದೆ/ವಿವರಿಸಲಾಗಿದೆ ಮತ್ತು ನಾನು ಇದನ್ನು ಅರ್ಥ ಮಾಡಿಕೊಂಡಿರುತೇನೆ. ಈ ಅಧ್ಯಯನದ ವಿವಿಧ ಅಂಶಗಳ ಬಗ್ಗೆ ಪ್ರಶ್ನೆಗಳನ್ನು ಕೇಳುವ ಅವಕಾಶವನ್ನು ನನಗೆ ನೀಡಲಾಗಿದೆ ಮತ್ತು ನನ್ನ ಪ್ರಶ್ನೆಗಳಿಗೆ ತೃಪ್ತಿಕರವಾದ ಉತ್ತರಗಳು ದೊರೆತಿರುತವೆ. ಈ ಅಧ್ಯಯನದ ಮೂಲಕ ಸಂಗ್ರಹಿಸಿರುವ ಮಾಹಿತಿಯನ್ನು ಸಂಶೋಧನೆಯ ಉದ್ದೇಶಕ್ಕೆ ಮಾತ್ರ ಬಳಸತಕ್ಕದ್ದು.

ಈ ಅಧ್ಯಯನದಿಂದ ಯಾವುದೇ ಸಂದರ್ಭದಲ್ಲಿ ಹಿಂದೆ ಸರಿಯುವ ಸ್ವಾತಂತ್ರ್ಯ ನನಗಿದೆ ಎಂಬುದನ್ನೂ, ಈ ಅಧ್ಯಯನದಲ್ಲಿ ಪಾಲ್ಗೊಳ್ಳುವುದರಿಂದ ನನಗೆ ಯಾವುದೇ ಹೆಚ್ಚುವರಿ ವೆಚ್ಚ ತಗಲುವುದಿಲ್ಲವೆಂಬುದನ್ನು ತಿಳಿದಿರುತ್ತೇನೆ.

ರೋಗಿಯ ಸಹಿ:

ಹೆಸರು:

ಸಾಕ್ಷಿಯ ಸಹಿ:

ಹೆಸರು:

ಪ್ರಧಾನ ಪರೀಕ್ಷಕರ ಹೆಸರು ಮತ್ತು ಸಹಿ:

ದಿನಾಂಕ:

PATIENT INFORMATION SHEET

DIAGNOSTIC POTENTIAL OF DIFFUSION WEIGHTED MRI IN DIFFERENTIATING BENIGN FROM MALIGNANT OVARIAN MASSES AND CORRELATING WITH HISTOPATHOLOGY

Patient Information Sheet

Principal Investigator: Dr. AMRUTHA RANGANATH / Dr. ANIL KUMAR SAKALECHA

I, Dr. AMRUTHA RANGANATH, post-graduate student in Department of Radio-Diagnosis at Sri Devaraj Urs Medical College, will be conducting a study titled "Diagnostic potential of diffusion weighted MRI in differentiating benign from malignant ovarian masses and correlating with histopathology" for my dissertation under the guidance of Dr. Anil Kumar Sakalecha, Professor, Department of Radio-Diagnosis. In this study, we will assess the diagnostic potential of diffusion weighted imaging in differentiating benign from malignant ovarian masses. You would have undergone MRI before entering the study. You will not be paid any financial compensation for participating in this research project.

All of your personal data will be kept confidential and will be used only for research purpose by this institution. You are free to participate in the study. You can also withdraw from the study at any point of time without giving any reasons whatsoever. Your refusal to participate will not prejudice you to any present or future care at this institution

Name and Signature of the Principal Investigator

Ph: 09845306442

Date

ರೋಗಿಯ ಮಾಹಿತಿ ಪತ್ರ

ಮುಖ್ಯ ಸಂಶೋಧಕರು: ಡಾ|| ಅಮೃತ ರಂಗನಾಥ್. / ಡಾ|| ಅನಿಲ್ ಕುಮಾರ್ ಸಕಲೇಚ

ನಾನು ಡಾ|| ಅಮೃತ ರಂಗನಾಥ್ ಶ್ರೀ ದೇವರಾಜ್ ಅರಸು ಮೆಡಿಕಲ್ ಕಾಲೇಜಿನ ರೇಡಿಯೊ ಡಯಾಗ್ನೋಸಿಸ್ ವಿಭಾಗದಲ್ಲಿ ಸ್ನಾತಕೋತ್ತರ ವಿದ್ಯಾರ್ಥಿನಿ. ನಾನು " ಮಾರಣಾಂತಿಕ ಅಂಡಾಶಯದ ದ್ರವ್ಯರಾಶಿಗಳಿಂದ ಬೆನಿಗ್ನ್ ಅನ್ನು ವಿಭಿನ್ನಗೊಳಿಸುವಲ್ಲಿ ಎಂ.ಆರ್.ಐ ಪಾತ್ರ " ನನ್ನ ಪ್ರಬಂಧಕ್ಕಾಗಿ ಡಾ|| ಅನಿಲ್ ಕುಮಾರ್ ಸಕಲೇಚ, ಪ್ರೊಫೆಸರ್, ರೇಡಿಯಾಲಜಿ ವಿಭಾಗ ಅವರ ಮಾರ್ಗದರ್ಶನದಲ್ಲಿ ಮಾಡುತ್ತೇನೆ.

ನೀವು ಈ ಅಧ್ಯಯನದ ಭಾಗವಾಗಲು ಒಪ್ಪಿಗೆ ಹೊಂದಿಲ್ಲದಿದ್ದರೆ ಅಥವಾ ಭಯಭೀತರಾಗುತಿದ್ದರೆ ನೀವು ಯಾವಾಗ ಬೇಕಾದರೂ ಅಧ್ಯಯನದಿಂದ ಹೊರಗುಳಿಯಲು ಮುಕ್ತರಾಗಿದ್ದೀರಿ. ನೀವು ಅಧ್ಯಯನದ ಭಾಗವಾಗಲು ನಿರಾಕರಿಸಿದರೆ ನಿಮ್ಮ ಚಿಕಿತ್ಸೆ ಮತ್ತು ಕಾಳಜಿಗೆ ಧಕ್ಕೆಯಾಗುವುದಿಲ್ಲ. ನೀವು ಅಧ್ಯಯನದ ಭಾಗವಾಗಿದ್ದರೆ ಅಧ್ಯಯನವು ನಿಮಗೆ ಯಾವುದೇ ಅಪಾಯ ಅಥವಾ ಆರ್ಥಿಕ ಹೊರೆಯಾಗುವುದಿಲ್ಲ.

ನಿಮ್ಮ ಗುರುತು ಮತ್ತು ವೈದ್ಯಕೀಯ ವಿವರಗಳು ಗೌಪ್ಯವಾಗಿರುತ್ತದೆ. ಅಧ್ಯಯನದ ಭಾಗವಾಗಿರುವುದರಿಂದ ನೀವು ಯಾವುದೇ ಆರ್ಥಿಕ ಲಾಭವನ್ನು ಪಡೆಯುವುದಿಲ್ಲ.

ನೀವು ಹೊಂದಿರುವ ಯಾವುದೇ ಅನುಮಾನ ಅಥವಾ ಸ್ಪಷ್ಟೀಕರಣಕ್ಕಾಗಿ ನೀವು ಡಾ|| ಅಮೃತ ರಂಗನಾಥ್ ಅಥವಾ ಮೇಲಿನ ಸಂಶೋಧನಾ ತಂಡದ ಯಾವುದೇ ಸದಸ್ಯರನ್ನು ಸಂಪರ್ಕಿಸಬಹುದು.

ಸಂಪರ್ಕ ವಿವರಗಳು:

ಡಾ|| ಅಮೃತ ರಂಗನಾಥ್. ದೂರವಾಣಿ: 9845306442

ಡಾ|| ಅನಿಲ್ ಕುಮಾರ್ ಸಕಲೇಚ.

ANNEXURE III
MASTER CHART

Sl. No	Trial ID	Age	Clinical features	Size AP (cm)	Size TR (cm)	Size CC (cm)	Septations < 3mm	Septations > 3mm	Papillary projection	Character of lesion	Fat	Calcification	Hemorrhage	Contrast	Other findings	Regional lypmh nodes	Acites	MRI diagnosis	MRI Diagnosis	DWI	ADC Value (10^{-3}mm^2/s)	DWI/ADC Diagnosis	Combined MRI & DWI/ADC Diagnosis	HPE B/M	HPE diagnosis
1	644890	55	PA	2.3	2.5	2.1	A	A	A	C	A	A	P	-	A		A	Hemorrhagic Cyst	B	R	0.9	M	B	B	Corpus hemorrhagic cyst
2	28755	60	MA	10.8	17.1	17.2	P	A	P	S & C	A	A	P	PCE +	A	A	P	Serous cystadenocarcinoma	M	R	0.8	M	M	M	Serous cystadenocarcinoma
3	49702	65	AD	8.6	11.6	13.5	A	P	A	S & C	A	A	P	PCE +	A	A	P	Mucinous cystadenocarcinoma	M	R	1.3	B	B	B	Benign seromucinous cystadenoma
4	795880	36	PA	12.8	21.7	31.7	P	A	A	S & C	A	A	A	PCE -	A	A	P	Mucinous cystadenoma	B	R	2	B	B	B	Mucinous cystadenoma
5	537379	68	MA	12.2	7.6	7.8	P	A	P	S & C	A	A	P	-	A	A	P	Malignant ovarian neoplasm	M	R	0.7	M	M	M	Granulosa cell tumor
6	343524	60	PAD	10.4	11.1	14.4	A	A	A	S & C	P	A	P	-	Fat fluid levels	A	A	Dermoid cyst	B	R	1	M	B	B	Mature teratoma
7	498783	42	PA	4.9	5	5.4	P	A	A	S & C	P	A	A	-	Fat fluid levels	A	A	Dermoid cyst	B	R	1.3	B	B	B	Mature Teratoma
8	918982	45	PA	6.3	9.8	8.7	A	A	A	C	A	A	A	-	A	A	A	Serous cystadenoma	B	NR	3.05	B	B	B	Serous cystadenoma
9	997057	60	MA	6.6	8.3	10.3	A	A	A	S & C	P	P	A	PCE +	Fat fluid levels	A	P	Teratoma with malignant transformation	M	R	1.1	M	M	B	Mature Teratoma
10	539319	50	PA	7.6	5.8	5.4	A	A	A	C	A	A	P	-	T2 shading, Few adhesive bands to bowel loops.	A	A	Endometriotic cyst	B	R	1.4	B	B	B	Endometrioma
11	361423	70	AD	8.2	6.4	9.1	P	A	A	C	A	A	A	-	A	A	A	Mucinous cystadenoma	B	NR	1.96	B	B	B	Mucinous cystadenoma
12	844740	46	PA	8.4	9.2	8.8	P	A	A	C	A	A	A	-	A	A	A	Serous cystadenoma	B	R	1.5	B	B	B	Serous cystadenoma
13	762061	46	MA	9.5	11	10.2	P	A	A	C	A	A	A	-	A	A	A	Serous cystadenoma	B	NR	2.8	B	B	B	Mucinous cystadenoma

A-Absent; AD- Abdominal Distention; ADC-Apparent Diffusion Coefficient; AP-Anteroposterior; B-Benign; CC-Craniocaudal; C-Cystic DWI-Diffusion Weighted Imaging; HPE-Histopathological Examination; IC- Irregular Cycles; M- Malignant; MA- Mass per abdomen; MRI-Magnetic Resonance Imaging; NR-No restricted diffusion on DWI; P-Present; PA- Pain Abdomen; PAD-Pain abdomen & Distension; PAM- Pain abdomen & Mass per abdomen; PCE-Post contrast enhancement; PD-Peritoneal Deposit; R-Restricted diffusion on DWI; S-Solid; S & C-Solid & Cystic; TR-Transverse.

ANNEXURE III
MASTER CHART

Sl. No	Trial ID	Age	Clinical features	Size AP (cm)	Size TR (cm)	Size CC (cm)	Septations < 3mm	Septations > 3mm	Papillary projection	Character of lesion	Fat	Calcification	Hemorrhage	Contrast	Other findings	Regional lypmh nodes	Acites	MRI diagnosis	MRI Diagnosis	DWI	ADC Value (10^{-3} mm^2/s)	DWI/ADC Diagnosis	Combined MRI & DWI/ADC Diagnosis	HPE B/M	HPE diagnosis
14	361173	65	PA	10.1	6.4	7.1	P	A	A	S & C	A	A	P	-	A	A	A	Serous cystadenoma	B	R	1.2	B	B	B	Serous cystadenoma
15	932894	48	PA	6.6	4.1	5.9	P	A	A	C	A	A	A	-	A	A	A	Mucinous cystadenoma	B	NR	2.7	B	B	B	Mucinous cystadenoma
16	749471	45	PAD	18	17.3	11	A	P	P	S & C	A	A	p	PCE +	Cyst within cyst. Enhancing PD	P	P	Mucinous cystadenocarcinoma	M	R	0.9	M	M	M	Serous cystadenocarcinoma.
17	433134	35	PA	12.1	6.8	1.2	P	A	A	C	A	A	A	-	A	A	A	Simple cyst	B	NR	2.7	B	B	B	Simple cyst
18	360804	65	MA	11.6	13.5	18.7	A	P	P	S	A	A	p	PCE +	PD in RIF & LIF	A	P	Serous cystadenocarcinoma	M	R	0.7	M	M	M	Serous cystadenocarcinoma
19	625297	25	PA	8.8	11.8	12.1	A	A	A	S & C	P	P	A	-	Pokeball sign, calcification, fat fluid levels	A	P	Dermoid cyst	B	R	1.1	M	B	B	Mature teratoma
20	859722	45	PAM	15	22.3	18.5	A	P	P	S & C	A	A	P	PCE +	A	P	A	Serous cystadenocarcinoma	M	R	0.4	M	M	M	Serous cystadenocarcinoma
21	165463	29	IC	8.4	12.1	13.5	P	A	A	C	A	A	A	-	A	A	A	Serous cystadenoma	B	NR	2.4	B	B	B`	Mucinous cystadenoma
22	333742	56	PA	6.9	14.1	13.7	A	A	A	C	A	A	A	-	A	A	P	Serous cystadenoma	B	NR	1.7	B	B	B	Serous cystadenoma
23	68926	23	AD	9	16.5	16.3	A	P	P	S & C	A	A	P	PCE +	PD	A	P	Ovarian carcinoma	M	R	0.6	M	M	M	Mucinous cystadenocarcinoma
24	916402	53	AD	10.6	14.1	10.4	A	P	A	S & C	A	A	P	PCE +	PD	A	P	Serous cystadenocarcinoma	M	R	0.5	M	M	M	Serous cystadenocarcinoma
25	496596	60	MA	RO 14.9	RO 12.8	RO 18.8	A	P	P	S & C	A	A	P	PCE +	A	A	P	Mucinous cystadenocarcinoma	M	R	1	M	M	M	Mucinous cystadenocarcinoma
26	818249	27	PA	12	9	5.5	A	A	A	C	P	p	A	-	A	A	A	Dermoid cyst	B	NR	1.6	B	B	B	Mature teratoma

A-Absent; AD- Abdominal Distention; ADC-Apparent Diffusion Coefficient; AP-Anteroposterior; B-Benign; CC-Craniocaudal; C-Cystic DWI-Diffusion Weighted Imaging; HPE-Histopathological Examination; IC- Irregular Cycles; M- Malignant; MA- Mass per abdomen; MRI-Magnetic Resonance Imaging; NR-No restricted diffusion on DWI; P-Present; PA- Pain Abdomen; PAD-Pain abdomen & Distension; PAM- Pain abdomen & Mass per abdomen; PCE-Post contrast enhancement; PD-Peritoneal Deposit; R-Restricted diffusion on DWI; S-Solid; S & C-Solid & Cystic; TR-Transverse.

ANNEXURE III
MASTER CHART

Sl. No	Trial ID	Age	Clinical features	Size AP (cm)	Size TR (cm)	Size CC (cm)	Septations < 3mm	Septations > 3mm	Papillary projection	Character of lesion	Fat	Calcification	Hemorrhage	Contrast	Other findings	Regional lypmh nodes	Acites	MRI diagnosis	MRI Diagnosis	DWI	ADC Value (10^{-3} mm^2/s)	DWI/ADC Diagnosis	Combined MRI & DWI/ADC Diagnosis	HPE B/M	HPE diagnosis
27	665984	66	MA	19.5	10.9	22.4	A	P	A	S & C	A	A	P	PCE +	A	A	P	Mucinous cystadenocarcinoma	**M**	R	1.3	B	B	B	Mucinous cystadenoma
28	861531	60	PA	10.9	7.6	8.9	A	P	A	S & C	A	A	A	PCE +	A	P	P	Serous cystadenocarcinoma	M	R	1.1	M	M	M	Serouc cystadenocarcinoma
29	873383	45	PA	11.9	13.2	8.3	A	P	A	S & C	A	A	P	PCE +	A	A	A	Mucinous cystadenocarcinoma	M	R	0.9	M	M	M	Mucinous cystadenocarcinoma
30	294802	56	PA	9.1	8.8	4.5	P	A	P	S & C	A	A	P	PCE +	A	P	A	Ovarian carcinoma	M	R	0.8	M	M	M	Serous cystadenocarcinoma
31	79540	48	MA	14.3	11.1	8.9	A	P	P	S & C	A	A	P	PCE+	A	A	P	Serouscystadeno carcinoma	M	R	0.68	M	M	M	Serous cystadenocarcinoma
32	973504	40	PA	18.5	9.2	5.6	A	P	P	S & C	A	A	P	PCE +	A	A	A	Ovarian carcinoma	M	R	1.15	M	M	M	Serous cystadenocarcinoma

A-Absent; AD- Abdominal Distention; ADC-Apparent Diffusion Coefficient; AP-Anteroposterior; B-Benign; CC-Craniocaudal; C-Cystic DWI-Diffusion Weighted Imaging; HPE-Histopathological Examination; IC- Irregular Cycles; M- Malignant; MA- Mass per abdomen; MRI-Magnetic Resonance Imaging; NR-No restricted diffusion on DWI; P-Present; PA- Pain Abdomen; PAD-Pain abdomen & Distension; PAM- Pain abdomen & Mass per abdomen; PCE-Post contrast enhancement; PD-Peritoneal Deposit; R-Restricted diffusion on DWI; S-Solid; S & C-Solid & Cystic; TR-Transverse.